

การดูดซับและการออกซิเดชันของเอทานอลบนตัวเร่งปฏิกิริยาโลหะคู่ที่  
ประกอบด้วยแพลทินัมและออกไซด์ของโลหะที่เป็นเบสบนตัวรองรับ

**RH-MCM-41**



นางสาวกมลวรรณ รินทราณี

วิทยานิพนธ์นี้เป็นส่วนหนึ่งของการศึกษาตามหลักสูตรปริญญาวิทยาศาสตรดุษฎีบัณฑิต

สาขาวิชาเคมี

มหาวิทยาลัยเทคโนโลยีสุรนารี

ปีการศึกษา 2554

**ADSORPTION AND OXIDATION OF ETHANOL ON  
BIMETALLIC CATALYSTS CONTAINING PLATINUM  
AND BASE METAL OXIDES SUPPORTED ON  
RH-MCM-41**

**Kamolwan Rinramee**



**A Thesis Submitted in Partial Fulfillment of the Requirements for the  
Degree of Doctor of Philosophy in Chemistry  
Suranaree University of Technology  
Academic Year 2011**

**ADSORPTION AND OXIDATION OF ETHANOL ON  
BIMETALLIC CATALYSTS CONTAINING PLATINUM  
AND BASE METAL OXIDES SUPPORTED ON  
RH-MCM-41**

Suranaree University of Technology has approved this thesis submitted in partial fulfillment of the requirements for the Degree of Doctor of Philosophy.

Thesis Examining Committee

---

(Asst. Prof. Dr. Kunwadee Rangriwatananon)

Chairperson

---

(Assoc. Prof. Dr. Jatuporn Wittayakun)

Member (Thesis Advisor)

---

(Dr. Karin Föttinger)

Member

---

(Asst. Prof. Dr. Thanaporn Manyum)

Member

---

(Asst. Prof. Dr. Sanchai Prayoonpokarach)

Member

---

(Prof. Dr. Sukit Limpijumng)

Vice Rector for Academic Affairs

---

(Assoc. Prof. Dr. Prapun Manyum)

Dean of Institute of Science

กมลวรรณ รินทราณี : การดูดซับและการออกซิเดชันของเอทานอลบนตัวเร่งปฏิกิริยา โลหะคู่ที่ประกอบด้วยแพลทินัม และออกไซด์ของโลหะที่เป็นเบสบนตัวรองรับ RH-MCM-41 (ADSORPTION AND OXIDATION OF ETHANOL ON BIMETALLIC CATALYSTS CONTAINING PLATINUM AND BASE METAL OXIDES SUPPORTED ON RH-MCM-41). อาจารย์ที่ปรึกษา : รองศาสตราจารย์ ดร.จตุพร วิทยาคณ, 91 หน้า.

เอทานอลในฐานะสารมลพิษที่ถูกปล่อยออกมาจากยานพาหนะที่ใช้เอทานอลเป็นเชื้อเพลิง ที่อุณหภูมิต่ำ หรือจากโรงงานอุตสาหกรรมในรูปสารอินทรีย์ระเหยได้ สามารถกำจัดได้โดยปฏิกิริยาออกซิเดชันที่มีตัวเร่งปฏิกิริยา วิทยานิพนธ์นี้ได้ศึกษาการดูดซับและการออกซิเดชันของเอทานอลบนตัวเร่งปฏิกิริยาที่เป็นโลหะเดี่ยวและโลหะคู่ผสม ซึ่งประกอบไปด้วยแพลทินัมในปริมาณร้อยละ 0.5 และออกไซด์ของโลหะที่เป็นเบสในปริมาณร้อยละ 5-15 โดยน้ำหนัก ได้แก่ โคบอลต์ คอปเปอร์ หรือแมงกานีส บนตัวรองรับ RH-MCM-41 ที่สังเคราะห์ด้วยซิลิกาจากแคลบข้าวด้วยเทคนิคไฮโดรเทอร์มัล ตัวเร่งปฏิกิริยาเตรียมด้วยวิธีการทำให้เอิบซุ่ม แล้วนำไปวิเคราะห์สมบัติทางเคมีและทางกายภาพ

RH-MCM-41 มีพื้นที่ผิวสูงถึง 1352 ตารางเมตรต่อกรัม เมื่อเติมด้วยโลหะแล้ว ลักษณะเฉพาะของ RH-MCM-41 ยังคงอยู่ แต่มีพื้นที่ผิวลดลง เพราะโลหะอยู่ที่ผิวหน้า และปิดรูพรุนบางส่วน ของ RH-MCM-41 การศึกษาโดยเทคนิค ethanol-TGA ยืนยันได้ว่าเอทานอลถูกดูดซับบนตัวเร่งปฏิกิริยาทั้งโดยหมู่ไฮดรอกซิลของ RH-MCM-41 บนโลหะ และบนออกไซด์ของโลหะ การตรวจสอบด้วยเทคนิค ethanol-TPD ทำให้ทราบชนิดของแก๊สที่เกิดขึ้นหลังการดูดซับ ทำให้เห็นบทบาทของออกไซด์ที่มีศักยภาพเป็นตัวให้ออกซิเจน สำหรับปฏิกิริยาออกซิเดชันของเอทานอล โดยตัวเร่งปฏิกิริยาโคบอลต์ในรูป  $Co_3O_4$  เป็นแหล่งให้ออกซิเจนที่ดีที่สุดเมื่อเทียบกับออกไซด์อื่นในตัวเร่งปฏิกิริยาทั้งแบบโลหะเดี่ยวและโลหะคู่ผสม เพราะทำให้เกิดคาร์บอนไดออกไซด์ออกมาได้มากที่สุด เมื่อเทียบกับตัวเร่งปฏิกิริยาทั้งหมดที่ศึกษา  $0.5Pt15Co/RH-MCM-41$  แสดงการปล่อยคาร์บอนไดออกไซด์ออกมาได้มากที่สุด ดังนั้นจึงศึกษาปฏิกิริยาออกซิเดชันของเอทานอลด้วยเทคนิค *in situ* FTIR เฉพาะบนตัวเร่งนี้เท่านั้น ข้อมูลที่ได้จากการศึกษาคือชนิดของสารมัธยันตร์และวิถีของปฏิกิริยา เมื่อทำการทดสอบปฏิกิริยาออกซิเดชันของเอทานอลในเครื่องปฏิกรณ์ แบบที่ให้แก๊สไหลผ่านตัวเร่งปฏิกิริยาที่อยู่กับที่ในท่อควอดซ์ พบว่าตัวเร่งปฏิกิริยาโลหะคู่ผสมของแพลทินัมและโคบอลต์ให้การแปลงผันของเอทานอล

ต่ำกว่าตัวเร่งปฏิกิริยาโลหะเดี่ยวแพลทินัม แต่ดูเหมือนจะแสดงเสถียรภาพที่ดีกว่าเพราะผลิตแอลดีไฮด์น้อยกว่า นอกจากนี้ โลหะคู่ผสมของแพลทินัมและโคบอลต์ ให้การแปลงผันของเอทานอลที่อุณหภูมิทำได้สูงกว่าโลหะเดี่ยวโคบอลต์ อาจเป็นเพราะผลของการอยู่ร่วมกันของแพลทินัมและโคบอลต์บนตัวรองรับเดียวกัน



KAMOLWAN RINTRAMEE : ADSORPTION AND OXIDATION OF  
ETHANOL ON BIMETALLIC CATALYSTS CONTAINING PLATINUM  
AND BASE METAL OXIDES SUPPORTED ON RH-MCM-41.

THESIS ADVISOR : ASSOC. PROF. JATUPORN WITTAYAKUN, Ph.D.

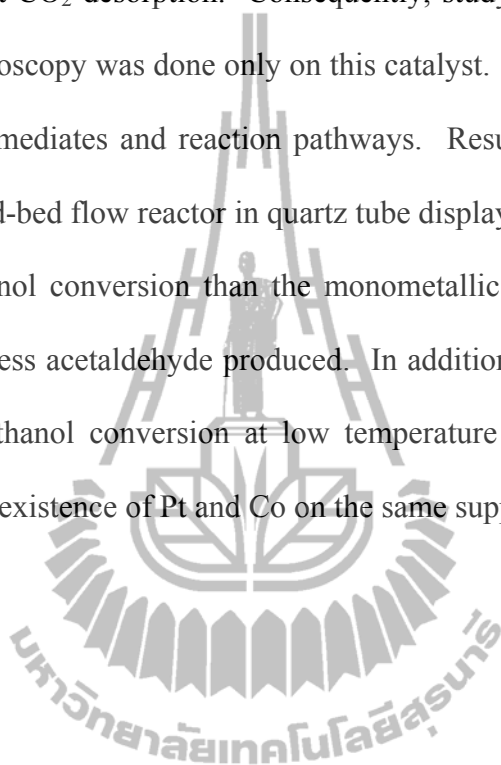
91 PP.

ETHANOL ADSORPTION/ETHANOL OXIDATION/BIMETALLIC  
CATALYST/MCM-41/PLATINUM/COBALT

Ethanol, as a pollutant emitted from ethanol-fueled vehicles at low temperature or released from industries as volatile organic compound (VOC), can be removed by catalytic oxidation. This thesis studied adsorption and oxidation of ethanol on mono- and bimetallic catalysts containing Pt with loading of 0.5 wt% and base metal oxides with loading of 5-15 wt% including Co, Cu, or Mn supported on RH-MCM-41 synthesized with rice husk silica by hydrothermal method. The catalysts were prepared by impregnation method and their chemical and physical properties were analyzed further.

The RH-MCM-41 had high surface area of 1352 m<sup>2</sup>/g. When it was loaded with metal, characteristic of RH-MCM-41 was still maintained but surface area was decreased because metal was on the surface and partially blocked the pores of RH-MCM-41. Studies by ethanol-TGA confirmed that ethanol could be adsorbed on the catalysts on silanol groups of RH-MCM-41, metal and metal oxide. Investigation with ethanol-TPD led to identification of gases produced during the adsorption which indicated the role of oxides as a potential oxygen supplier for ethanol oxidation.

The Co catalyst in the form of  $\text{Co}_3\text{O}_4$  was the best oxygen supplier when compared with other oxides on mono- and bimetallic catalysts because more amount of  $\text{CO}_2$  was produced. Among all studied catalysts, the bimetallic 0.5Pt-15Co/RH-MCM-41 showed the highest  $\text{CO}_2$  desorption. Consequently, study of ethanol oxidation by *in situ* infrared spectroscopy was done only on this catalyst. Information from this study was types of intermediates and reaction pathways. Results from testing on ethanol oxidation in a fixed-bed flow reactor in quartz tube displayed that the bimetallic Pt-Co gave a lower ethanol conversion than the monometallic Pt but seemed to be more stable because of less acetaldehyde produced. In addition, bimetallic Pt-Co catalysts gave the higher ethanol conversion at low temperature than the monometallic Co possibly due to co-existence of Pt and Co on the same support.



School of Chemistry

Student's Signature \_\_\_\_\_

Academic Year 2011

Advisor's Signature \_\_\_\_\_

## ACKNOWLEDGEMENT

I would like to express my gratitude to all those who gave me the possibility to complete this thesis.

This work was supported by a Ph.D. Scholarship from Strategic Scholarships Fellowships Frontier Research Networks of Commission on Higher Education and Suranaree University of Technology (SUT). The equipments for the research were available at Center for Scientific and Technological Equipment (CSTE), SUT, Institute of Material Chemistry at Vienna University of Technology (TU Vienna), Austria and Synchrotron Light Research Institute (SLRI).

I would like to thank my thesis advisor, Assoc. Prof. Dr. Jatuporn Wittayakun, for giving me the chance to study at SUT, his kind support, stimulating suggestions and encouragement throughout my research and thesis writing.

Special thanks were also given to Prof. Dr. Günther Rupprechter, Dr. Karin Föttinger, Dr. Katrin Zorn and all people in Institute of Material Chemistry, TU Vienna for supporting the equipments for characterization and a reactor for catalytic activity study and for their kindness, instruction, advices and assistance during my studies in Vienna.

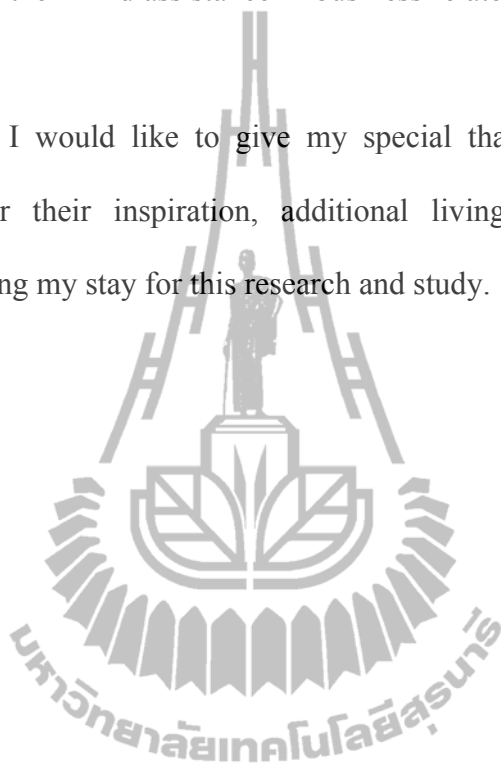
Also, I would like to thank Asst. Prof. Dr. Kunwadee Rangriwatananon, Asst. Prof. Dr. Thanaporn Manyum and Asst. Prof. Dr. Sanchai Prayoonpokarach for their valuable comments and suggestions during my defense and on the thesis itself.



Special thanks to Pongtanawat Khemthong, Jitlada Chumee, Surachai Artkla, Sirinuch Loiha, Supattra Khabuanchalad, Piaw Phatai, Sittichai Kulawong, Nuttinee Supamathanon, Yuttakarn Rattanachai, Oratai Saisa-ard and all of my friends at SUT, for their kind assistance in business related to my studies and work at this university.

Especially, I would like to give my special thank to my parents and my younger sister for their inspiration, additional living allowance, patience and understanding during my stay for this research and study.

Kamolwan Rinramee



# CONTENTS

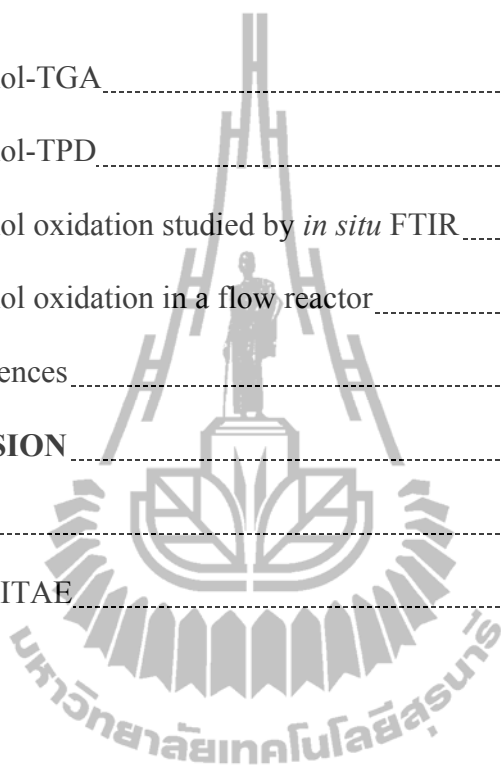
	<b>Page</b>
ABSTRACT IN THAI.....	I
ABSTRACT IN ENGLISH.....	III
ACKNOWLEDGEMENT.....	V
CONTENTS.....	VII
LIST OF TABLES.....	X
LIST OF FIGURES.....	XI
<b>CHAPTER</b>	
<b>I INTRODUCTION.....</b>	<b>1</b>
1.1 Goal of thesis.....	1
1.2 Ethanol pollutant and its oxidation.....	2
1.3 Ethanol adsorption.....	3
1.4 Proposed oxidation mechanism.....	4
1.5 Background of MCM-41.....	5
1.6 Scope and limitation of the study.....	7
1.7 References.....	7
<b>II LITERATURE REVIEW.....</b>	<b>10</b>
2.1 Ethanol oxidation on noble metal catalysts.....	10
2.2 Ethanol oxidation on base metal oxide catalysts.....	12

## CONTENTS (Continued)

	<b>Page</b>
2.3 Combination of noble metal and base metal oxide as catalyst for oxidation.....	13
2.4 Supported catalysts for ethanol oxidation.....	16
2.5 References.....	18
<b>III EXPERIMENTS</b> .....	<b>21</b>
3.1 Chemicals.....	21
3.2 Extraction of rice husk silica.....	21
3.3 RH-MCM-41 synthesis.....	22
3.4 Catalyst preparation.....	22
3.5 Catalyst characterization.....	23
3.6 Ethanol adsorption by thermogravimetric analysis (ethanol-TGA).....	25
3.7 Temperature programmed desorption of ethanol (ethanol-TPD).....	26
3.8 Ethanol oxidation studied by <i>in situ</i> Fourier transform infrared spectroscopy ( <i>in situ</i> FTIR).....	26
3.9 Ethanol oxidation in a fixed-bed flow reactor.....	27
3.10 References.....	28
<b>IV RESULTS AND DISCUSSION</b> .....	<b>30</b>
4.1 Catalyst characterization by ICP-MS.....	30
4.2 N <sub>2</sub> adsorption-desorption and TEM.....	31
4.3 Catalyst characterization by XRD and XANES.....	41

**CONTENTS (Continued)**

	<b>Page</b>
4.4 Ethanol-TGA.....	54
4.5 Ethanol-TPD.....	57
4.6 Ethanol oxidation studied by <i>in situ</i> FTIR.....	65
4.7 Ethanol oxidation in a flow reactor.....	76
4.8 References.....	81
<b>V CONCLUSION</b> .....	<b>85</b>
APPENDIX.....	87
CURRICULUM VITAE.....	91



## LIST OF TABLES

<b>Table</b>	<b>Page</b>
2.1 Conditions for ethanol oxidation on various catalysts and testing results.....	14
4.1 Metal contents in the studied catalysts.....	30
4.2 BET surface area, average pore size, and total pore volume of RH-MCM-41 and catalysts.....	33
4.3 $2\theta$ , $d_{100}$ , and $a_0$ values of RH-MCM-41 and catalysts.....	45
4.4 Edge energy, edge shift, and oxide components in catalysts.....	54
4.5 Change of catalysts weight from ethanol adsorption from ethanol-TGA.....	55
4.6 Band assignments and vibration modes during ethanol oxidation on 0.5Pt/RH-MCM-41 and 0.5Pt15Co/RH-MCM-41.....	68

## LIST OF FIGURES

<b>Figure</b>	<b>Page</b>
1.1 Proposed mechanism of ethanol chemisorption on Pt (modified from Nagai and Gonzalez, 1985).....	4
1.2 Proposed role of base metal oxide as oxygen storage and its regeneration by oxidation.....	5
4.1 Nitrogen adsorption-desorption isotherm of RH-MCM-41 (A) and 0.5Pt/RH-MCM-41 (B)); filled: adsorption and open: desorption.....	32
4.2 TEM images of RH-MCM-41 viewed along (A) and perpendicular to (B) the axis of the hexagonally arranged mesopores.....	35
4.3 Nitrogen adsorption-desorption isotherm of RH-MCM-41 supported mono- and bimetallic Co catalysts; filled: adsorption and open: desorption.....	36
4.4 Nitrogen adsorption-desorption isotherm of RH-MCM-41 supported mono- and bimetallic Cu catalysts; filled: adsorption and open: desorption.....	37
4.5 Nitrogen adsorption-desorption isotherm of RH-MCM-41 supported mono- and bimetallic Mn catalysts; filled: adsorption and open: desorption.....	37
4.6 TEM images of 15Co/RH-MCM-41.....	39
4.7 TEM images of 0.5Pt-15Co/RH-MCM-41.....	40

## LIST OF FIGURES (Continued)

<b>Figure</b>	<b>Page</b>
4.8 XRD powder pattern of RH-MCM-41.....	42
4.9 XRD powder patterns at low angle of mono- and bimetallic Co catalysts.....	43
4.10 XRD powder patterns at low angle of mono- and bimetallic Cu catalysts.....	43
4.11 XRD powder patterns at low angle of mono- and bimetallic Mn catalysts.....	44
4.12 XRD powder patterns at high angle of mono- and bimetallic Co catalysts.....	46
4.13 XRD powder patterns at high angle of mono- and bimetallic Cu catalysts.....	47
4.14 XRD powder patterns at high angle of mono- and bimetallic Mn catalysts.....	47
4.15 XRD powder pattern of 0.5Pt/RH-MCM-41.....	48
4.16 TEM images of 0.5Pt/RH-MCM-41.....	49
4.17 The XANES spectra of Co reference materials (A) and 15Co/RH-MCM-41 and 0.5Pt15Co/RH-MCM-41 catalysts compared with Co <sub>3</sub> O <sub>4</sub> standard (B).....	51

## LIST OF FIGURES (Continued)

Figure	Page
4.18 The XANES spectra of Cu reference materials (A) and 15Cu/RH-MCM-41 and 0.5Pt15Cu/RH-MCM-41 catalysts compared with CuO standard (B).....	52
4.19 The XANES spectra of Mn reference materials (A) and 15Mn/RH-MCM-41 and 0.5Pt15Mn/RH-MCM-41 catalysts compared with MnO <sub>2</sub> standard (B).....	53
4.20 Ethanol-TPD profiles on RH-MCM-41.....	59
4.21 Ethanol-TPD profiles on 0.5Pt/RH-MCM-41.....	60
4.22 Ethanol-TPD profiles on 15Co/RH-MCM-41 (A), 15Cu/RH-MCM-41 (B), and 15Mn/RH-MCM-41 (C).....	62
4.23 Ethanol-TPD profiles on 0.5Pt-15Cu/RH-MCM-41 (A) and 0.5Pt-15Mn/RH-MCM-41 (B).....	63
4.24 Ethanol-TPD profiles on 0.5Pt-15Co/RH-MCM-41.....	64
4.25 <i>in situ</i> IR spectra measured on 0.5Pt/RH-MCM-41 (A) and 0.5Pt-15Co/RH-MCM-41 (B) during ethanol oxidation. Spectrum of both samples were recorded at (a) 30 °C (under vacuum), (b)-(g) at 30, 100, 150, 200, 250, and 300 °C (under a flow of ethanol and air).....	66

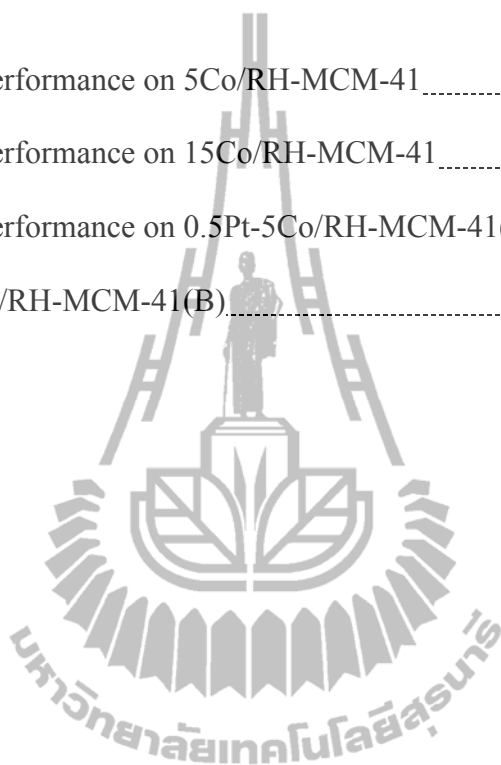


## LIST OF FIGURES (Continued)

<b>Figure</b>	<b>Page</b>
4.26 <i>In situ</i> IR spectra measured on 0.5Pt/RH-MCM-41 (red line) and 0.5Pt-15Co/RH-MCM-41 (black line) during ethanol oxidation at 30 °C .....	71
4.27 <i>In situ</i> IR spectra measured on 0.5Pt/RH-MCM-41 (red line) and 0.5Pt-15Co/RH-MCM-41 (black line) during ethanol oxidation at 100 °C .....	72
4.28 <i>In situ</i> IR spectra measured on 0.5Pt/RH-MCM-41 (red line) and 0.5Pt-15Co/RH-MCM-41 (black line) during ethanol oxidation at 150 °C .....	72
4.29 <i>In situ</i> IR spectra measured on 0.5Pt/RH-MCM-41 (red line) and 0.5Pt-15Co/RH-MCM-41 (black line) during ethanol oxidation at 200 °C .....	73
4.30 <i>In situ</i> IR spectra measured on 0.5Pt/RH-MCM-41 (red line) and 0.5Pt-15Co/RH-MCM-41 (black line) during ethanol oxidation at 250 °C .....	73
4.31 <i>In situ</i> IR spectra measured on 0.5Pt/RH-MCM-41 (red line) and 0.5Pt-15Co/RH-MCM-41 (black line) during ethanol oxidation at 300 °C .....	74
4.32 Catalytic performance on RH-MCM-41 .....	76
4.33 Catalytic performance on 0.5Pt/RH-MCM-41 .....	77

**LIST OF FIGURES (Continued)**

<b>Figure</b>		<b>Page</b>
4.34	Catalytic performance on 5Co/RH-MCM-41.....	78
4.35	Catalytic performance on 15Co/RH-MCM-41.....	79
4.36	Catalytic performance on 0.5Pt-5Co/RH-MCM-41(A) and 0.5Pt-15Co/RH-MCM-41(B).....	80



# CHAPTER I

## INTRODUCTION

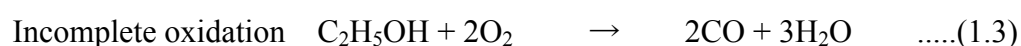
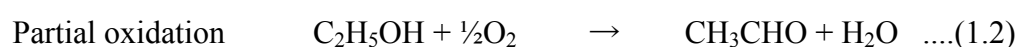
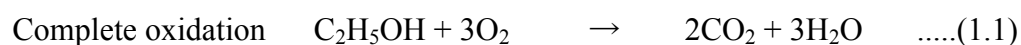
### 1.1 Goal of thesis

The goal of this work was to study adsorption and oxidation of ethanol on mono- and bimetallic catalysts supported on MCM-41 synthesized by using rice husk silica (referred to as RH-MCM-41) including Pt (0.5 wt%) and oxides of Co, Cu, and Mn (5-15 wt%). The catalysts were prepared by impregnation method and their chemical and physical properties were investigated by several techniques including X-ray diffraction (XRD), X-ray absorption near edge structure (XANES), inductively coupled plasma-mass spectroscopy (ICP-MS), nitrogen adsorption-desorption, and transmission electron microscopy (TEM). Adsorption of ethanol on these catalysts was studied by thermogravimetric analysis (ethanol-TGA) to determine the adsorption ability. Temperature programmed desorption of ethanol (ethanol-TPD) in the absence of air was investigated to determine the role of oxides as oxygen supplier for surface oxidation. The oxide with highest oxygen involvement was further studied for ethanol oxidation by air using *in situ* Fourier transform infrared spectroscopy (*in situ* FTIR) to identify the reaction intermediates which could lead to an understanding of the reaction mechanism. Finally, the ethanol oxidation by air was studied using a fixed-bed flow reactor connected to a gas chromatograph (GC) to determine the catalytic performance at various temperatures.

## 1.2 Ethanol pollutant and its oxidation

Ethanol (C<sub>2</sub>H<sub>5</sub>OH) has been used as an additive or substitute to gasoline to improve octane number and to reduce an emission of carbon monoxide (CO) from automotive exhaust. However, ethanol can be classified as a pollutant when it is emitted from low-efficient ethanol-fueled vehicles or during cold-start operation of vehicles. Moreover, an incomplete combustion of ethanol can generate other toxic compounds such as CO and acetaldehyde (CH<sub>3</sub>CHO). These pollutants are considered to be harmful to human health and recognized as contributors to pollution and photochemical formation of smog (Trawczyński, Bielak, and Miśta, 2005). In another aspect, ethanol can be thought of as a volatile organic compound (VOC). It has been used widely in manufacture of many products, such as chemical and textile industries, manufacture of electronic components, paints and printing (Bastos, Órfão, Freitas, Pereira, and Figueiredo, 2009).

An effective method to remove ethanol is catalytic oxidation which can be operated at low temperature. In general, the products from the ethanol oxidation depend on the amount of oxygen (Rajesh and Ozkan, 1993). In excess of oxygen, only a complete oxidation (Equation 1.1) is expected but it also depends on catalyst and reaction conditions. Both partial and incomplete oxidation (Equation 1.2 and 1.3) should be minimized because they produce acetaldehyde and CO, respectively.



### 1.3 Ethanol adsorption

Study of ethanol adsorption on catalysts at conditions similar to the testing conditions can provide understanding on the mechanism of ethanol oxidation and the role of the metal catalysts. The ethanol adsorption study could be used as a screening test to find suitable catalysts for ethanol oxidation. For example, Yee, Morrison, and Idriss (2000) studied intermediates and products of ethanol oxidation on reduced and unreduced  $\text{CeO}_2$  and Pd supported on  $\text{CeO}_2$  ( $\text{Pd/CeO}_2$ ) by Fourier transform infrared spectroscopy (FTIR) and temperature programmed desorption (TPD). They reported an increase in dehydrogenation of ethanol to acetaldehyde in the presence of Pd. Sanchez-Sanchez, Yerga, Kondarides, Verykios, and Fierro (2010) investigated adsorbed species and products on Pt, Ni and PtNi catalysts supported on alumina ( $\text{Al}_2\text{O}_3$ ) with combined analysis of ethanol-TPD and diffuse reflectance infrared Fourier transform spectroscopy (DRIFTS) spectra. The gas products from the PtNi bimetallic catalyst showed the lowest desorption temperature suggesting that the activity in the C-C bond rupture was higher than that of monometallic counterparts.

Wu and Kawi (2009) found that high surface area of catalyst support showed significant effects on the catalytic performance. A high surface area catalyst support is generally used to disperse metallic particles, which would make the catalyst not only active but also stable due to the low coke formation on highly dispersed metallic particles. Consequently, MCM-41, which has a mesoporous structure with high surface area, was chosen in this study as the catalyst support for active Pt metal particle. MCM-41 may prevent sintering of Pt at high temperature.

## 1.4 Proposed oxidation mechanism

Nagai and Gonzalez (1985) studied reaction intermediates on the catalyst surface during the oxidation of ethanol on Pt/SiO<sub>2</sub> at 100 °C by *in situ* FTIR. They proposed mechanism of ethanol chemisorption on Pt which produced various surface species and could be dissociated further or react with surface oxygen to produce CO<sub>2</sub> and H<sub>2</sub>O (Figure 1.1). Although some surface species could react with each other to form undesired products, the modification with metal oxides as oxygen storage is expected to minimize the by-products. The regeneration of the base metal oxide can be done by a reaction with oxygen in the reactant stream as shown in Figure 1.2.

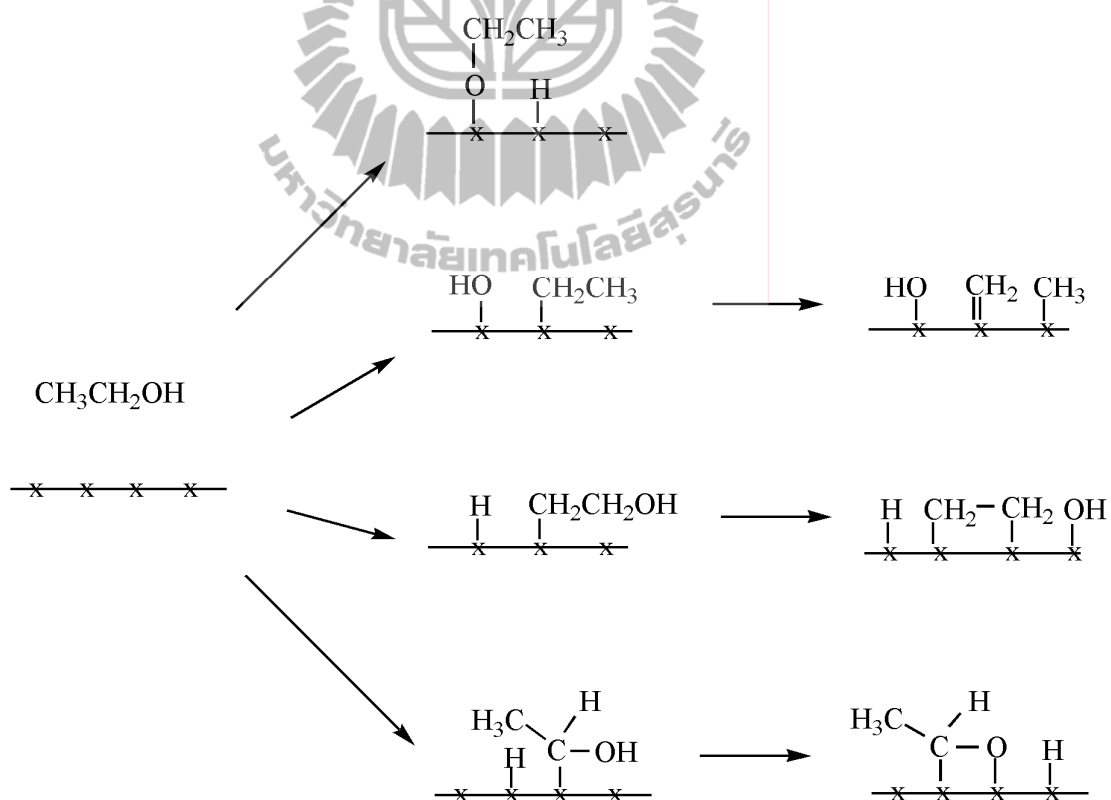


**Figure 1.1** Proposed mechanism of ethanol chemisorption on Pt (modified from Nagai and Gonzalez, 1985).

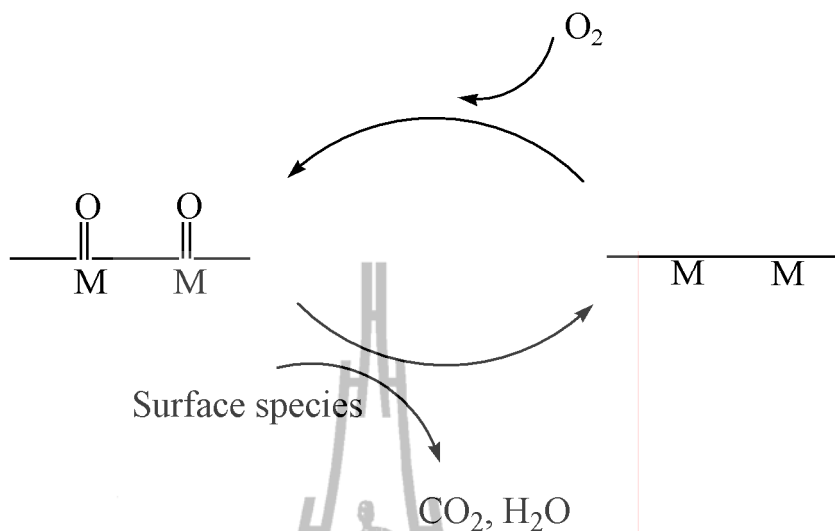


**Figure 1.2** Proposed role of base metal oxide as oxygen storage and its regeneration by oxidation.

## 1.5 Background of MCM-41

MCM-41 is a mesoporous molecular sieve consisting of hexagonal arranged cylindrical uniform channels. It has high surface area, narrow pore size distribution, and thermal stability (Kumar *et al.*, 2004).

### 1.5.1 MCM-41 synthesis

The formation of the MCM-41 phase occurs according to the liquid crystal template (LCT) mechanism in which tetrahedral  $\text{SiO}_4$  species bonded with micelles of surfactant template and further condensed to form the hexagonal array of channels under hydrothermal conditions (Beck *et al.*, 1992). Edler and White (1997) studied MCM-41 preparation under various conditions such as acid-treated, pH values during synthesis. They found that the most suitable acid to adjust pH was sulfuric acid which improved long range order of MCM-41 and the material prepared at pH around 11 had large crystallite sizes.

Chemicals in a typical preparation of MCM-41 include solvent, template (surfactant molecule), and silica source. Various silica sources could be used in the synthesis including sodium silicate, fumed silica, tetraethyl orthosilicate (TEOS), and rice husk silica. Rice husk silica is good choice because rice husk is a by-product of rice milling and could be considered as an agricultural waste. Purity of the rice husk silica could be greater than 98 wt% when extracted by acid leaching and calcination (Chumee, Grisdanurak, Neramittagapong, and Wittayakun, 2009). Chiarakorn, Areerob, and Grisdanurak (2007) compared MCM-41 from rice husk silica (RH-MCM-41) and that from commercial silica source and found that they had similar porosity. The average pore diameters were in a range of 20-30 Å.

### 1.5.2 Application of MCM-41

MCM-41 could be applied as an adsorbent of pollutant. Lee *et al.* (2007) and Yang, Guan, and Li (2011) studied potential of MCM-41 for the removal of dyes and aniline from wastewater, respectively. The effect of nanometer pore sizes of MCM-41 could separate large molecules from aqueous solution.

MCM-41 can be used as a catalyst support because its high surface area can improve a dispersion of active metal resulting in better performance. For instance, when Cu-Mn was deposited on MCM-41 support, the catalytic activity of toluene oxidation was improved more than that on  $\beta$ -zeolite and  $\text{SiO}_2$  support because high dispersion of Cu-Mn was obtained on the support with high surface area (Li, Zhuang, Xiao, and Green, 2006). In general,  $\text{Al}_2\text{O}_3$  is widely used as a support for ethanol oxidation; however, it causes undesired by-products as a result of its acidity. On the other hand, MCM-41 has mild acidic property due to the presence of Si-OH groups leading to concentration of acid sites about  $0.79 \text{ mmol g}^{-1}$  (Jentys, Kleestorfer, and



Vinek, 1999). Consequently, the MCM-41 may serve as a good choice of support for ethanol oxidation because it is less acidic than  $\text{Al}_2\text{O}_3$ .

## 1.6 Scope and limitation of the study

MCM-41 was synthesized with rice husk silica under hydrothermal method from a method in literature (Chumee *et al.*, 2009). Catalysts containing Pt and base metal oxides (Co, Cu, or Mn) were prepared by sequential impregnation, i.e., impregnation of metal oxide precursor followed by Pt precursor. The Pt loading on the catalysts was fixed at 0.5 wt% and the base metal oxide loading was varied from 5 to 15 wt%. Ethanol adsorption on catalyst could determine ability of ethanol oxidation and role of metal on catalyst by using ethanol-TGA and ethanol-TPD. The study of mechanism and intermediates of ethanol oxidation was investigated by *in situ* FTIR spectroscopy. The catalytic testing on ethanol oxidation was studied in a fixed-bed flow reactor at 100-400 °C. The reactants and products from the reactions were analyzed by an on-line GC.

## 1.7 References

- Bastos, S. S. T., Órfão, J. J. M., Freitas, M. M. A., Pereira, M. F. R., and Figueiredo, J. L. (2009). Manganese oxide catalysts synthesized by exotemplating for the total oxidation of ethanol. **Appl. Catal. B: Environ.** 93: 30-37.
- Beck, J. S., Vartuli, J. C., Roth, W. J., Leonowicz, M. E., Kresge, C. T., Schmitt, K. D., Chu, C. T. W., Olson, D. H., and Sheppard, E. W. (1992). A new family of mesoporous molecular sieves prepared with liquid crystal templates. **J. Am. Chem. Soc.** 114: 10834-10843.

- Chiarakorn, S., Areerob, T., and Grisdanurak, N. (2007) Influence of functional silanes on hydrophobicity of MCM-41 synthesized from rice husk. **Sci. Technol. Adv. Mat.** 8: 110-115.
- Chumee, J., Grisdanurak, N., Neramittagapong, A., and Wittayakun, J. (2009). Characterization of platinum–iron catalysts supported on MCM-41 synthesized with rice husk silica and their performance for phenol hydroxylation. **Sci. Technol. Adv. Mater.** 10: 1-6.
- Edler, K. J., and White, J. W. (1997). Further improvements in the long-range order of MCM-41 materials. **Chem. Mater.** 9: 1226-1233.
- Jentys, A., Kleestorfer, K., and Vinek, H. (1999). Concentration of surface hydroxyl groups on MCM-41. **Micropor. Mesopor. Mat.** 27: 321-328.
- Kumar, N., Mäki-Arvela, P., Hajek, J., Salmi, T., Murzin, D. Y., Heikkilä, T., Laine, E., Laukkanen, P., and Väyrynen, J. (2004). Physico-chemical and catalytic properties of Ru–MCM-41 mesoporous molecular sieve catalyst: influence of Ru modification methods. **Micropor. Mesopor. Mat.** 69: 173-179.
- Lee, C. K., Liu, S. S., Juang, L. C., Wang, C. C., Lin, K. S., and Lyu, M. D. (2007). Application of MCM-41 for dyes removal from wastewater. **J. Hazard. Mater.** 147: 997-1005.
- Li, W. B., Zhuang, M., Xiao, T. C., and Green, M. L. H. (2006). MCM-41 supported Cu–Mn catalysts for catalytic oxidation of toluene at low temperatures. **J. Phys. Chem. B.** 110: 21568-21571.
- Nagai, M., and Gonzalez, R. D. (1985). Oxidation of ethanol and acetaldehyde on silica-supported platinum catalysts: preparative and pretreatment effects on catalyst selectivity. **Ind. Eng. Chem. Prod. Res. Dev.** 24: 525-531.

- Rajesh, H., and Ozkan, U. S. (1993). Complete oxidation of ethanol, acetaldehyde, and ethanol/methanol mixtures over copper oxide and copper-chromium oxide catalysts. **Ind. Eng. Chem. Res.** 32: 1622-1630.
- Sanchez-Sanchez, M. C., Yerga, R. M., Kondarides, D. I., Verykios, X. E., and Fierro, J. L. G. (2009). Mechanistic aspects of the ethanol steam reforming reaction for hydrogen production on Pt, Ni and PtNi catalysts supported on  $\gamma$ -Al<sub>2</sub>O<sub>3</sub>. **J. Phys. Chem. A.** 114: 3873-3882.
- Trawczyński, J., Bielak, B., and Miśta, W. (2005). Oxidation of ethanol over supported manganese catalysts-effect of the carrier. **Appl. Catal. B: Environ.** 55: 277-285.
- Wu, X., and Kawi, S. (2009). Rh/Ce-SBA-15: active and stable catalyst for CO<sub>2</sub> reforming of ethanol to hydrogen. **Catal. Today.** 148: 251-259.
- Yang, X., Guan, Q., and Li, W. (2011). Effect of template in MCM-41 on the adsorption of aniline from aqueous solution. **J. Environ. Manage.** 92: 2939-2943.
- Yee, A., Morrison, S. J., and Idriss, H. (2000). A study of ethanol reactions over Pt/CeO<sub>2</sub> by temperature-programmed desorption and *in situ* FT-IR spectroscopy: evidence of benzene formation. **J. Catal.** 191: 30-45.

## CHAPTER II

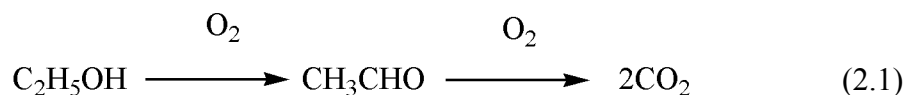
### LITERATURE REVIEW

Ethanol is a renewable fuel that can be used as an additive or substitute of gasoline with the advantage of octane enhancement and CO decrease from exhaust emissions. On the other hand, unburned ethanol is considered as a pollutant when it is emitted as an exhaust gas from ethanol-fueled vehicles or as VOC from manufacture relating to chemicals or electronic components. Because unburned ethanol could further produce toxic gases such as acetaldehyde and CO, researchers have been interested to study elimination of the unburned ethanol. One effective method is catalytic oxidation, which can proceed at low temperature.

#### 2.1 Ethanol oxidation on noble metal catalysts

Noble metals such as Pt, Pd, and Rh are good catalysts for ethanol oxidation. Yao (1984) studied ethanol oxidation on various metal-containing catalysts and found that Pt/Al<sub>2</sub>O<sub>3</sub> and Pd/Al<sub>2</sub>O<sub>3</sub> were effective because they produced CO<sub>2</sub> as a major product with less acetaldehyde than base metal oxide catalysts. In addition, reaction temperature of Pt/Al<sub>2</sub>O<sub>3</sub> was lower than that of base metal oxide catalysts. McCabe and Mitchell (1983) studied mechanism of ethanol oxidation on catalysts containing Cu or Pt by varying the space velocity through a reactor. From selectivity data, ethanol oxidation proceeded almost exclusively by a combined series-direct reaction

mechanism (Reaction 2.1 and 2.2) over Pt catalyst whereas Cu oxide catalyst exhibited only series reaction mechanism (Reaction 2.1).



Petkovic, Rashkeev, and Ginosar (2009) studied the role of Pt-containing catalysts by a combination of first-principles density-functional theory (DFT) based calculations and *in situ* diffuse reflectance infrared spectroscopy (DRIFTS). They suggested that the surface of Pt nanoparticles were the active sites that could trap and accumulate oxygen for ethanol oxidation. However, the noble metal catalysts could be easily poisoned by undesired reaction intermediates such as surface ethyl from ethanol dehydration which leads to deactivation by coking (Chen *et al.*, 2010). Several reactions responsible for coke formation were proposed in the following equations.



They studied the deactivation of Rh/Ca-Al<sub>2</sub>O<sub>3</sub> catalyst that deactivated after 7.5 h, accompanied by obvious increments in the CH<sub>3</sub>CHO and CO selectivity. In the case of CO oxidation over Pt/SiO<sub>2</sub>, the activity of Pt could be inhibited by strong

adsorption of CO but the problem could be solved by adding metal oxides to serve as oxygen sources for the surface reaction (Mergler, van Aalst, van Delft, and Nieuwenhuys, 1996).

## 2.2 Ethanol oxidation on base metal oxide catalysts

Deactivation of noble metal catalysts could be improved by substitute them with base metal oxide catalysts, due to their higher resistance to poisoning and lower price. Base metal oxides are used informally to refer to a metal that is oxidized easily so the metal could be quickly regenerated to active oxide form. Examples include Fe, Ni, Co, Mn, and Cu. It was reported that, CuO-MnO<sub>2</sub> catalyst was only slightly less active than Pt/Al<sub>2</sub>O<sub>3</sub> catalyst for the same volume in the combustion of ethanol (McCabe and Mitchell, 1984). Cu/Al<sub>2</sub>O<sub>3</sub> was reported to be active for oxidation of ethanol and acetaldehyde (Rajesh and Ozkan, 1993). The activity varied with Cu loading and the complete oxidation was the major reaction. The CO<sub>2</sub> yield could be improved by mixing Cu with Cr to create a synergy between two metal oxides by providing different sites in close proximity of each other. Those sites would activate the ethanol molecule through an initial dehydration step before a further reaction with oxides to complete oxidation.

Mn oxides were among the most efficient transition-metal compounds in catalytic combustion and they were considered to be environment-friendly materials (Morales, Barbero, and Cadús, 2006). Oxides of Mn were active for ethanol oxidation and the catalytic performance depended on oxidation state of Mn and amount of the lattice oxygen (Bastos, Órfão, Freitas, Pereira, and Figueiredo, 2009). Lamaita, Peluso, Sambeth, and Thomas (2005) reported that the activity of Mn could

be related to both of their oxidation states ( $\text{Mn}^{3+}$  and  $\text{Mn}^{4+}$ ) and the presence of  $\text{Mn}^{4+}$  vacancies. Beside, adsorption of ethanol on Mn oxide catalyst generated ethoxy species which transformed to carboxylate, acetaldehyde, and  $\text{CO}_2$  that were confirmed by *in situ* DRIFT spectroscopy. The catalytic activity of supported manganese oxides was higher than the un-supported one. The activity also depended on support type which caused variation in manganese reducibility and mobile oxygen species (Trawczyński, Bielak, and Mišta, 2005).

Cobalt oxides could act as catalysts for total oxidation reactions because they can be quickly regenerated to oxide form (Pope, Walker, and Moss, 1976). This effect is important to facilitate complete oxidation of ethanol and maintain catalyst stability. Song and Ozkan (2009) studied ethanol adsorption over  $\text{Co/CeO}_2$  by *in situ* DRIFTS and found that the vibration peaks characteristic for acetate species were present at room temperature. When increasing temperature, acetate species transformed to other species and disappeared at  $400^\circ\text{C}$ . This result indicated that the oxidation of surface species was facilitated by ceria. This observation was consistent with the resistance to coking seen over the Co catalysts.

As a single component, base metal oxide catalyst cannot rival a noble metal oxide catalyst. Hence, improvement in their activities has been attempted by combining base metal oxide and small amount of noble metal.

### **2.3 Combination of noble metal and base metal oxide as catalyst for oxidation**

Many researchers have studied a catalyst mixture between a small amount of noble metal and base metal oxide to improve catalytic activity and properties of both

components because they compensate each other's drawback. The role of metal oxides is to diminish the CO inhibition which is typical for Pt catalysts at low temperatures (Mergler *et al.*, 1996). For example, the addition of oxides of Co, Mn, and Ce to Pt/SiO<sub>2</sub> could promote the CO oxidation because the metal oxides serve as oxygen source for the surface reaction (Chen *et al.*, 2010). On the other hand, Pt helps metal oxides with multi-oxidation states to accelerate the oxygen transfer from gas phase to the catalyst (Ménézo, Rivière, and Barbier, 1993). In the elimination of CO and NO by oxidation, the temperature for Pd-Cu/CeO<sub>2</sub>-Al<sub>2</sub>O<sub>3</sub> catalyst in reaching 50% conversion, T<sub>50</sub>, of CO was 50 °C lower than that for Pd/CeO<sub>2</sub>-Al<sub>2</sub>O<sub>3</sub> catalyst (Fernandez-Garcia *et al.*, 2000). The role of Cu was to stabilize the zero-valence Pd.

Table 2.1 demonstrates conditions of ethanol oxidation for various catalysts and the testing results. The T<sub>x%</sub> is the temperature that gives x % ethanol conversion and the T<sub>Yx</sub> is the temperature at which x % CO<sub>2</sub> yield is obtained.

**Table 2.1** Conditions for ethanol oxidation on various catalysts and testing results.

Catalysts	Conditions	Conversion	Comment	Reference
0.1 wt% Pt/Al <sub>2</sub> O <sub>3</sub>	0.1 V% C <sub>2</sub> H <sub>5</sub> OH: 1 V% O <sub>2</sub> in N <sub>2</sub> (1000 ppm ethanol)	T <sub>90%</sub> ~145 °C T <sub>Y90</sub> ~227 °C	Pt/Al <sub>2</sub> O <sub>3</sub> reduces unburned fuel during engine cold-starting.	McCabe and Mitchell, 1984
0.3 wt% Pt/Al <sub>2</sub> O <sub>3</sub> (K/Al = 0.1)	500 ppm ethanol in air	T <sub>100%</sub> ~210 °C T <sub>Y100</sub> ~196 °C	K was added to Al <sub>2</sub> O <sub>3</sub> to minimize undesired products.	Avgouropoulos, Oikonomopoulos, Kanistras, and Ioannides, 2006



**Table 2.1** (Continued).

Catalysts	Conditions	Conversion	Comment	Reference
Commercial hopcalite (CuO-MnO <sub>2</sub> )	0.1 V% C <sub>2</sub> H <sub>5</sub> OH: 1 V% O <sub>2</sub> in N <sub>2</sub>	T <sub>90%</sub> ~148 °C T <sub>Y90</sub> ~230 °C	Hopcalite catalyst had similar activity to Pt/Al <sub>2</sub> O <sub>3</sub> .	McCabe and Mitchell, 1984
Mn <sub>9</sub> CuO	C <sub>2</sub> H <sub>5</sub> OH:O <sub>2</sub> :H <sub>2</sub> = 1:20.8:78.2 (100 mL min <sup>-1</sup> )	T <sub>100%</sub> ~192 °C T <sub>Y100</sub> ~208 °C	Poor crystalline of Mn are the best performance in ethanol combustion to CO <sub>2</sub> .	Morales, Barbero, and Cadús, 2008
Cu/Al <sub>2</sub> O <sub>3</sub>	0.35 V% C <sub>2</sub> H <sub>5</sub> OH: 3.83 V% O <sub>2</sub> : 95.82 V% N <sub>2</sub>	T <sub>95%</sub> ~250 °C T <sub>Y95</sub> ~250 °C	Cu favored complete ethanol oxidation.	Rajesh and Ozkan, 1993
Cr/Al <sub>2</sub> O <sub>3</sub>	0.35 V% C <sub>2</sub> H <sub>5</sub> OH: 3.83 V% O <sub>2</sub> : 95.82 V% N <sub>2</sub>	T <sub>95%</sub> ~250 °C T <sub>Y50</sub> ~250 °C	Cr favored dehydrogenation or partial oxidation.	Rajesh and Ozkan, 1993

**Table 2.1** (Continued).

Catalysts	Conditions	Conversion	Comment	Reference
0.5 wt% Pd- 1 wt% Cu /CeO <sub>2</sub> -Al <sub>2</sub> O <sub>3</sub>	1 V% CO: 0.1 V% NO: 0.45 V% O <sub>2</sub> in N <sub>2</sub>	T <sub>98%</sub> ~174 °C	Cu improved activity by enhancing the rate of CO oxidation.	Fernandez-Garcia <i>et al.</i> , 2000
0.5 wt% Pd /Co <sub>3</sub> O <sub>4</sub> -CeO <sub>2</sub>	1 V% CO: 5 V% O <sub>2</sub> in N <sub>2</sub>	T <sub>Y100</sub> ~90 °C	A synergy effect between Pd and Co <sub>3</sub> O <sub>4</sub> -CeO <sub>2</sub> was responsible for the activity enhancement.	Luo <i>et al.</i> , 2008

From Table 2.1, a number of catalysts were tested and the activity of noble metal combined with metal oxide merited attention as catalysts for total oxidation. Ferrandon (2001) reported the improving of catalytic activity for the oxidation reaction by modification of Pt catalyst with Co, Cu, and Mn.

## 2.4 Supported catalysts for ethanol oxidation

The selectivity of ethanol oxidation depends on various conditions and acid-basic properties of catalysts. McCabe and Mitchell (1984) studied catalyst behavior for the reactions of ethanol including oxidation to acetaldehyde (CH<sub>3</sub>CHO) and CO<sub>2</sub> and dehydration to diethyl ether (C<sub>2</sub>H<sub>5</sub>)<sub>2</sub>O (Reaction 2.6) and ethylene (C<sub>2</sub>H<sub>4</sub>)

(Reaction 2.7). The oxidation was favorable on catalysts with strong base character whereas dehydration was favorable on catalysts with strong acid character.



Effect of kind of carrier on activity and selectivity in the ethanol oxidation was investigated. Trawczyński *et al.* (2005) studied  $\text{MnO}_x$  catalysts supported on  $\text{Al}_2\text{O}_3$ ,  $\text{TiO}_2$ , or yttria-stabilized zirconia (YSZ) in ethanol oxidation. They found that dehydration of ethanol (to diethyl ether and/or ethylene) was catalyzed by acid sites. The total acidity of investigated carriers increases in the following order:  $\text{TiO}_2 < \text{YSZ} < \text{Al}_2\text{O}_3$ . Relatively large amounts of diethyl ether were found in the products of reaction carried out over  $\text{Al}_2\text{O}_3$  and YSZ whereas only negligible amounts of this compound were detected in the reaction products over  $\text{TiO}_2$ .

To prevent ethanol dehydration, MCM-41 may serve as a better choice of support for ethanol oxidation because it has weaker acidity than  $\text{Al}_2\text{O}_3$ . When metals are deposited on a support with high surface area, the catalytic performance could be improved because of an improvement in metal dispersion. In this work, mesoporous MCM-41 type structure was chosen as a catalyst support because of its uniform pore system and high surface area (Beck *et al.*, 1992; Selvam, Bhatia, and Sonwane, 2001). In addition, the interconnectivity of the mesopores and the uniformity of the channel dimensions had an influence on the catalytic activity. Tsoncheva, Ivanova, Rosenholm, and Linden (2009) studied ethyl acetate oxidation on Co supported on

SBA-15 (same structure as MCM-41 with larger pore size), KIT-5 (interconnected cage-like mesoporous silica), and KIT-6 (two interpenetrating branched networks of cylindrical pores) and found that Co/SBA-15 exhibited better catalytic activity than that Co/KIT-6 and Co/KIT-5. This was because more open pore structure of SBA-15 could facilitate the catalytic process due to enhanced mass-transfer.

## 2.5 References

- Avgouropoulos, G., Oikonomopoulos, E., Kanistras, D., and Ioannides, T. (2006). Complete oxidation of ethanol over alkali-promoted Pt/Al<sub>2</sub>O<sub>3</sub> catalysts. **Appl. Catal. B: Environ.** 65: 62-69.
- Bastos, S. S. T., Órfão, J. J. M., Freitas, M. M. A., Pereira, M. F. R., and Figueiredo, J. L. (2009). Manganese oxide catalysts synthesized by exotemplating for the total oxidation of ethanol. **Appl. Catal. B: Environ.** 93: 30-37.
- Beck, J. S., Vartuli, J. C., Roth, W. J., Leonowicz, M. E., Kresge, C. T., Schmitt, K. D., Chu, C. T. W., Olson, D. H., and Sheppard, E. W. (1992). A new family of mesoporous molecular sieves prepared with liquid crystal templates. **J. Am. Chem. Soc.** 114: 10834-10843.
- Chen, L., Choong, C. K. S., Zhong, Z., Huang, L., Ang, T. P., Hong, L., and Lin, J. (2010). Carbon monoxide-free hydrogen production via low-temperature steam reforming of ethanol over iron-promoted Rh catalyst. **J. Catal.** 276: 197-200.
- Fernandez-Garcia, M., Martinez-Arias, A., Belver, C., Anderson, J. A., Conesa, J. C., and Soria, J. (2000). Behavior of palladium-copper catalysts for CO and NO elimination. **J. Catal.** 190: 387-395.

- Ferrandon, M. (2001). **Mixed metal catalysts for total oxidation of volatile organic compounds and carbon monoxide.** Ph.D. thesis, Royal Institute of Technology, Stockholm, Sweden.
- Lamaita, L., Peluso, M. A., Sambeth, J. E., and Thomas, H. J. (2005). Synthesis and characterization of manganese oxides employed in VOCs abatement. **Appl. Catal. B: Environ.** 61: 114-119.
- Luo, J. Y., Meng, M., Li, X., Li, X. G., Zha, Y. Q., Hu, T. D., Xie, Y. N., and Zhang, J. (2008). Mesoporous  $\text{Co}_3\text{O}_4\text{-CeO}_2$  and  $\text{Pd/Co}_3\text{O}_4\text{-CeO}_2$  catalysts: synthesis, characterization and mechanistic study of their catalytic properties for low-temperature CO oxidation. **J. Catal.** 254: 310-324.
- McCabe, R. W., and Mitchell, P. J. (1983). Oxidation of ethanol and acetaldehyde over alumina-supported catalysts. **Ind. Eng. Chem. Prod. Res. Dev.** 22: 212-217.
- McCabe, R. W., and Mitchell, P. J. (1984). Reactions of ethanol and acetaldehyde over noble metal and metal oxide catalysts. **Ind. Eng. Chem. Prod. Res. Dev.** 23: 196-202.
- Ménézo, J. C., Rivière, J., and Barbier, J. (1993). Effect of the doping of a metal oxide by platinum on its oxidizing properties. **React. Kinet. Catal. Lett.** 49: 293-298.
- Mergler, Y. J., van Aalst, A., van Delft, J., and Nieuwenhuys, B. E. (1996). CO oxidation over promoted Pt catalysts. **Appl. Catal. B: Environ.** 10: 245-261.
- Morales, M. R., Barbero, B. P., and Cadús, L. E. (2006). Total oxidation of ethanol and propane over Mn-Cu mixed oxide catalysts. **Appl. Catal. B: Environ.** 67: 229-236.

- Morales, M. R., Barbero, B. P., and Cadús, L. E. (2008). Evaluation and characterization of Mn-Cu mixed oxide catalysts for ethanol total oxidation: influence of copper content. **Fuel**. 87: 1177-1186.
- Petkovic, L. M., Rashkeev, S. N., and Ginosar, D. M. (2009). Ethanol oxidation on metal oxide-supported platinum catalysts. **Catal. Today**. 147: 107-114.
- Pope, D., Walker, D. S., and Moss, R. L. (1976). Evaluation of cobalt oxide catalysts for the oxidation of low concentrations of organic compounds in air. **Atmos. Environ.** 10: 951-956.
- Rajesh, H., and Ozkan, U. S. (1993). Complete oxidation of ethanol, acetaldehyde and ethanol/methanol mixtures over copper oxide and copper-chromium oxide catalysts. **Ind. Eng. Chem. Res.** 32: 1622-1630.
- Selvam, P., Bhatia, S. K., and Sonwane, C. G. (2001). Recent advances in processing and characterization of periodic mesoporous MCM-41 silicate molecular sieves. **Ind. Eng. Chem. Res.** 40: 3237-3261.
- Song, H., and Ozkan, U. S. (2009). Ethanol steam reforming over Co-based catalysts: Role of oxygen mobility. **J. Catal.** 261: 66-74.
- Trawczyński, J., Bielak, B., and Miśta, W. (2005). Oxidation of ethanol over supported manganese catalysts – effect of the carrier. **Appl. Catal. B: Environ.** 55: 277-285.
- Tsoncheva, T., Ivanova, L., Rosenholm, J., and Linden, M. (2009). Cobalt oxide species supported on SBA-15, KIT-5 and KIT-6 mesoporous silicas for ethyl acetate total oxidation. **Appl. Catal. B: Environ.** 89: 365-374.
- Yao, Y. F. Y. (1984). Catalytic oxidation of ethanol at low concentrations. **Ind. Eng. Chem. Proc. Des. Dev.** 23: 60-67.

## CHAPTER III

### EXPERIMENTS

#### 3.1 Chemicals

The chemical for rice husk silica preparation was hydrochloric acid (HCl) 37% supplied by Carlo Erba. The chemicals for MCM-41 synthesis were cetyl trimethylammonium bromide (CTAB) supplied by Fluka; anhydrous sodium hydroxide pellet (NaOH) and sulfuric acid (H<sub>2</sub>SO<sub>4</sub>) 96%, both supplied by Carlo Erba.

The chemicals for catalyst preparation were dihydrogen hexachloroplatinate(IV) hexahydrate (H<sub>2</sub>PtCl<sub>6</sub>·6H<sub>2</sub>O) supplied by Alfa; cobalt(II) nitrate hexahydrate (Co(NO<sub>3</sub>)<sub>2</sub>·6H<sub>2</sub>O), copper(II) nitrate trihydrate (Cu(NO<sub>3</sub>)<sub>2</sub>·3H<sub>2</sub>O), and manganese(II) nitrate tetrahydrate (Mn(NO<sub>3</sub>)<sub>2</sub>·4H<sub>2</sub>O), all supplied by Merck.

The chemicals for catalytic testing were ethanol (C<sub>2</sub>H<sub>5</sub>OH) 99.9% supplied by Merck; synthetic air (O<sub>2</sub> 20% and N<sub>2</sub> 80%), hydrogen (H<sub>2</sub>) 99.99%, and nitrogen (N<sub>2</sub>) 99.99%.

#### 3.2 Extraction of rice husk silica

The preparation of silica from rice husk was similar to a method in literature (Wittayakun, Khemthong, and Prayoonpokarach, 2008). Rice husk was washed by H<sub>2</sub>O, dried at 100 °C overnight and refluxed at 70 °C in 3M HCl solution. The obtained solid material was washed with water until pH of the washing water was ~7,

dried at 100 °C overnight, and calcined at 550 °C for 6 h. The sample was referred to as rice husk silica.

### 3.3 RH-MCM-41 synthesis

The RH-MCM-41 was synthesized by hydrothermal method with a procedure modified from the literature (Chumee, Grisdanurak, Neramittagapong, and Wittayakun, 2009). A clear solution of sodium silicate was prepared by mixing rice husk silica (3.0 g) with NaOH solution (5 M, 30 mL prepared from pellets) under stirring in a polypropylene bottle. This mixture was added to an aqueous solution of cetyltrimethyl ammonium bromide (CTAB, 0.14 M, 90 mL, prepared from solid) and stirred at room temperature for 4 h. The solution pH was adjusted to 11 by 2.5 M H<sub>2</sub>SO<sub>4</sub>. The resulting mixture was transferred to a teflon-lined stainless steel autoclave and heated at 100 °C for 3 days. The solid product, as-synthesized RH-MCM-41, was separated by centrifugation, washed thoroughly with deionized water, and dried at 100 °C. Finally, the organic template was removed by calcination in atmospheric pressure at 540 °C for 6 h.

### 3.4 Catalyst preparation

Monometallic Pt/RH-MCM-41 with Pt loading of 0.5 wt% and M/RH-MCM-41 (M = Co, Cu, and Mn) with M loading of 5, 10, or 15 wt% were prepared by impregnation method with an aqueous of H<sub>2</sub>PtCl<sub>6</sub>·6H<sub>2</sub>O, Co(NO<sub>3</sub>)<sub>2</sub>·6H<sub>2</sub>O, Cu(NO<sub>3</sub>)<sub>2</sub>·3H<sub>2</sub>O, and Mn(NO<sub>3</sub>)<sub>2</sub>·4H<sub>2</sub>O, respectively. The samples were dried at 70 °C for 1 h and then 100 °C overnight and calcined at 500 °C for 2 h. The catalysts



were named as xM/RH-MCM-41 where x was the extent of loading by weight and M was the type of metal.

The bimetallic Pt-M/RH-MCM-41 catalysts with 0.5 wt% Pt and 5, 10, or 15 wt% M were prepared by sequential impregnation method. The monometallic catalysts, prepared as mentioned above, were impregnated with an aqueous solution of  $\text{H}_2\text{PtCl}_6 \cdot 6\text{H}_2\text{O}$ , dried at 70 °C for 1 h and then 100 °C overnight and calcined at 500 °C for 2 h. The catalysts were named as 0.5Pt-yM/RH-MCM-41 where y was the extent of loading by weight of metal.

### 3.5 Catalyst characterization

Metal contents of catalysts were analyzed by inductively coupled plasma-mass spectroscopy (ICP-MS) with an Agilent 7500ce. A 50-mg sample was dissolved in HCl/HNO<sub>3</sub>/HF/H<sub>3</sub>BO<sub>3</sub> solution (0.8/1.2/0.4/6 by mL).

Physical characteristics of the samples were studied by nitrogen adsorption-desorption analysis at -196 °C at relative pressure ( $P/P_0$ ) from 0.01 to 0.99 on a Micromeritics ASAP 2010. Before measurement, each sample was degassed with heat at 300 °C under vacuum for 4 h. The surface area, average pore size and total pore volume were calculated using the Brunauer-Emmett-Teller (BET) method from the adsorption data.

Powder XRD patterns were obtained from a Bruker axs D5005 diffractometer. The Cu K<sub>α</sub> X-ray ( $\lambda = 1.54 \text{ \AA}$ ) was generated with a current of 35 mA and a potential of 35 kV. The catalysts were scanned in two  $2\theta$  ranges, low angle from 1 to 10 degrees and wide angle from 20 to 70 degrees. The powder pattern of each catalyst was recorded in the same day with the same amount, so that the intensity of the peaks

could be roughly compared. Equation (3.1) correlates the inter-planar distances with the value of the mesoporous parameter (Beck *et al.*, 1992). The unit cell dimension,  $a_0$ , was calculated from the  $d_{100}$  value extracted from XRD according to Equation (3.2).

$$\frac{1}{d(hkl)^2} = \frac{4(h^2 + hk + l^2)}{3a_0^2} + \frac{l^2}{c^2} \quad (3.1)$$

$$a_0 = \frac{2d(100)}{\sqrt{3}} \quad (3.2)$$

X-ray absorption near edge structure (XANES) spectra of mono- and bimetallic containing Co, Cu, and Mn were recorded in a transmission mode at the Beamline 8 of the Synchrotron Light Research Institute, Thailand (Klysubun *et al.*, 2007). The storage ring was normally operated with the electron energy of 1.2 GeV and electron current between 90 and 140 mA. Using a synchrotron X-ray monochromator equipped with double Ge (2 2 0) crystals, the photon energy was scanned from 7690 to 7780 eV, 8950 to 9060 eV, and 6510 to 6620 eV for the samples containing Co, Cu and Mn, respectively. The energy calibration for scanning the X-ray energy was performed using standard foils of Co, Cu, and Mn (Exafs Material, Inc.) at their K-edges. The percentages of oxide phases of Co, Cu, and Mn were determined by comparing the XANES spectrum of each catalyst to those of standard materials using a Linear Combination Fitting tool available in the ATHENA program (Ravel and Newville, 2005). Beside the foils, the oxide standards of Co, Cu and Mn were: CoO, Co<sub>3</sub>O<sub>4</sub>; CuO, Cu<sub>2</sub>O; MnO, MnO<sub>2</sub>, and Mn<sub>2</sub>O<sub>3</sub>, respectively.

Transmission electron microscopy was performed on a JEOL JEM 2010. For the TEM analysis, the samples were suspended in 95% ethanol solution, dispersed by sonication, deposited on a grid with a holey carbon copper and dried at 70 °C with UV lamp. Electron for the analysis was accelerated at 120 kV.

### **3.6 Ethanol adsorption by thermogravimetric analysis (ethanol-TGA)**

Ethanol adsorption of each catalyst was analyzed by thermogravimetric analysis (TGA) (NETZSCH; STA 409 PC). In the TGA, the catalyst (50 mg) was pretreated by heat under a flow of N<sub>2</sub> (50 mL/min) from room temperature to 300 °C with a ramping rate of 5 °C/min and holding at 300 °C for 1 h. Then, the catalyst was reduced under a flow of H<sub>2</sub> (30 mL/min) at 200 °C with a ramping rate of 5 °C/min. After cooled down to 30 °C, the catalyst was purged by N<sub>2</sub> (25 mL/min) until a constant weight was obtained. Then vapor, generated by flowing N<sub>2</sub> through a saturator containing ethanol, was flowed over the catalyst at 30 °C. When a saturated adsorption was obtained, i.e., the weight became constant, the catalyst was purged by a flow of N<sub>2</sub> to remove physisorbed species. Finally, weight of ethanol on catalyst was recorded.

### 3.7 Temperature programmed desorption of ethanol (ethanol-TPD)

The ethanol-TPD analysis was performed in a tubular flow reactor connected to a mass spectrometer (Balzers Prisma 260). First, the monometallic 15M/RH-MCM-41 catalysts (M = Co, Cu, or Mn) were tested to observe the ability of the oxides to react with adsorbed ethanol to produce CO<sub>2</sub>. Then the 0.5Pt/RH-MCM-41 and bimetallic 0.5Pt-15M/RH-MCM-41 were studied.

In the ethanol-TPD procedure, each catalyst (50 mg) was packed on a quartz wool bed in a quartz tube, topped with quartz wool, heated under a flow of He (50 mL/min) at 300 °C (ramping rate of 5 °C/min) for 4 h, and reduced under a flow of H<sub>2</sub> (30 mL/min) at 200 °C for 2 h. Then H<sub>2</sub> was switched to He (25 mL/min) to remove the adsorbed hydrogen on the catalyst. The ethanol adsorption was carried out by flowing He (25 mL/min) into a saturator containing ethanol and then through the catalyst at 30 °C for 2 h. After that, the catalyst was purged by He (25 mL/min) at 30 °C for 4 h. The ethanol-TPD was performed at ambient temperature to 400 °C with a heating rate of 5 °C/min and holding at 400 °C for 30 min. The signal of ethanol and desorbed gases were monitored by the mass spectrometer.

### 3.8 Ethanol oxidation studied by *in situ* Fourier transform infrared spectroscopy (*in situ* FTIR)

A self-support wafer (~0.6 cm diameter) of a catalyst powder, prepared by a hydraulic press, was put into an *in situ* sample holder, heated under a flow of He (50 mL/min) at 300 °C with a ramping rate of 10 °C/min for 1 h, and reduced under a

flow of H<sub>2</sub> (30 mL/min) at 300 °C for 1 h. Then H<sub>2</sub> was switched to He (25 mL/min) to remove hydrogen residue on the catalyst. The ethanol vapor, mixed with synthetic air, was introduced to the *in situ* cell at 30 °C and heated to 300 °C with a ramping rate of 10 °C/min. The *in situ* IR spectra of species during the oxidation were recorded at 30, 100, 150, 200, 250, and 300 °C on a Bruker IFS 28 spectrometer over the 4,000-1,000 cm<sup>-1</sup> range at a resolution of 4 cm<sup>-1</sup>. The spectra were normalized using the intensity of the MCM-41 structural vibrations which was in the range of 2100-1770 cm<sup>-1</sup> (Bellat *et al.*, 1999).

### 3.9 Ethanol oxidation in a fixed-bed flow reactor

Each catalyst was tested in a continuous-flow fixed bed reactor connected to a GC. Before the test, approximately 100 mg of catalyst was packed on a quartz wool bed in a quartz tube, heated under flowing He (50 mL/min) at 400 °C for 2 h and then reduced under flowing H<sub>2</sub> (30 mL/min) for 2 h. Ethanol vapor was generated by a syringe pump through a tube furnace which was heated at 100 °C and mixed with synthetic air (100 mL/min) before entering the reactor. The total flow rate was 100.2 mL/min. The concentration of ethanol was 1974 ppm and space velocity (SV) was 9550 h<sup>-1</sup>. All of the reactor inlet and outlet lines were heated to prevent condensation and to preheat the feed. The reaction was studied from 100 to 400 °C and the gas components before and after the reaction were analyzed by GC (Hewlett-Packard 5890) equipped with a thermal conductivity detector. After the testing was complete, the catalyst was cooled down to 100 °C under the feed of the reactants. The second

run was conducted; the temperature was increased again and the reaction products were analyzed by the GC.

Because the products observed were both CO<sub>2</sub> and acetaldehyde, the ethanol conversion and product yield were calculated by using carbon balance according to Equation (3.3) and (3.4), respectively.

$$\% \text{CH}_3\text{CH}_2\text{OH conversion} = \frac{1/2 \text{CO}_2 + 1 \text{CH}_3\text{CHO}}{1/2 \text{CO}_2 + 1 \text{CH}_3\text{CHO} + 1 \text{CH}_3\text{CH}_2\text{OH (residue)}} \quad (3.3)$$

$$\% \text{Yield} = \frac{\text{Conc. of product}}{\text{Conc. of ethanol (in put)}} \times \frac{\text{No. of C-atom of product}}{\text{No. of C-atom of ethanol}} \times 100\% \quad (3.4)$$

### 3.10 References

- Beck, J. S., Vartuli, J. C., Roth, W. J., Leonowicz, M. E., Kresge, C. T., Schmitt, K. D., Chu, C. T. W., Olson, D. H., and Sheppard, E. W. (1992). A new family of mesoporous molecular sieves prepared with liquid crystal templates. **J. Am. Chem. Soc.** 114: 10834-10843.
- Bellat, J. P., Bertrand, O., Bouvier, F., Broyer, M., François, V., Maure, S., and Weber, G. (1999). Characterization and utilization of MFI zeolites and MCM-41 materials for gaseous pollutant adsorption. **Stud. Surf. Sci. Catal.** 125: 737-744.

- Chumee, J., Grisdanurak, N., Neramittagapong, A., and Wittayakun, J. (2009). Characterization of platinum-iron catalysts supported on MCM-41 synthesized with rice husk silica and their performance for phenol hydroxylation. **Sci. Technol. Adv. Mater.** 10: 1-6.
- Klysubun, W., Sombunchoo, P., Wongprachanukul, N., Tarawarakarn, P., Klinkhieo, S., Chaiprapa, J., and Songsiriritthigul, P. (2007). Commissioning and performance of X-ray absorption spectroscopy beamline at the Siam Photon Laboratory. **Nucl. Instrum. Meth. A.** 582: 87-89.
- Ravel, B., and Newville, M. (2005). ATHENA, ARTEMIS, HEPHAESTUS: data analysis for X-ray absorption spectroscopy using IFEFFIT. **J. Synchrotron Radiat.** 12: 537-541.
- Wittayakun, J., Khemthong, P., and Prayoonpokarach, S. (2008). Synthesis and characterization of zeolite NaY from rice husk silica. **Korean J. Chem. Eng.** 25: 861-864.

## CHAPTER IV

### RESULTS AND DISCUSSION

#### 4.1 Catalyst characterization by ICP-MS

Metal content in each catalyst was analyzed by ICP-MS. The results in Table 4.1 demonstrate that the extents of metal loading in the catalysts prepared by the impregnation method were similar to the nominal values.

**Table 4.1** Metal contents in the studied catalysts.

Catalysts	Metals content (wt%)			
	Pt	Co	Cu	Mn
MCM-41	-	-	-	-
15Co/RH-MCM-41	-	15.17	-	-
15Cu/RH-MCM-41	-	-	14.91	-
15Mn/RH-MCM-41	-	-	-	14.76
0.5Pt-15Co/RH-MCM-41	0.47	14.23	-	-
0.5Pt-15Cu/RH-MCM-41	0.37	-	14.80	-
0.5Pt-15Mn/RH-MCM-41	0.48	-	-	14.11
0.5Pt/RH-MCM-41	0.50	-	-	-



## 4.2 N<sub>2</sub> adsorption-desorption and TEM

The N<sub>2</sub> adsorption-desorption isotherm of RH-MCM-41 (Figure 4.1A) was type IV which is the characteristic of ordered mesoporous materials, as classified by the International Union of Pure and Applied Chemistry (IUPAC) (Rouquerol and Sing, 1999). The isotherm of RH-MCM-41 consisted of three regions. The adsorptions at relative pressure from 0.0 to 0.2 corresponded to monolayer-multilayer adsorption on the pore walls. The adsorption and desorption isotherms showed a sharp inflection at intermediate relative pressures ranging from 0.25 to 0.35, which was due to capillary condensation of nitrogen inside the mesopores. The last stage was a plateau at high relative pressures associated with multilayer adsorption on the external surface of the crystals (Paulino and Schuchardt, 2002). The isotherm of 0.5Pt/RH-MCM-41 (Figure 4.1B) was also type IV. The volume of N<sub>2</sub> adsorbed was lower than that of the bare RH-MCM-41 indicating a decrease in surface area. The BET surface area, average pore diameter, and total pore volume of all catalysts are presented in Table 4.2.

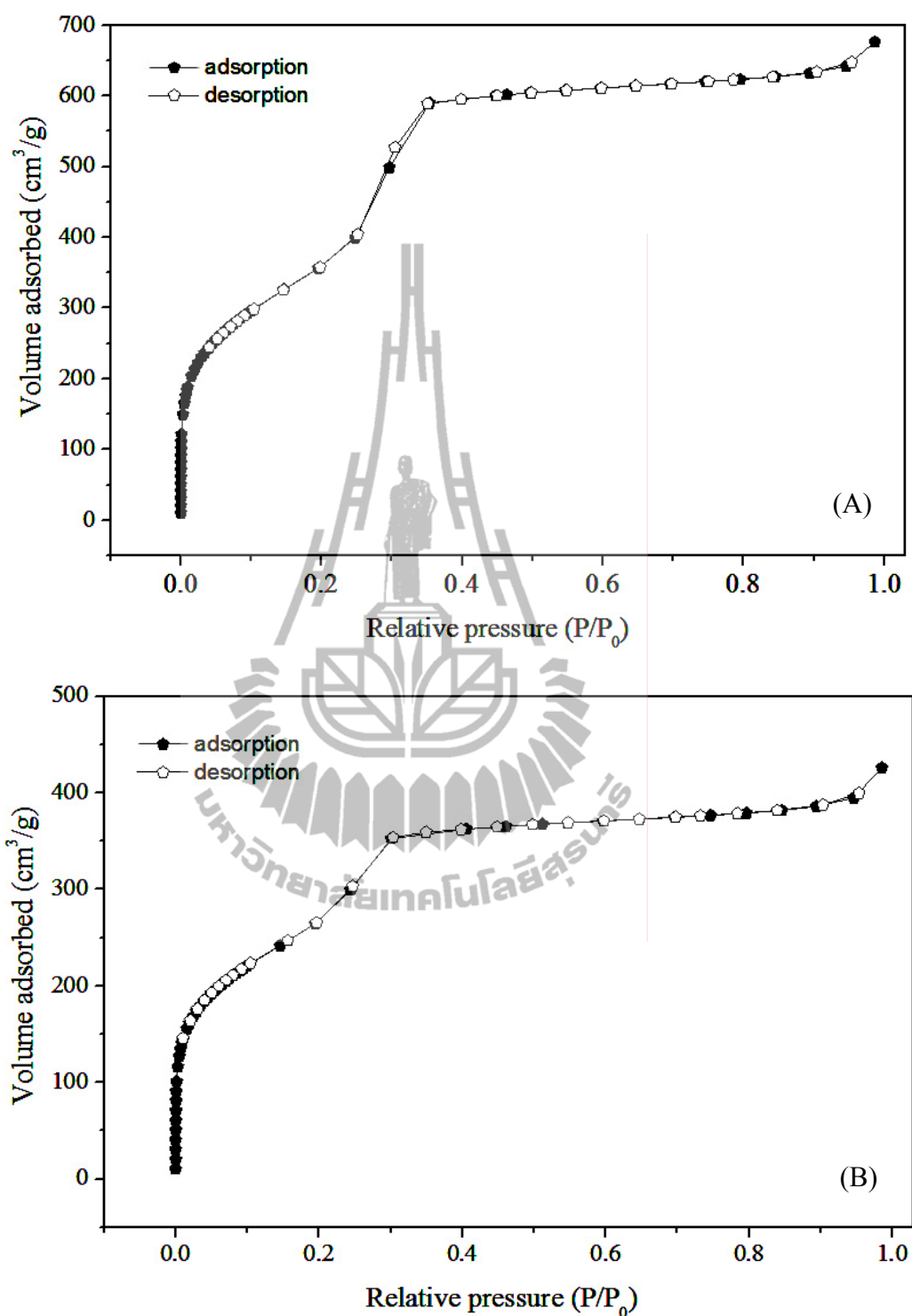


**Figure 4.1** Nitrogen adsorption-desorption isotherm of RH-MCM-41 (A) and 0.5Pt/RH-MCM-41 (B); filled: adsorption and open: desorption.

**Table 4.2** BET surface area, average pore size, and total pore volume of RH-MCM-41 and catalysts.

Catalysts	BET surface area (m <sup>2</sup> /g)	Average pore size (nm)	Total pore volume (cm <sup>3</sup> /g)
RH-MCM-41	1352	3.1	1.05
0.5Pt/RH-MCM-41	992	2.7	0.66
5Co/RH-MCM-41	669	2.9	0.49
10Co/RH-MCM-41	574	3.1	0.45
15Co/RH-MCM-41	535	3.0	0.41
0.5Pt-5Co/RH-MCM-41	755	2.7	0.50
0.5Pt-10Co/RH-MCM-41	821	2.7	0.55
0.5Pt-15Co/RH-MCM-41	809	2.7	0.55
5Cu/RH-MCM-41	626	2.9	0.46
10Cu/RH-MCM-41	505	3.2	0.41
15Cu/RH-MCM-41	745	2.9	0.54
0.5Pt-5Cu/RH-MCM-41	830	2.6	0.54
0.5Pt-10Cu/RH-MCM-41	863	2.6	0.57
0.5Pt-15Cu/RH-MCM-41	807	2.6	0.52

**Table 4.2** (Continued).

Catalysts	BET surface area (m <sup>2</sup> /g)	Average pore size (nm)	Total pore volume (cm <sup>3</sup> /g)
5Mn/RH-MCM-41	554	3.1	0.43
10Mn/RH-MCM-41	912	2.7	0.63
15Mn/RH-MCM-41	904	2.8	0.63
0.5Pt-10Mn/RH-MCM-41	860	2.7	0.57
0.5Pt-15Mn/RH-MCM-41	710	2.8	0.49

Characteristic of RH-MCM-41 relative with ordered mesoporous materials was exhibited in TEM images (shown in Figure 4.2). TEM images showed uniform order and mesoporosity in RH-MCM-41 particles.

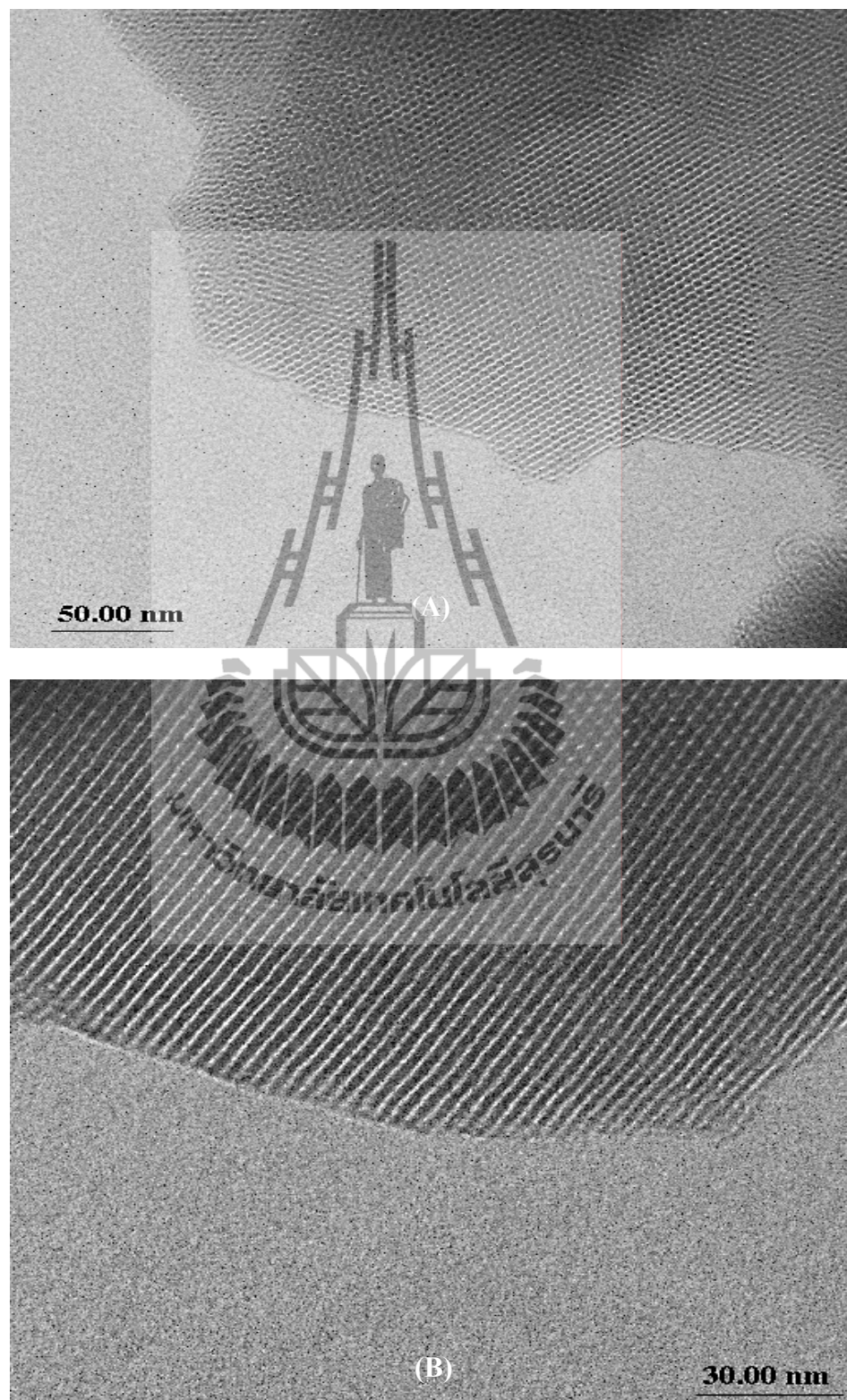


**Figure 4.2** TEM images of RH-MCM-41 viewed along (A) and perpendicular to (B) the axis of the hexagonally arranged mesopores.

The nitrogen adsorption-desorption isotherm of RH-MCM-41 supported mono- and bimetallic catalysts containing Co, Cu, and Mn are shown in Figure 4.3A, B, and C, respectively. All samples still showed type IV isotherms. These isotherms can be compared to that of 0.5Pt/RH-MCM-41 in Figure 4.1B.

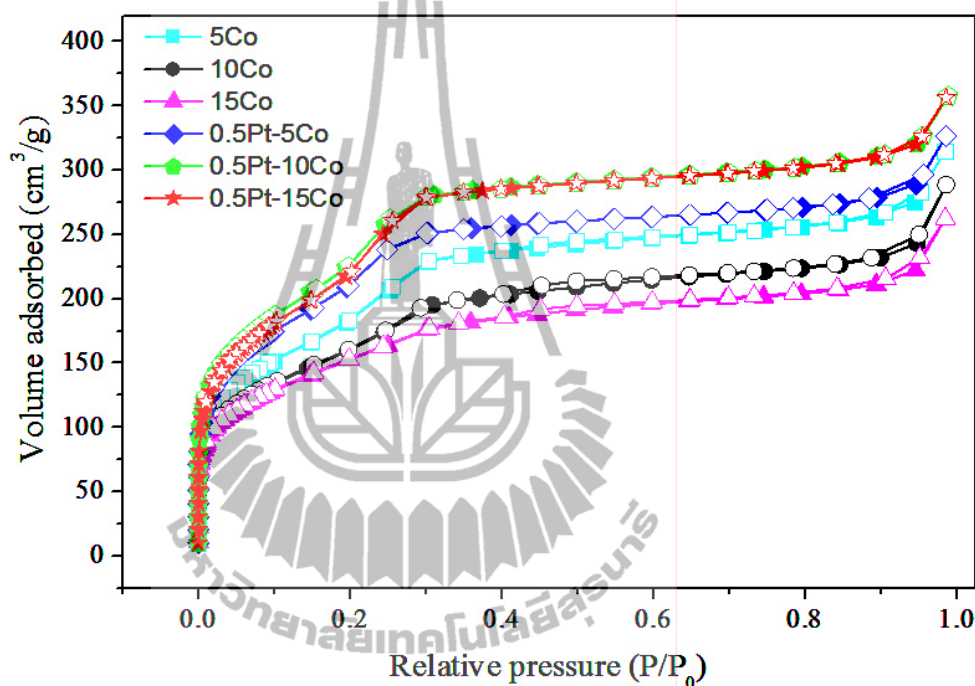


**Figure 4.3** Nitrogen adsorption-desorption isotherm of RH-MCM-41 supported mono- and bimetallic Co catalysts; filled: adsorption and open: desorption.

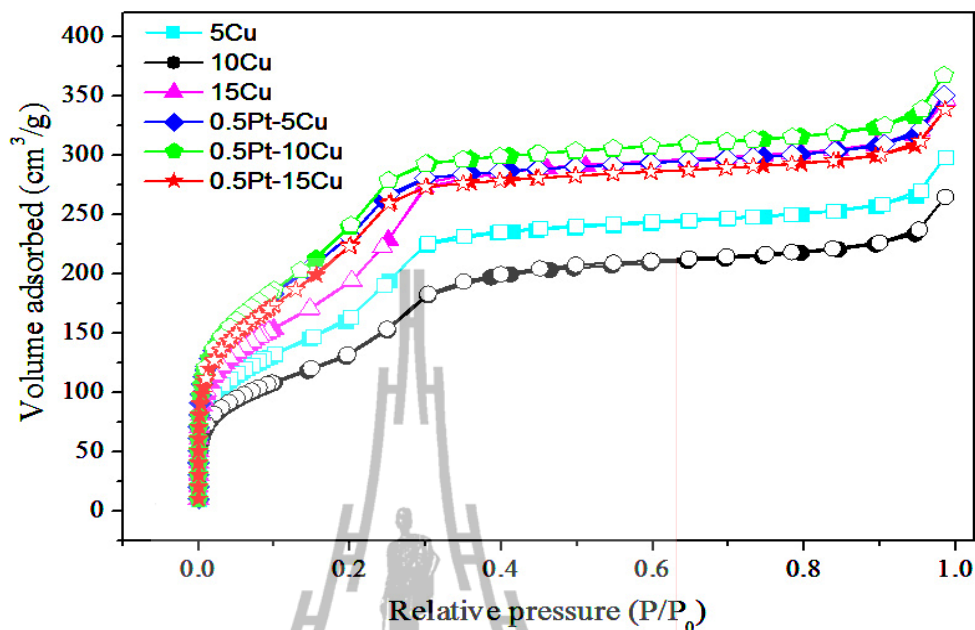


**Figure 4.4** Nitrogen adsorption-desorption isotherm of RH-MCM-41 supported mono- and bimetallic Cu catalysts; filled: adsorption and open: desorption.

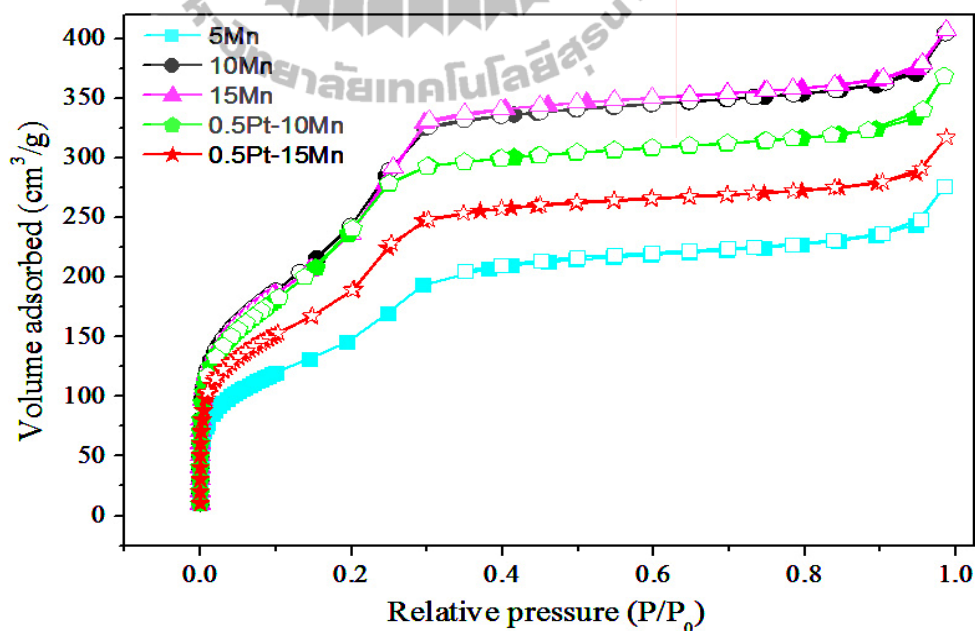


**Figure 4.5** Nitrogen adsorption-desorption isotherm of RH-MCM-41 supported mono- and bimetallic Mn catalysts; filled: adsorption and open: desorption.

After calcination, RH-MCM-41 had surface area of 1352 m<sup>2</sup>/g. After it was loaded with metal, the surface area, average pore diameter, and total pore volume decreased indicating that the pores of RH-MCM-41 were partially filled after impregnation (Xu, Song, Andresen, Miller, and Scaroni, 2002). All catalysts had surface areas in the range of 992-505 m<sup>2</sup>/g and total pore volume in the range of 0.66-0.41 cm<sup>3</sup>/g. In 0.5Pt/RH-MCM-41, BET surface area was higher than other catalysts because only low loading of Pt was used. Most of catalysts showed decrease in both average pore size and surface area which indicated that metal resided in the pore of the support or they had less pore blocking.

The isotherm of 10Co/RH-MCM-41 and 15Co/RH-MCM-41 catalysts were different from others because the adsorption corresponded to mesopore filling almost disappeared indicating a loss of surface of mesoporous silica. Although both catalysts showed strongly decreased surface area, average pore size was not different from that of the bare RH-MCM-41. The result suggested that most of metal did not incorporate inside the mesopores but formed large oxide particles and settled on RH-MCM-41 external surface or blocked mesopores.

Evidence of large particles outside mesopores could be seen by TEM. For examples, TEM images of 15Co/RH-MCM-41 in Figure 4.6 showed non-uniform particles, expected to be oxides with the size about 30 nm (circle area).

0.5Pt-15Co/RH-MCM-41 catalyst had higher BET surface area than 15Co/RH-MCM-41 probably because of better metal dispersion. This statement could be confirmed by comparing TEM images of both catalysts. In the case of bimetallic catalyst (Figure 4.7), large particles from agglomeration of cobalt oxides were not observed.



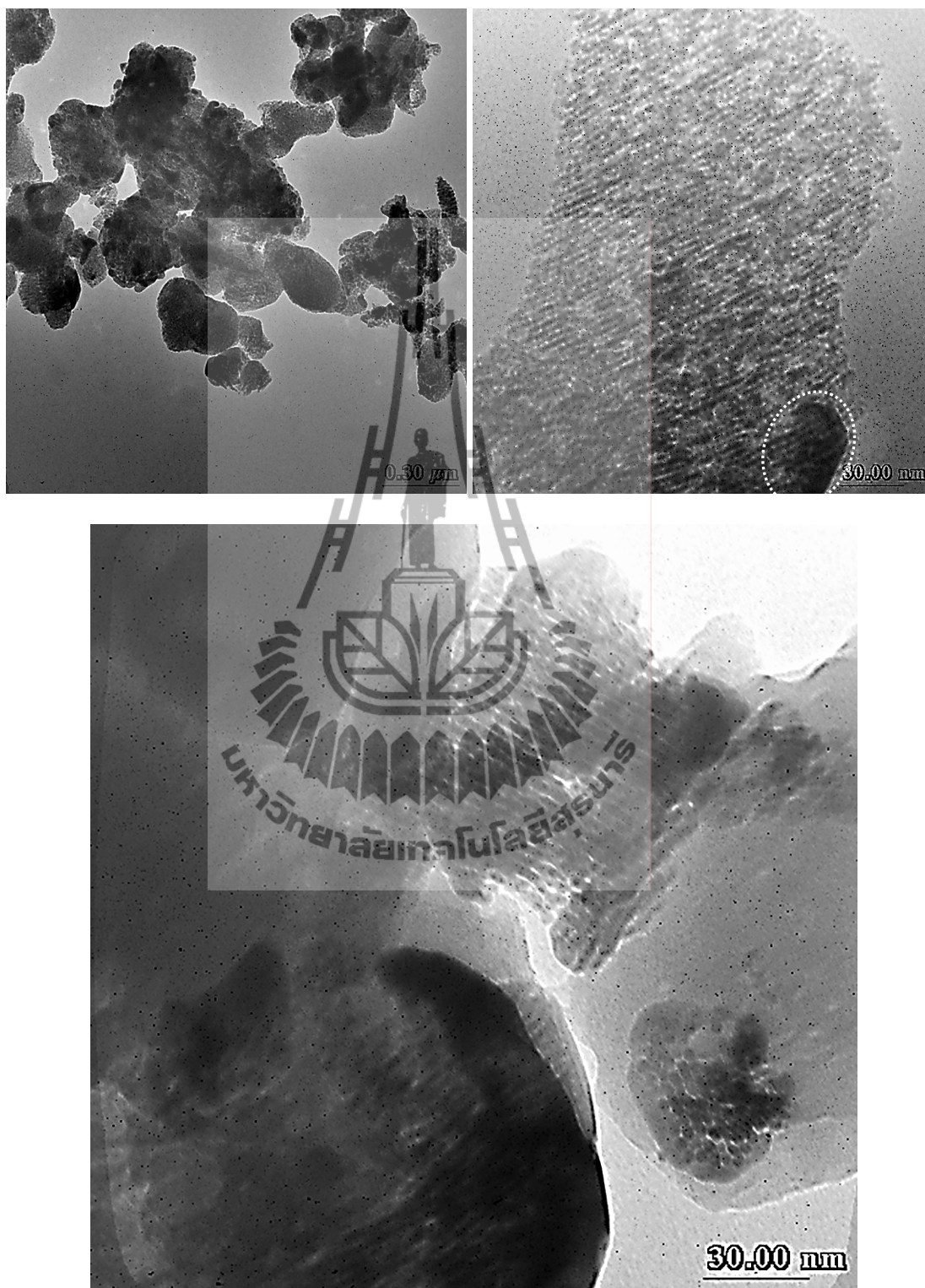


**Figure 4.6** TEM images of 15Co/RH-MCM-41.

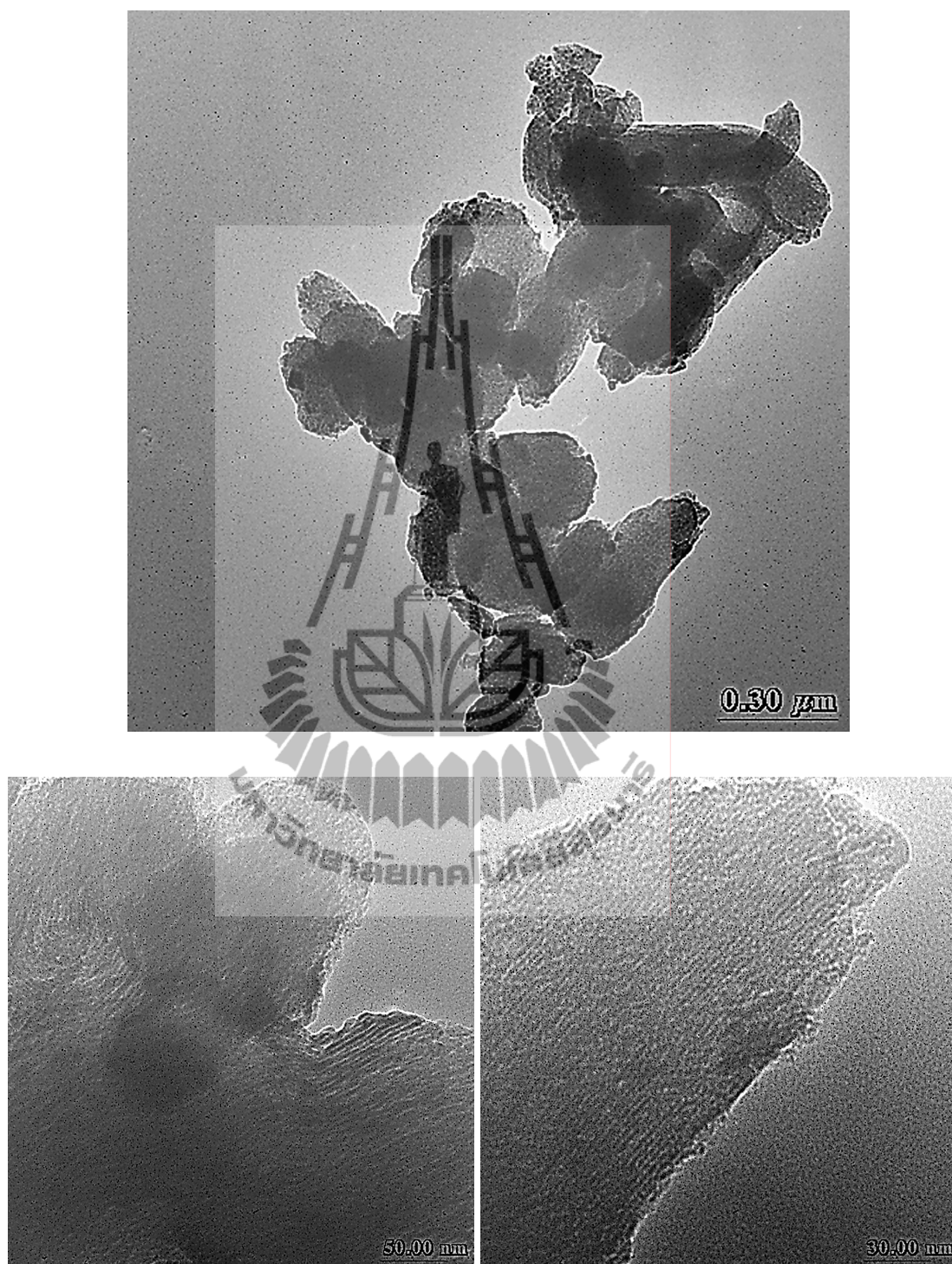


**Figure 4.7** TEM images of 0.5Pt-15Co/RH-MCM-41.

From surface area results, 0.5Pt-5Co/RH-MCM-41 and 0.5Pt-10Co/RH-MCM-41 had higher surface area than 5Co/RH-MCM-41 and 10Co/RH-MCM-41 because of well dispersion of metals on RH-MCM-41 support. This result was evidenced by TEM images, as shown in Appendix. The TEM images of 0.5Pt-5Co/RH-MCM-41 and 0.5Pt-10Co/RH-MCM-41 did not show large metal particles on RH-MCM-41. Thus the average pore diameter of bimetallic Co catalysts was less than that of monometallic Co catalysts because some part of Co was inside the pore of RH-MCM-41.

### 4.3 Catalyst characterization by XRD and XANES

The XRD pattern of the RH-MCM-41 support (Figure 4.8) consisted of characteristic peaks of MCM-41 similar to that in the literature (Chumee, Grisdanurak, Neramittagapong, and Wittayakun, 2009) with a strong peak at  $2.3^\circ$  and weak peaks at  $4.0$ ,  $4.6$ ,  $6.0$ , and  $8.2^\circ$  corresponding to the (100), (110), (200), (210), and (300) plane of a hexagonal lattice, respectively. These peaks indicated long range order of the mesoporous channels (Kresge, Leonowicz, Roth, Vartuli, and Beck, 1992).

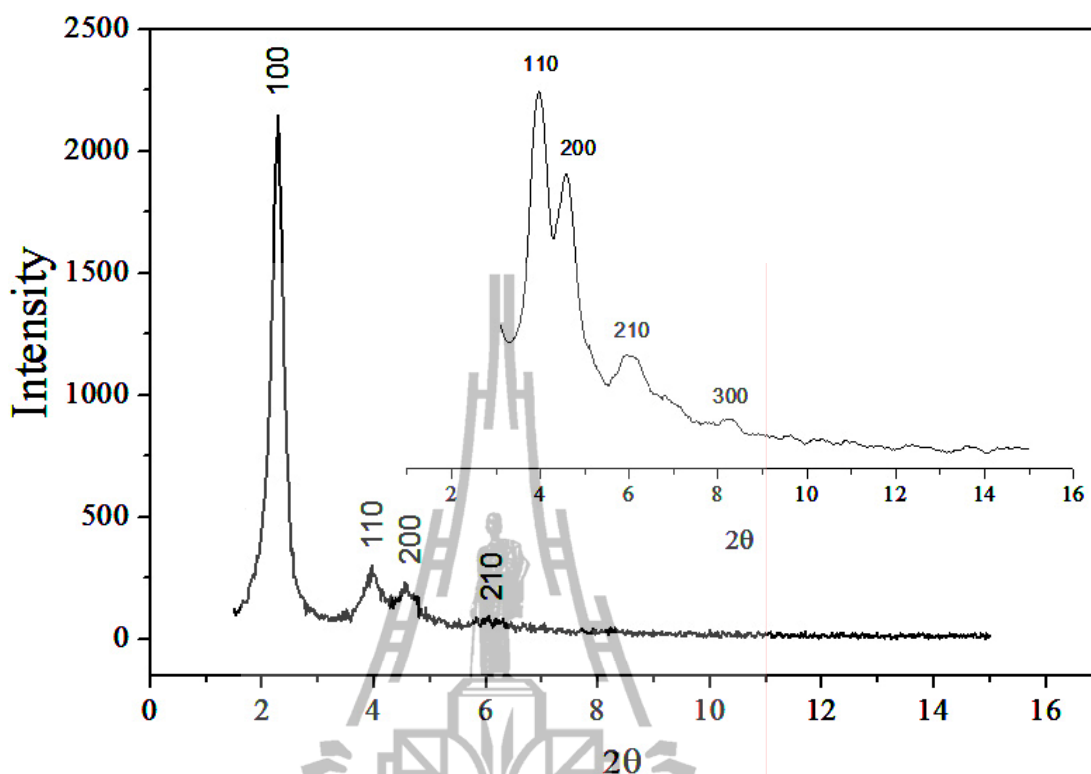


**Figure 4.8** XRD powder pattern of RH-MCM-41.

The XRD patterns of all mono- and bimetallic catalysts containing Co, Cu, and Mn at low angle region (Figure 4.9, 4.10, and 4.11, respectively) still showed characteristic peaks of MCM-41. After deposition with metal, the intensity of the main peak decreased and those of weak peaks were not observed. With metal loading, the presence of oxides on the support surface could scatter out the X-ray resulting in lower diffracted intensity. Similar behavior was observed when 10 wt% of nanoparticles of  $\text{TiO}_2$  were loaded on RH-MCM-41 (Artkla, Kim, Choi, and Wittayakun, 2009). In addition, the lower MCM-41-peak intensity and peak broadening was reported on Co/MCM-41 with Co loading of 7-8 wt% due to secondary scattering and less ordered structure of MCM-41 (Panpranot, Kaewkun, Prasertthdam, and Goodwin, 2003).

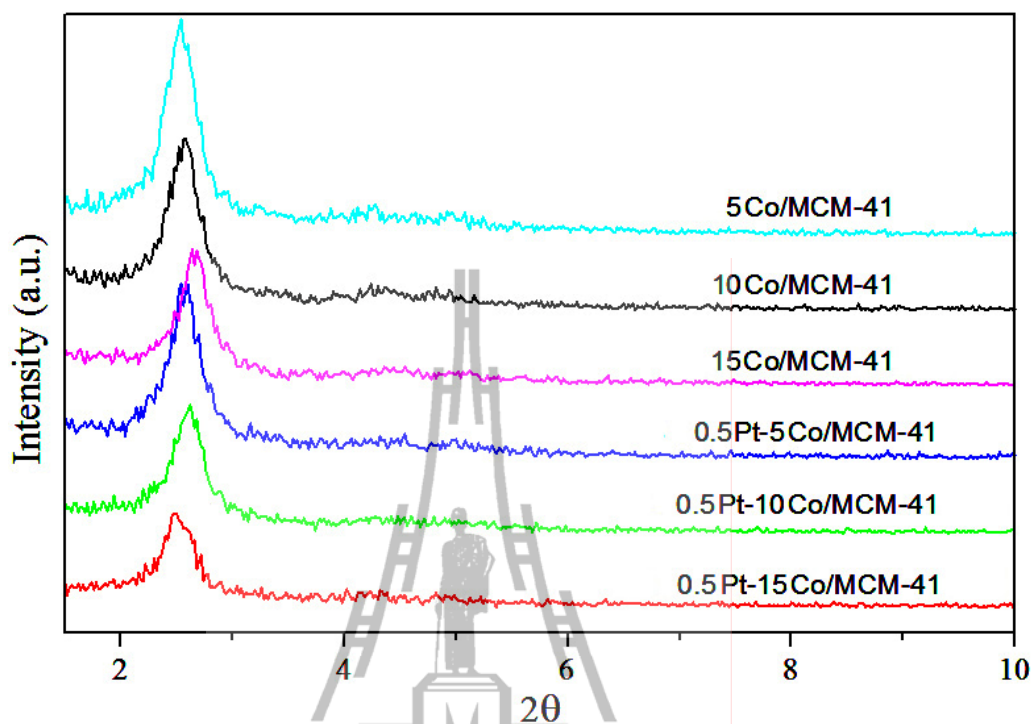


Figure 4.9 XRD powder patterns at low angle of mono- and bimetallic Co catalysts.

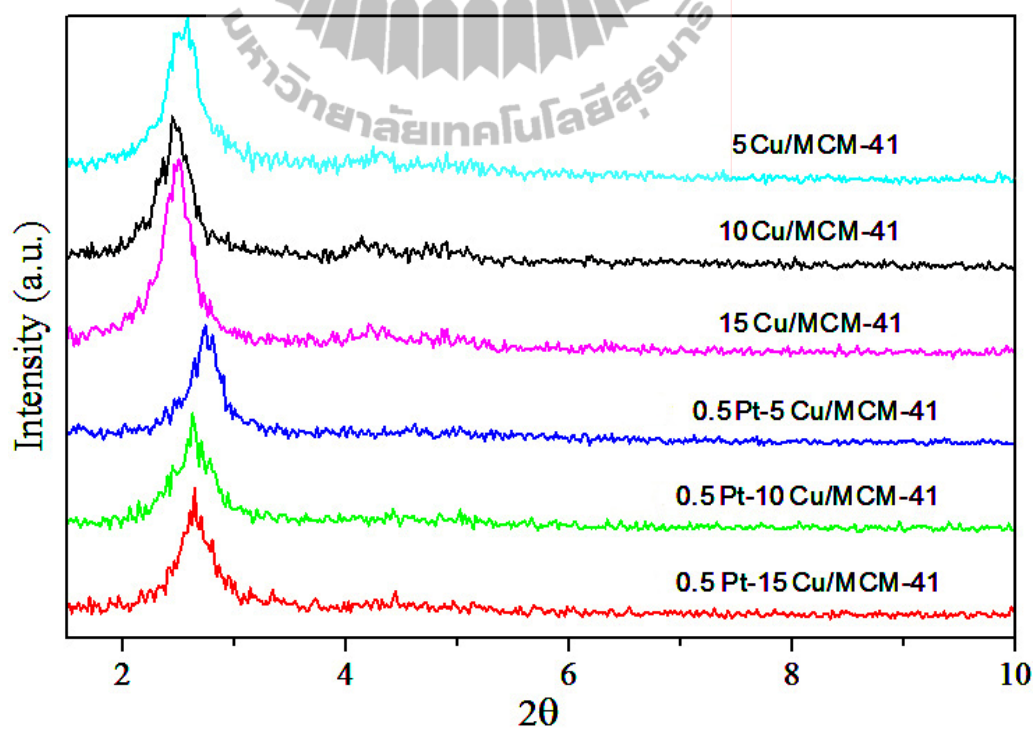
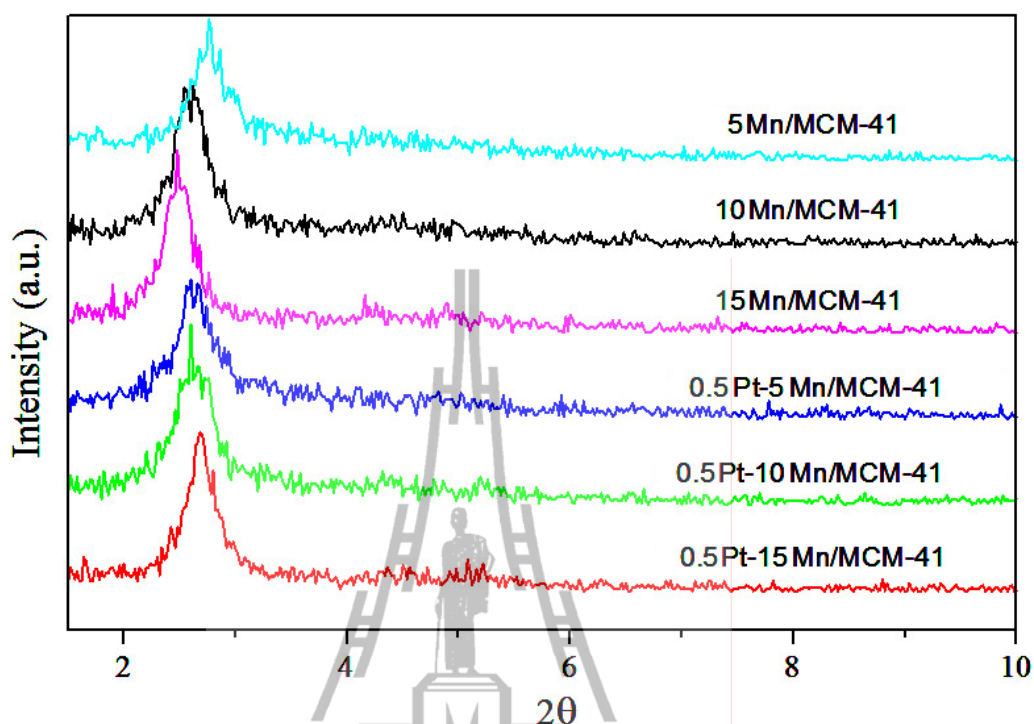


Figure 4.10 XRD powder patterns at low angle of mono- and bimetallic Cu catalysts.



**Figure 4.11** XRD powder patterns at low angle of mono- and bimetallic Mn catalysts.

With Co loading of fewer than 3 wt%, Bhoware and Singh (2007) reported that the peak of the (100) plane decreased as the loading of cobalt increased. In addition, the peak position of the (100) plane of the supported catalysts shifted slightly toward the higher angle suggesting that some metal oxide settled on pore wall or blocked mesoporous channels of MCM-41. From  $d_{100}$  values calculated from Bragg equation, all catalysts exhibited decreasing  $d_{100}$  spacing values compared to bare RH-MCM-41. In addition, unit cell parameter value of all catalysts,  $a_0$  (calculated using  $a_0 = 2d_{100}/3^{1/2}$  (Beck *et al.*, 1992)), were in a range of 3.70-4.17, lower than that of bare RH-MCM-41 which was 4.48 (Table 4.3). The  $N_2$  adsorption-desorption and XRD results suggested that loaded metal dispersed on external surface and inside pore of RH-MCM-41. Consequently, pores of RH-MCM-41 were partially blocked.

**Table 4.3**  $2\theta$ ,  $d_{100}$ , and  $a_0$  values of RH-MCM-41 and catalysts.

Catalysts	$2\theta$	$d_{100}$	$a_0$
RH-MCM-41	2.28	3.87	4.48
5Co/RH-MCM-41	2.54	3.48	4.02
10Co/RH-MCM-41	2.57	3.44	3.97
15Co/RH-MCM-41	2.66	3.32	3.84
5Cu/RH-MCM-41	2.57	3.44	3.97
10Cu/RH-MCM-41	2.45	3.60	4.17
15Cu/RH-MCM-41	2.50	3.53	4.08
5Mn/RH-MCM-41	2.76	3.20	3.70
10Mn/RH-MCM-41	2.59	3.41	3.94
15Mn/RH-MCM-41	2.49	3.55	4.10
0.5Pt-5Co/RH-MCM-41	2.57	3.44	3.97
0.5Pt-10Co/RH-MCM-41	2.62	3.37	3.90
0.5Pt-15Co/RH-MCM-41	2.49	3.55	4.10
0.5 Pt-5Cu/RH-MCM-41	2.74	3.22	3.73
0.5Pt-10Cu/RH-MCM-41	2.64	3.34	3.87
0.5Pt-15Cu/RH-MCM-41	2.65	3.33	3.85
0.5Pt-5Mn/RH-MCM-41	2.63	3.36	3.88
0.5Pt-10Mn/RH-MCM-41	2.60	3.40	3.93
0.5Pt-15Mn/RH-MCM-41	2.68	3.29	3.81

The XRD patterns at high angle of all mono- and bimetallic Co, Cu, and Mn catalysts are shown in Figure 4.12, 4.13, and 4.14, respectively. The Co catalysts

exhibited characteristic peaks of  $\text{Co}_3\text{O}_4$  with diffraction peaks at  $2\theta$  of ca.  $31^\circ$ ,  $37^\circ$ ,  $45^\circ$ ,  $59^\circ$ , and  $65^\circ$  (Panpranot *et al.*, 2003; JCPDS: PDF 43-1003). The Cu catalysts showed peaks corresponding to CuO around  $2\theta$  of  $35^\circ$ ,  $38^\circ$ , and  $48^\circ$  (Wu, Wang, and Zhu, 2005; JCPDS: PDF 44-706). The Mn catalysts displayed weak peaks of  $\beta$ - $\text{MnO}_2$  or pyrolusite phase around  $2\theta$  of  $28^\circ$ ,  $37^\circ$ , and  $57^\circ$  (Lamaita, Peluso, Sambeth, and Thomas, 2005; JCPDS: PDF 24-735). The XRD patterns of all catalysts showed the evidence that metal oxides were formed on RH-MCM-41. The intensity of these peaks increased when metal loading increased because of the increase of particle size of metal oxides.

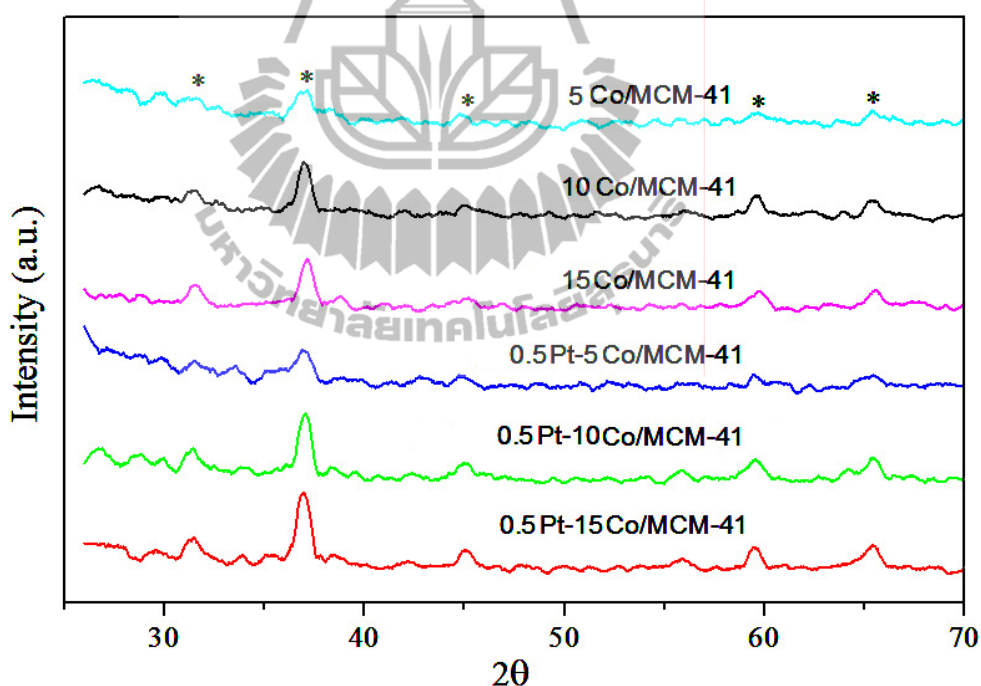


**Figure 4.12** XRD powder patterns at high angle of mono- and bimetallic Co catalysts.



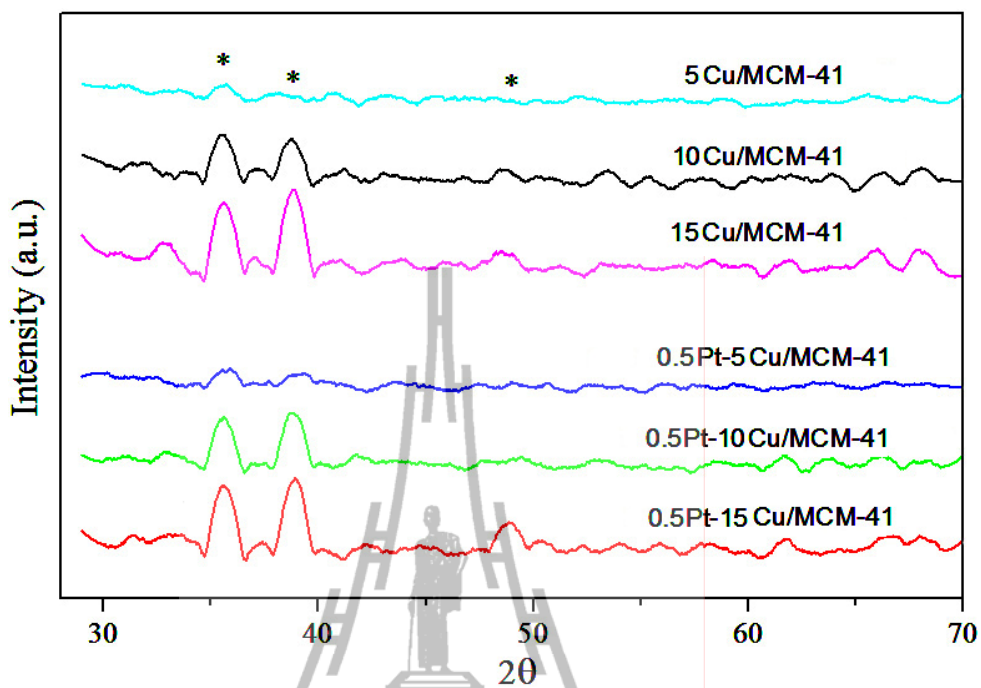


Figure 4.13 XRD powder patterns at high angle of mono- and bimetallic Cu catalysts.

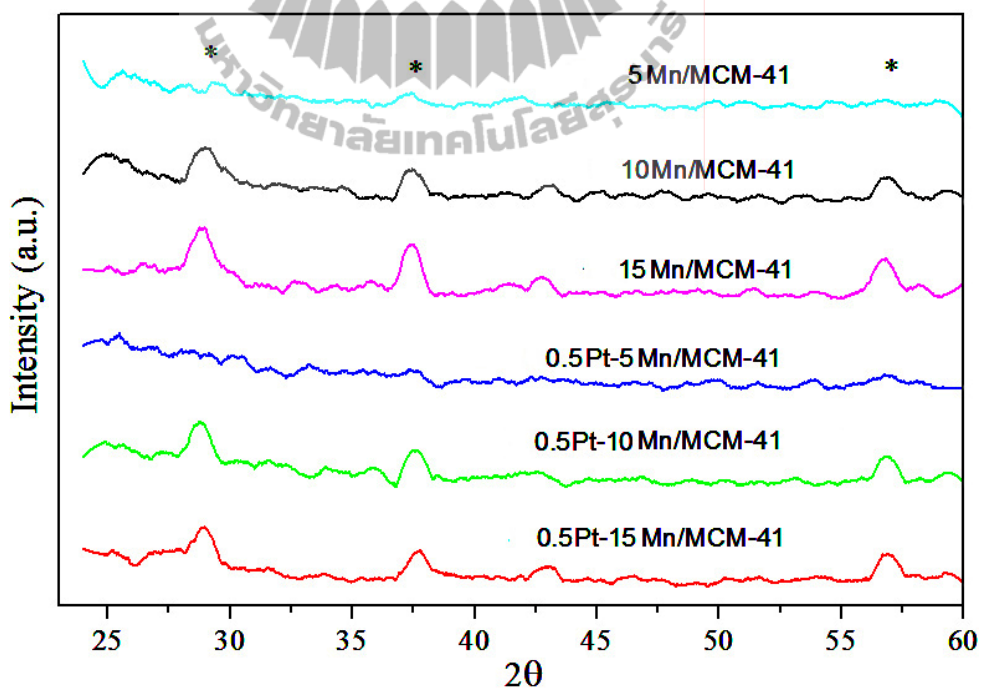
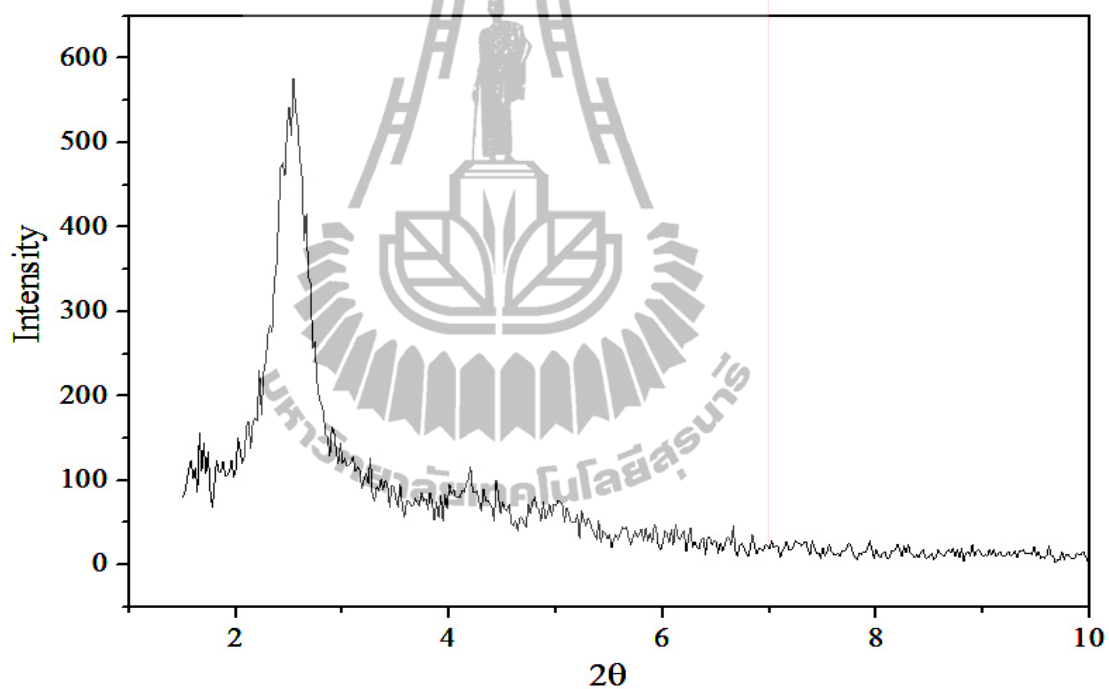
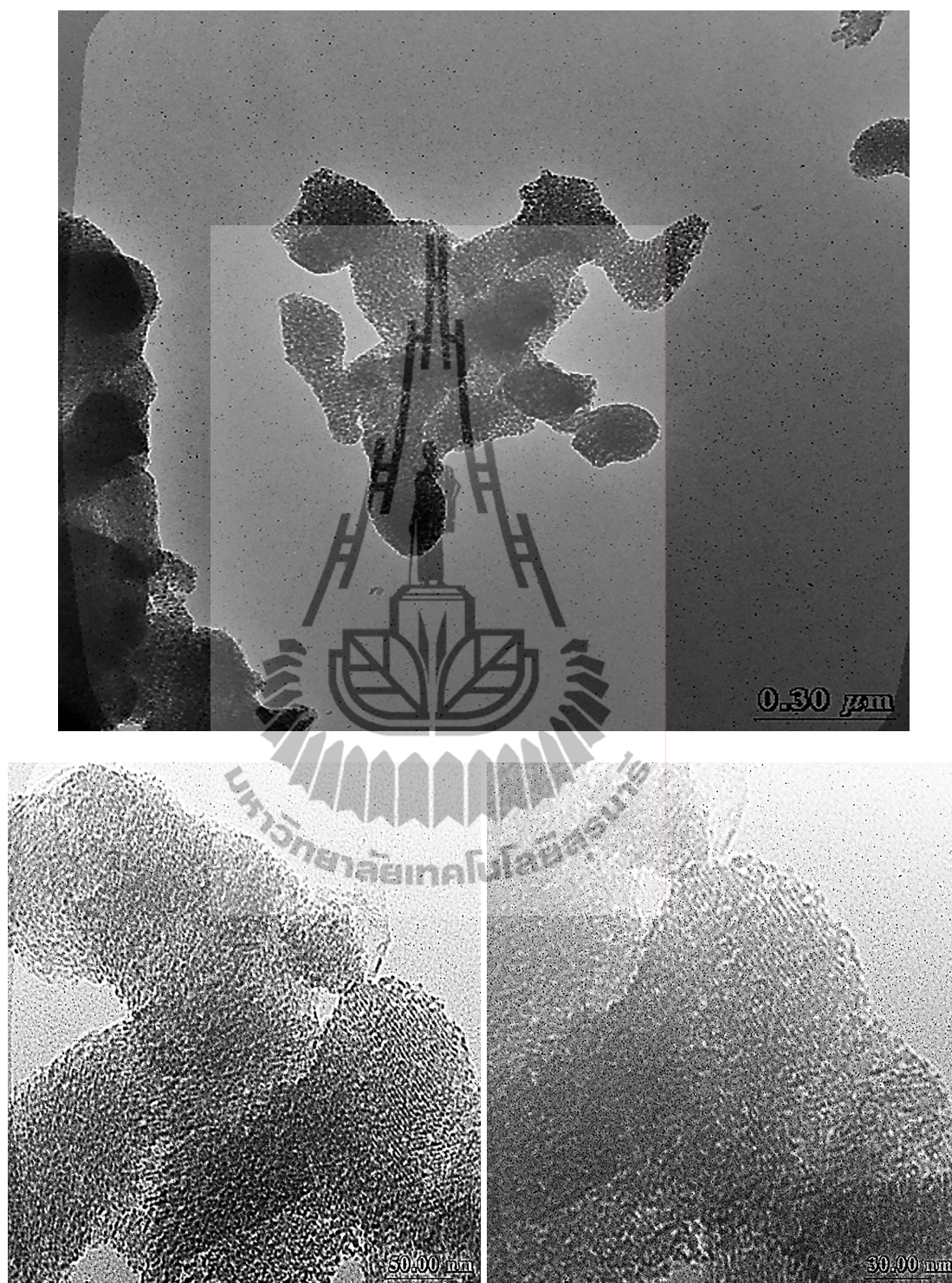


Figure 4.14 XRD powder patterns at high angle of mono- and bimetallic Mn catalysts.

The XRD pattern of 0.5Pt/RH-MCM-41 catalyst was shown in Figure 4.15. The intensity of the main peak of RH-MCM-41 slightly decreased compared to that of bare RH-MCM-41. An attempt to observe Pt particles by TEM images (Figure 4.16) was not successful because of low Pt loading. Pt particles were well dispersed on RH-MCM-41 support. Besides, uniform mesostructure of the support was still observed.

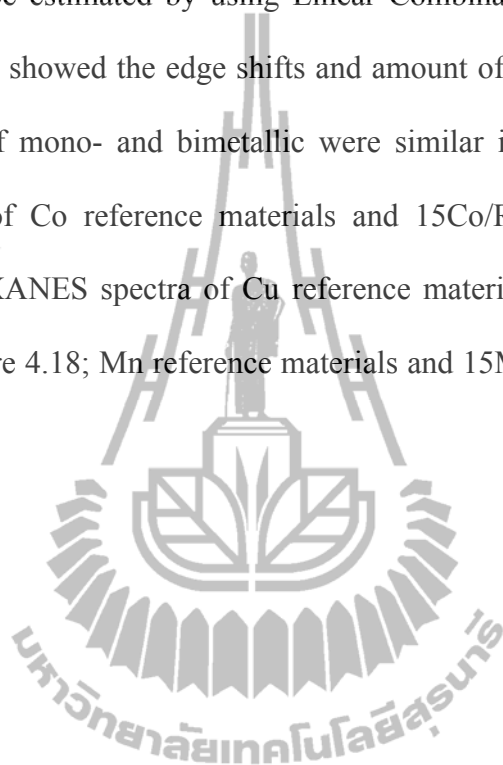


**Figure 4.15** XRD powder pattern of 0.5Pt/RH-MCM-41.



**Figure 4.16** TEM images of 0.5Pt/RH-MCM-41.

The forms of Co, Cu, and Mn on RH-MCM-41 in the mono- and bimetallic catalysts were studied by XANES. The oxidation state of each metal could be determined from the edge shift from that of the corresponding foil and the amount of oxide forms can be estimated by using Linear Combination Fitting of the XANES spectra. Table 4.4 showed the edge shifts and amount of oxide forms of each metal. The edge shifts of mono- and bimetallic were similar indicating the similar form. XANES spectra of Co reference materials and 15Co/RH-MCM-41 are shown in Figure 4.17; the XANES spectra of Cu reference materials and 15Cu/RH-MCM-41 are shown in Figure 4.18; Mn reference materials and 15Mn/RH-MCM-41 are shown in Figure 4.19.



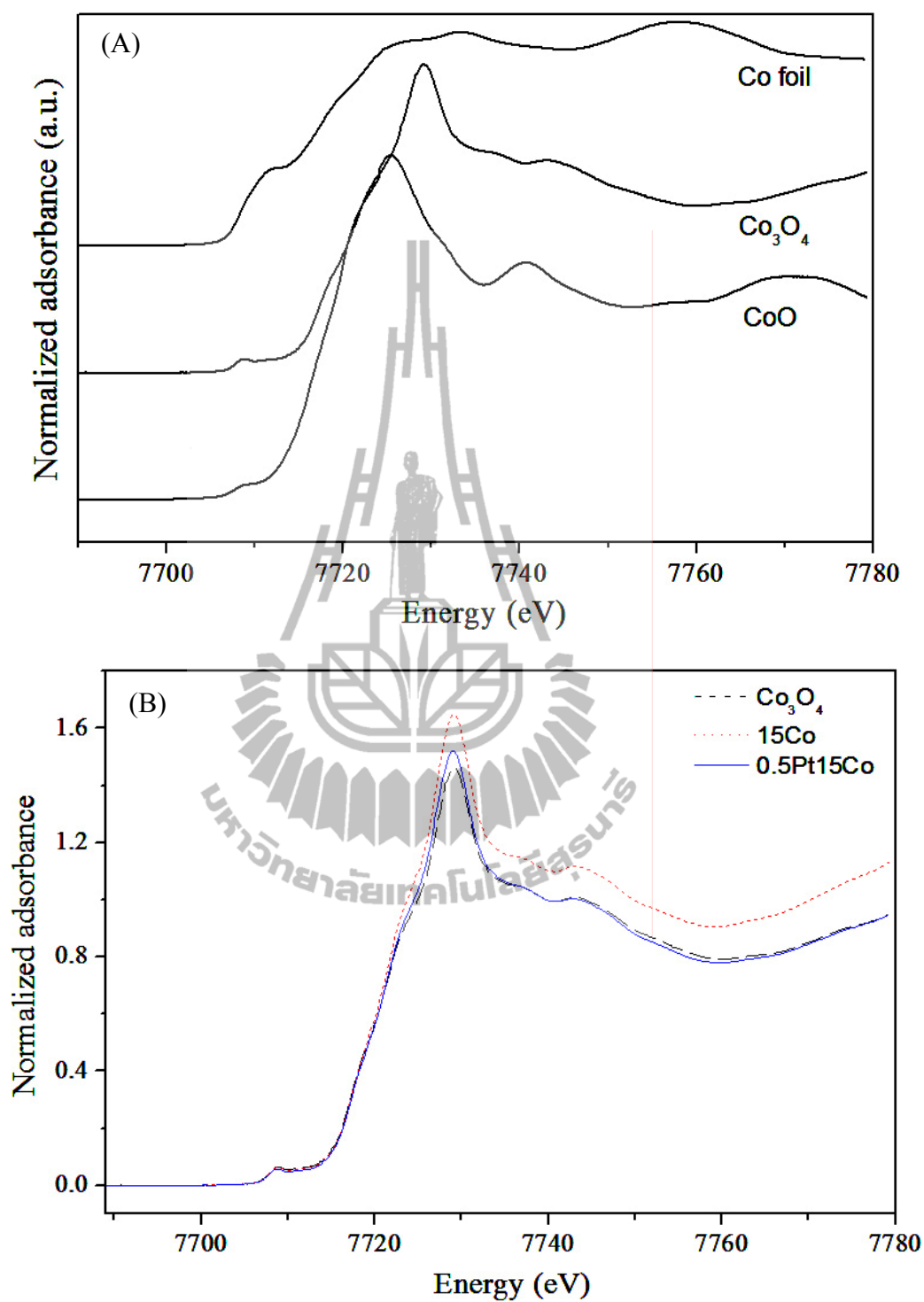


**Figure 4.17** The XANES spectra of Co reference materials (A) and 15Co/RH-MCM-41 and 0.5Pt15Co/RH-MCM-41 catalysts compared with  $\text{Co}_3\text{O}_4$  standard (B).

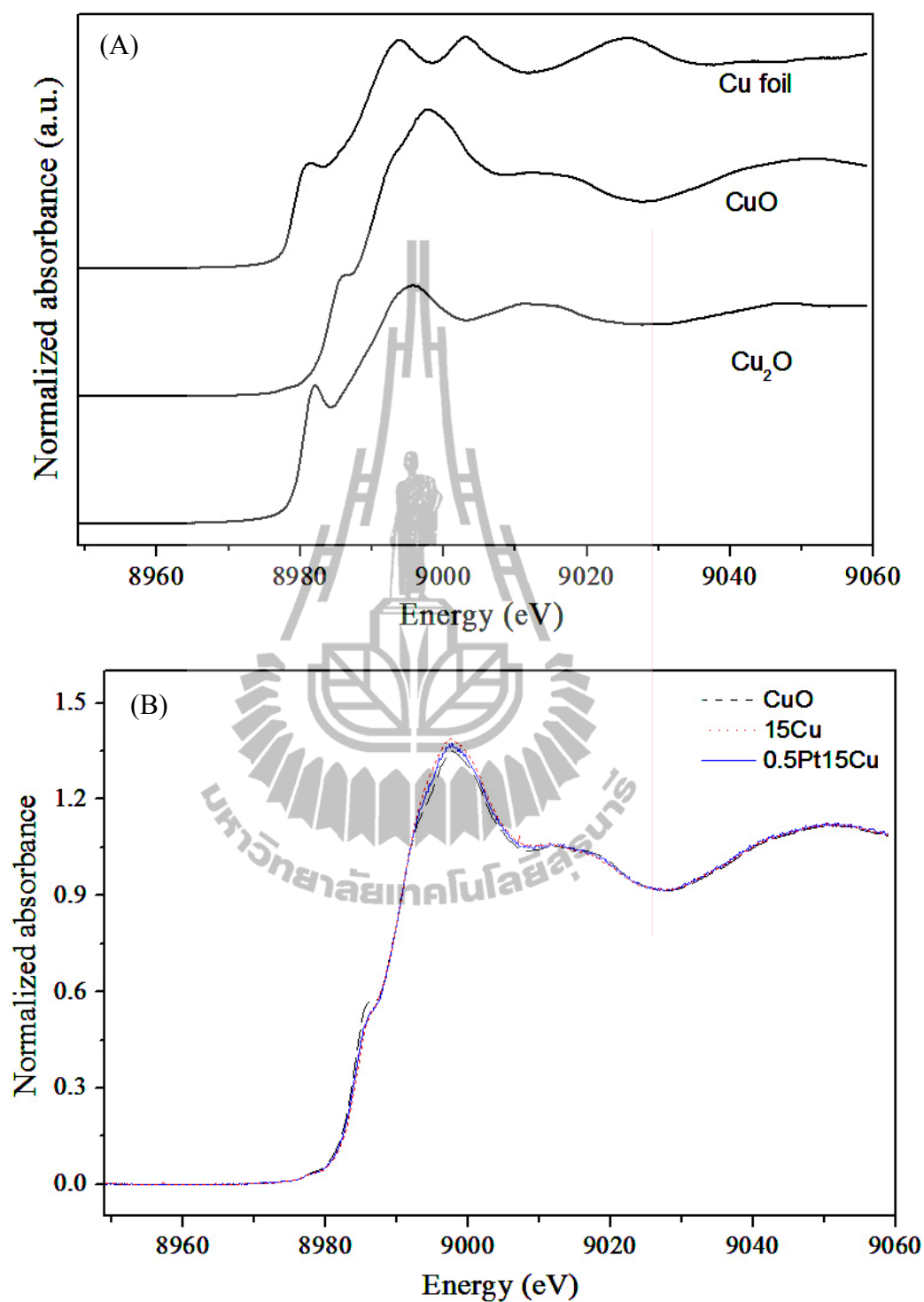


**Figure 4.18** The XANES spectra of Cu reference materials (A) and 15Cu/RH-MCM-41 and 0.5Pt15Cu/RH-MCM-41 catalysts compared with CuO standard (B).

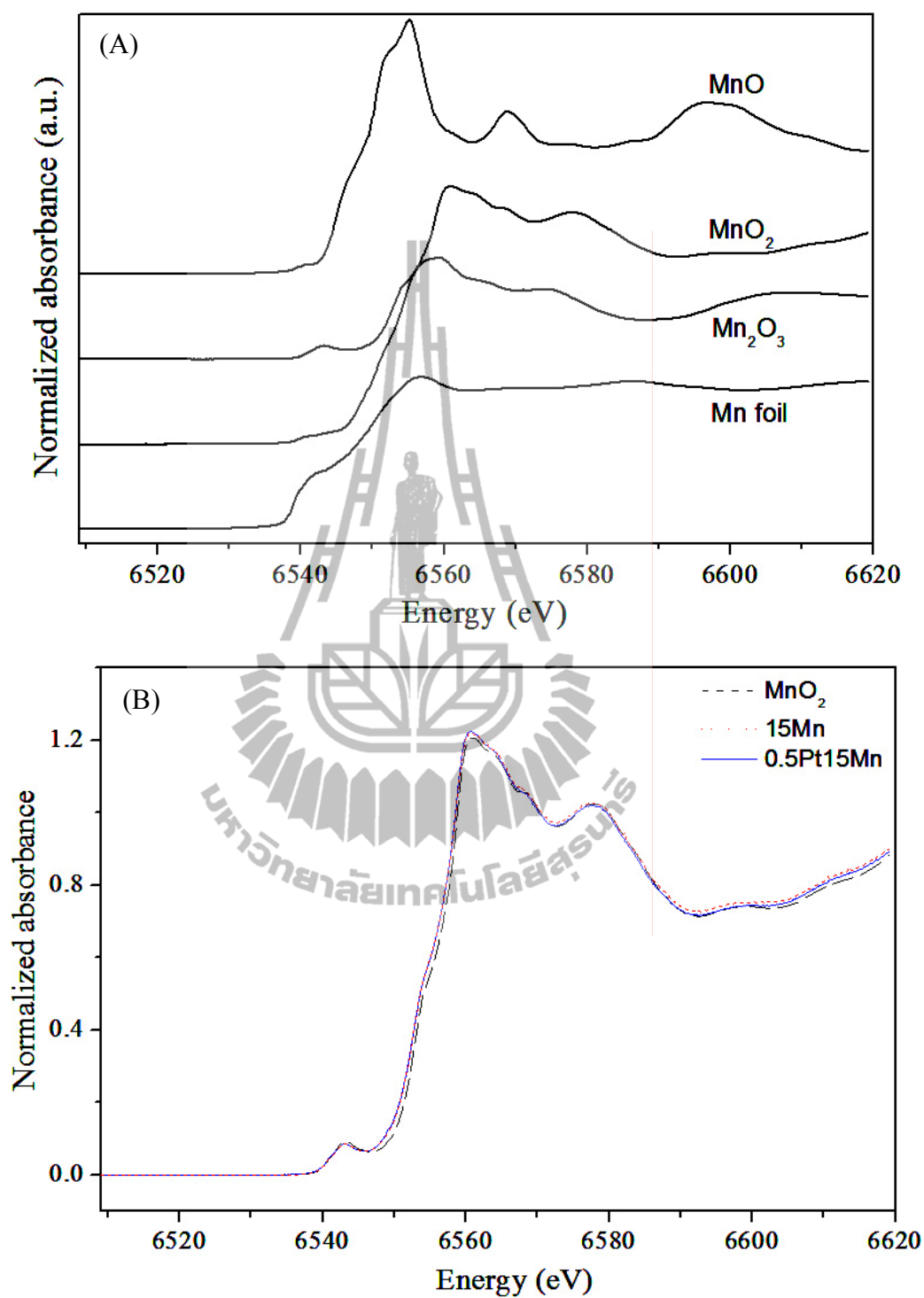


**Figure 4.19** The XANES spectra of Mn reference materials (A) and 15Mn/RH-MCM-41 and 0.5Pt15Mn/RH-MCM-41 catalysts compared with MnO<sub>2</sub> standard (B).

The edge shift and linear combination fitting corroborated that  $\text{Co}_3\text{O}_4$ ,  $\text{CuO}$ , and  $\text{MnO}_2$  were the only oxide form of Co, Cu, and Mn, respectively. (Table 4.4). The oxide forms suggested by the XANES results were consistent with the XRD results.

**Table 4.4** Edge energy, edge shift, and oxide components in catalysts.

Catalysts	K-edge position (eV)	Edge shift from corresponding foil (eV) <sup>a</sup>	Oxide components (wt%)	R-factor	Chi-square
15Co/RH-MCM-41	7727	18	$\text{Co}_3\text{O}_4$ (100%)	0.0013	0.26
0.5Pt-15Co/RH-MCM-41	7727	18	$\text{Co}_3\text{O}_4$ (100%)	0.0021	0.39
15Cu/RH-MCM-41	8991	12	$\text{CuO}$ (100%)	0.0007	0.16
0.5Pt-15Cu/RH-MCM-41	8991	12	$\text{CuO}$ (100%)	0.0004	0.07
15Mn/RH-MCM-41	6559	20	$\text{MnO}_2$ (90.3%), $\text{Mn}_2\text{O}_3$ (9.7%)	0.0001	0.01
0.5Pt-15Mn/RH-MCM-41	6559	20	$\text{MnO}_2$ (89.8%), $\text{Mn}_2\text{O}_3$ (10.2%)	0.0001	0.02

<sup>a</sup> K-edge of Co, Cu and Mn foil were 7709, 8979, and 6539 eV, respectively.

#### 4.4 Ethanol-TGA

Ability of catalysts in ethanol adsorption was investigated by ethanol-TGA in the absence of air. As shown in Table 4.5, the amount of ethanol adsorbed on RH-MCM-41 and all catalysts were in the range of 4.3-6.5 wt%. The RH-MCM-41



support adsorbed ethanol by using silanol groups (Zhao, Lu, Whittaker, Millar, and Zhu, 1997). Although all catalysts except 0.5Pt-15Cu/RH-MCM-41 had lower surface area than RH-MCM-41, they showed higher ethanol adsorption than RH-MCM-41 indicating that ethanol also adsorbed on the metal and metal oxides. The ability to adsorb ethanol had a similar trend to that of BET surface area of the catalysts. On the bimetallic catalysts, the ability to adsorb ethanol decreased when BET surface area decreased due to poor dispersion of metals, i.e, large particles had low surface area.

**Table 4.5** Change of catalysts weight from ethanol adsorption from ethanol-TGA.

Sample	Weight (mg)	Weight gain (mg)	Wt% ethanol adsorption
RH-MCM-41	45.1	2.1	4.7
0.5Pt/RH-MCM-41	49.3	2.8	5.7
0.5Pt-5Co/RH-MCM-41	49.5	2.7	5.5
0.5Pt-10Co/RH-MCM-41	49.4	3.2	6.5
0.5Pt-15Co/RH-MCM-41	49.3	3.1	6.3
0.5Pt-5Cu/RH-MCM-41	49.2	3.2	6.5
0.5Pt-10Cu/RH-MCM-41	48.6	2.6	5.4
0.5Pt-15Cu/RH-MCM-41	48.5	2.1	4.3
0.5Pt-5Mn/RH-MCM-41	48.7	3.0	6.2
0.5Pt-10Mn/RH-MCM-41	49.9	3.1	6.2
0.5Pt-15Mn/RH-MCM-41	47.8	2.8	5.9

In the ethanol-TGA experiment, catalysts were reduced by H<sub>2</sub> at 200 °C. Tsoncheva, Rosenholm, Linden, Ivanova, and Minchev (2007) found that oxide of Cu in CuO/SBA-15 was reduced to metallic form at 200 °C whereas Co and Mn were only partially reduced. Temperature programmed reduction (TPR) study of Mn/SBA-15 and Co/SBA-15 suggested that Mn and Co could be reduced to metallic form at 400 °C (Pérez, Navarro, Delgado, and Montes, 2011; Tsoncheva, Ivanova, Rosenholm, and Linden, 2009). Because amounts of adsorbed ethanol on Co and Mn catalysts were higher than that on the Cu one, ethanol adsorption was not favorable on supported Cu.

Although 0.5Pt/RH-MCM-41 contained a small amount of Pt, it showed high ethanol adsorption capacity. In general, Pt oxide could be reduced completely by H<sub>2</sub> at 200 °C. The ethanol-TGA result indicated that ethanol adsorbed on both Pt and RH-MCM-41.

In bimetallic Co catalysts, the ethanol adsorption on 0.5Pt5Co/RH-MCM-41 was lower than that on 0.5Pt/RH-MCM-41 possibly because Co at this loading was not reduced to metallic form due to strong metal-support interaction. The ethanol adsorption occurred mainly on the reduced Pt and RH-MCM-41. Because Co covered some silanol groups (Si-OH) of RH-MCM-41, the adsorption sites were decreased.

The ethanol adsorptions on 0.5Pt10Co/RH-MCM-41 and 0.5Pt15Co/RH-MCM-41 were higher than that of 0.5Pt/RH-MCM-41. The results suggested that additional adsorption took place on Co. With high Co loading, large particles of cobalt oxides were expected and they could be more easily reduced (Khemthong, Klysubun, Prayoonpokarach, Roessner, and Wittayakun, 2010). However, higher Co

loading in 0.5Pt15Co/RH-MCM-41 resulted in a poorer dispersion, i.e., large particles of Co oxides. After reduction, this catalyst had less active Co site.

On the bimetallic Cu catalysts, ethanol also adsorbed on the Cu sites. However, the adsorbed ethanol decreased when Cu loading increased. Because supported Cu could be reduced easily (Tsoncheva *et al.*, 2007), the metal-support interaction was weak. Consequently, Cu could migrate easily on the support and agglomerate to form large particles resulting in less active surface sites.

On the bimetallic Mn catalysts, ethanol also adsorbed on the Mn sites. With increase of Mn loading, the amount adsorbed did not increase suggesting large particle and blocking of silanol groups of RH-MCM-41. The degree of agglomeration in Mn catalysts was less than that in the Cu catalysts.

#### 4.5 Ethanol-TPD

In the ethanol-TPD analysis in the absence of air, the desorbed species were detected by a mass spectrometer (MS). The recorded MS fragments from possible desorbed species had several  $m/e$  values and can be ranged from the highest intensity, for examples, ethanol, 31, 45, 46, and 29; acetaldehyde, 29, 44, 43, and 15; and  $\text{CO}_2$ , 44, 28, and 16. For simplicity in the following figures, only the most intense peak of each species was displayed; the existence of other peaks was used to assist the identification. Although the fraction with  $m/e$  of 44 could be from either acetaldehyde or  $\text{CO}_2$ , it was reported that desorption of  $\text{CO}_2$  occurred at above 300 °C. Consequently, the position at low temperature was assigned to acetaldehyde and that at above 300 °C was assigned to  $\text{CO}_2$ .

The main desorbed species from all catalysts were ethanol followed by acetaldehyde which was observed at around 100 °C. The results implied that ethanol adsorbed associatively (i.e., without any bond cleavage) on all catalysts (see the adsorption mode 1 in Scheme 4.1). This adsorbed species could desorb as molecular ethanol or convert simultaneously to other surface species including acetaldehyde precursors. Desorption of acetaldehyde occurred through ethanol dehydrogenation by breaking the O–H bond to produce ethoxy species (see the adsorption mode 2 in Scheme 4.1). Further arrangement to remove another hydrogen atom resulted in acetaldehyde.

TPD profile on bare RH-MCM-41 (Figure 4.20) shows ethanol desorption peaks at 100 and 250 °C. The result suggested that there were two types of adsorption sites on RH-MCM-41 and the interactions were possibly via hydrogen bond with silanol groups. Zhao *et al.* (1997) studied types of silanol groups on MCM-41 by using pyridine-TPD and reported the desorption activation energies of 54.2 and 91.4 kJ/mol from hydrogen-bonded (SiOH---OHSi) and free SiOH groups, respectively. In addition, a small amount of ethylene (C<sub>2</sub>H<sub>4</sub>) was detected at 400 °C as a result from dehydration of ethanol adsorbed on acid sites (Trawczyński, Bielak, and Mišta, 2005). The reaction occurred via a dissociative adsorption of ethanol via C–O bond cleavage, as shown in the third adsorption mode in Scheme 4.1 to produce surface ethyl and hydroxyl groups. Trawczyński *et al.* (2005) reported that an acidic support like Al<sub>2</sub>O<sub>3</sub> has high acid sites which facilitate the formation of diethyl ether and/or ethylene via dehydration of ethanol. In contrast, titania (TiO<sub>2</sub>) which is a weak acid support generated only negligible amounts of these compounds. Because the siliceous of RH-MCM-41 in this work contained only weakly acidic silanol groups

(Jentys, Kleestorfer, and Vinek, 1999), only a small amount of  $C_2H_4$  was detected. When metal precursors were deposited on RH-MCM-41, metal ions interacted with acid site of RH-MCM-41. Therefore, acid sites decreased and the products from dehydration were not observed in the TPD results.

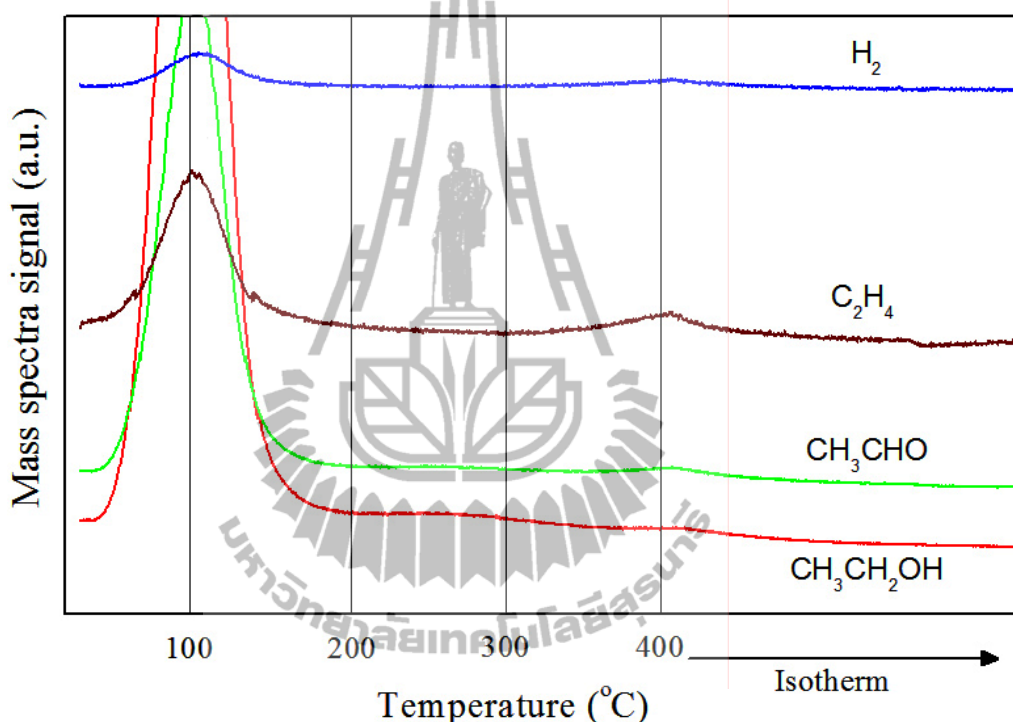


**Figure 4.20** Ethanol-TPD profiles on RH-MCM-41.

After reduced at 200 °C, Pt species on the catalyst was likely converted to metallic form which is active for dissociative adsorption of ethanol by breaking C–O and C–C bonds (de Lima *et al.*, 2009) (adsorption mode 3 and 4 in Scheme 4.1). From C–O bond breaking, ethylene and water could be attributed as ethanol dehydration products. From C–C bond breaking generated CO,  $CH_4$ , and  $H_2$  could be attributed as ethanol decomposition products. The availability of hydrogen could be

responsible for hydrogenation of the surface ethylene which produced  $C_2H_6$  as detected in the ethanol-TPD of Pt catalyst at high temperature (Figure 4.21).

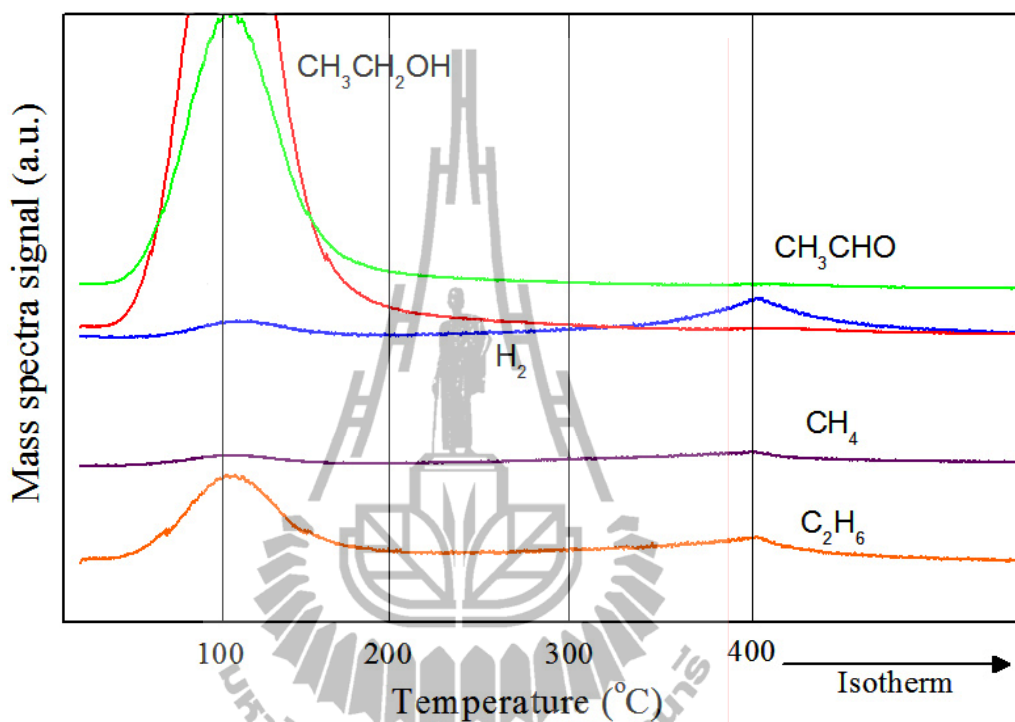
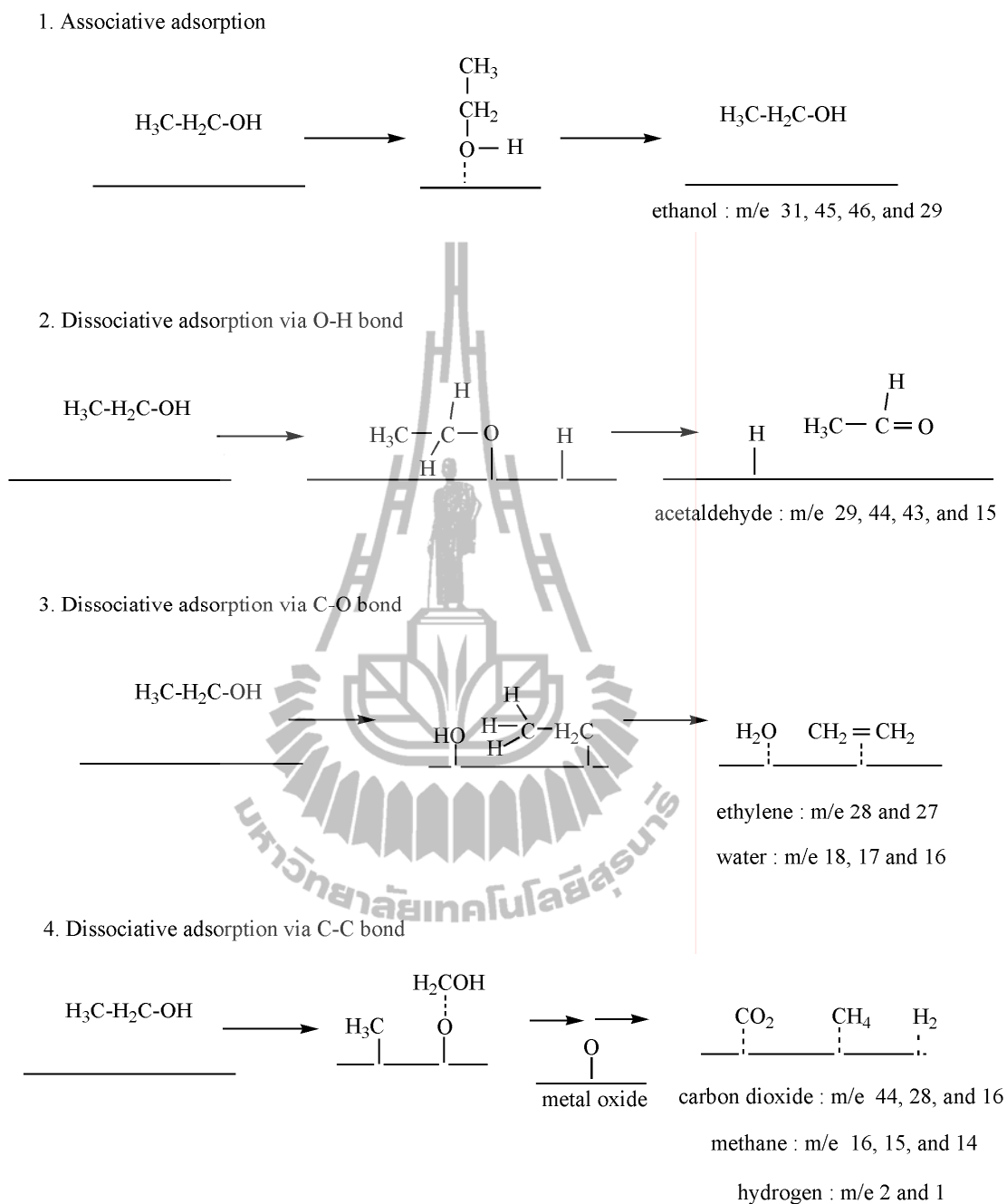


**Figure 4.21** Ethanol-TPD profiles on 0.5Pt/RH-MCM-41.

On the monometallic 15Co/RH-MCM-41, the decomposition products and  $CO_2$  were detected in the ethanol-TPD profile (Figure 4.22A). These products could be derived from decomposition of ethanol and/or acetaldehyde. The adsorption could be through a cleavage of the C–C bond and generated  $-CH_2OH$  surface species which was further converted to  $CO_2$  at 300-400 °C (adsorption mode 4 in Scheme 4.1).



**Scheme 4.1** Possible adsorption modes of ethanol and surface species derived from ethanol-TPD results.

Ethanol-TPD profiles of 15Mn/RH-MCM-41 (Figure 4.22C) only showed a small amount of CO<sub>2</sub> while that of 15Cu/RH-MCM-41 (Figure 4.22B) did not show

any  $\text{CO}_2$  peaks. In addition,  $\text{CH}_4$  was not observed on both catalysts, so they were not active for the rupture of ethanol molecule.

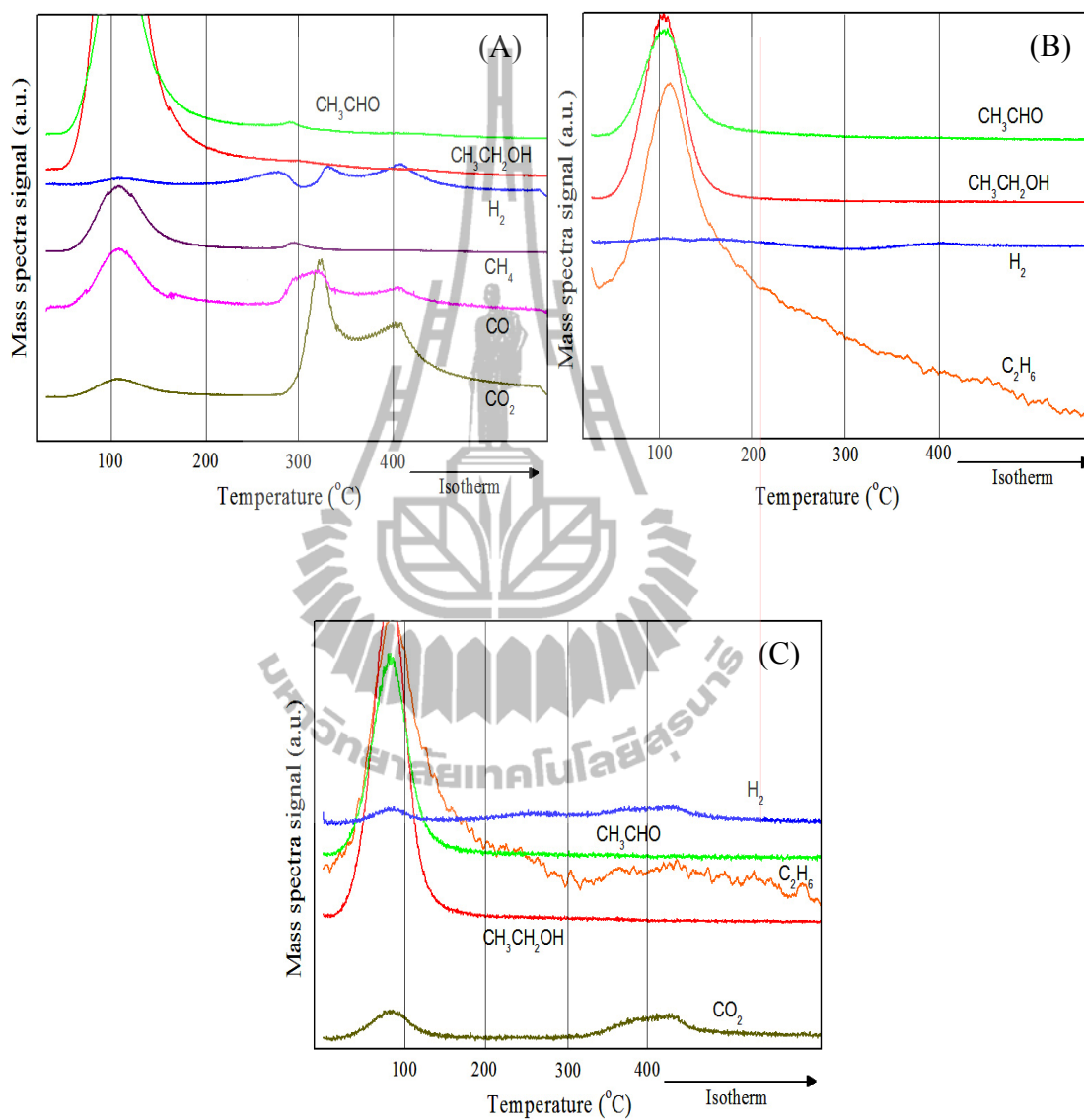


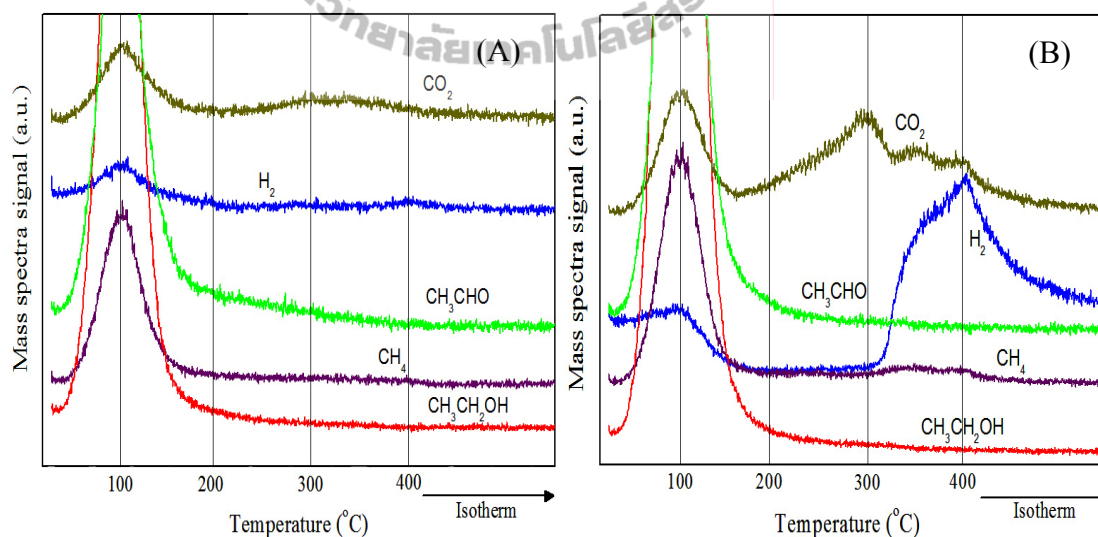
**Figure 4.22** Ethanol-TPD profiles on 15Co/RH-MCM-41 (A), 15Cu/RH-MCM-41 (B), and 15Mn/RH-MCM-41 (C).

Before the ethanol-TPD experiment, all catalysts were reduced by  $\text{H}_2$  at 200 °C. In such condition Cu in both mono- and bimetallic catalysts was converted to



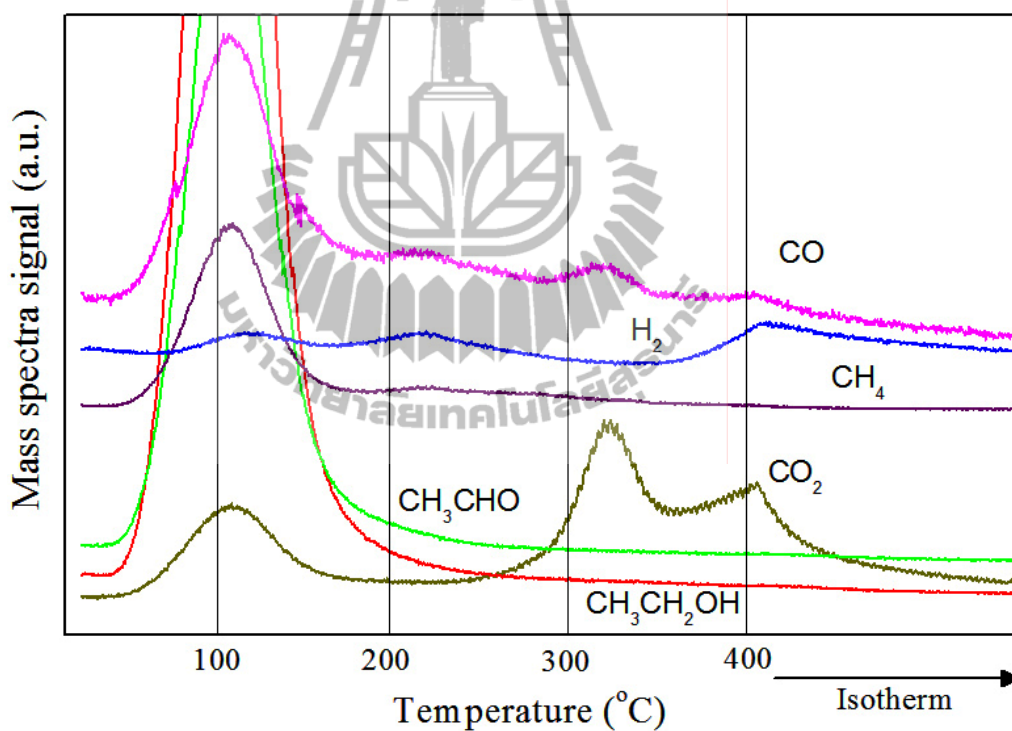
metallic form. In contrast, Co and Mn were still mainly in oxide forms (Tsoncheva *et al.*, 2009; Pérez *et al.*, 2010) and could supply oxygen for ethanol oxidation to generate  $\text{CO}_2$ . The form of Mn in 15Mn/RH-MCM-41 was mainly  $\text{MnO}_2$  as confirmed by XRD and XANES results. However, this form was not very active for ethanol oxidation (Lamaita *et al.*, 2005) because only a small amount of  $\text{CO}_2$  was observed.

From bimetallic 0.5Pt-15Cu/RH-MCM-41 and 0.5Pt-15Mn/RH-MCM-41, ethanol Decomposition was observed. Ethanol-TPD of 0.5Pt-15Cu/RH-MCM-41 (Figure 4.23A) and 0.5Pt-15Mn/RH-MCM-41 (Figure 4.23B) showed higher amount of  $\text{CO}_2$ ,  $\text{CH}_4$  and  $\text{H}_2$  than those of monometallic 15Cu/RH-MCM-41 and 15Mn/RH-MCM-41, respectively. These results suggested that the co-existence of Pt and base metal oxides on the same support could improve catalytic activity.



**Figure 4.23** Ethanol-TPD profiles on 0.5Pt-15Cu/RH-MCM-41 (A) and 0.5Pt-15Mn/RH-MCM-41 (B).

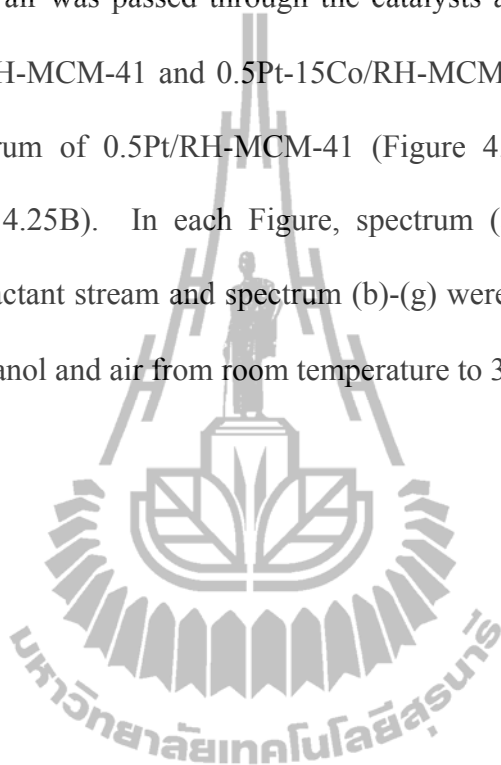
The ethanol-TPD of 0.5Pt-15Co/RH-MCM-41 (Figure 4.24) revealed the formation of CH<sub>4</sub>, CO, CO<sub>2</sub>, and H<sub>2</sub> similar to that of 15Co/RH-MCM-41. The similarity could be a result from the similar form of Co in both catalysts. However, CH<sub>4</sub> and H<sub>2</sub> were observed at temperature about 40 °C lower than 15Co/RH-MCM-41. In addition, CO<sub>2</sub> was clearly produced on 0.5Pt-15Co/RH-MCM-41 more than bimetallic Cu and Mn catalysts. From these results, only the catalysts containing oxides of cobalt were studied by *in situ* IR and in the flow reactor.



**Figure 4.24** Ethanol-TPD profiles on 0.5Pt-15Co/RH-MCM-41.

#### 4.6 Ethanol oxidation studied by *in situ* IR

The information obtained during ethanol oxidation from *in situ* IR was useful for an elaboration of reaction mechanism on the catalyst surface. After the mixture of ethanol vapor and air was passed through the catalysts at 30-300 °C, the *in situ* IR spectra of 0.5Pt/RH-MCM-41 and 0.5Pt-15Co/RH-MCM-41 were collected. Figure 4.25 shows spectrum of 0.5Pt/RH-MCM-41 (Figure 4.25A) and 0.5Pt-15Co/RH-MCM-41 (Figure 4.25B). In each Figure, spectrum (a) was recorded before an exposure to the reactant stream and spectrum (b)-(g) were recorded after an exposure to a mixture of ethanol and air from room temperature to 300 °C.



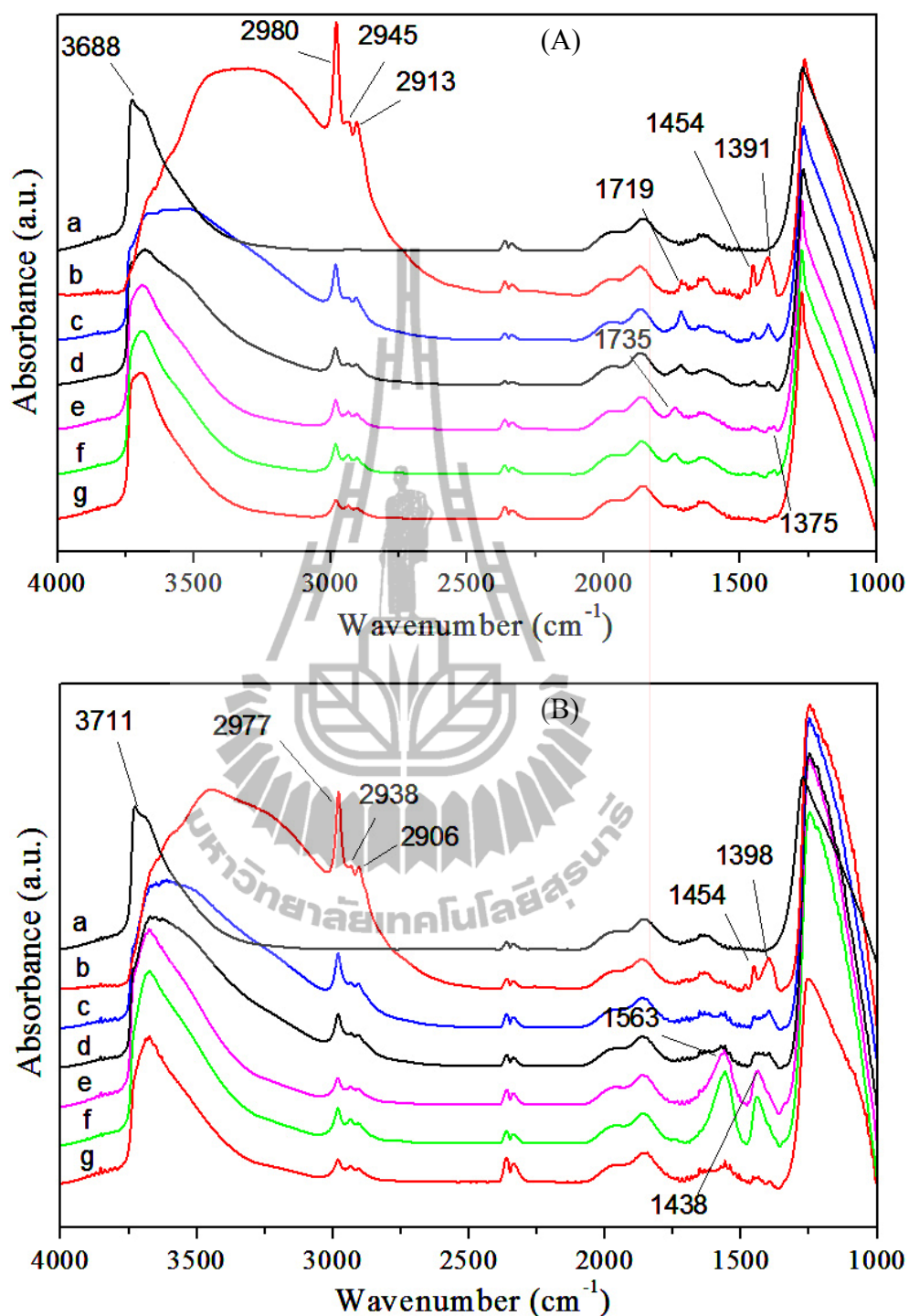


**Figure 4.25** *in situ* IR spectra measured on 0.5Pt/RH-MCM-41 (A) and 0.5Pt-15Co/RH-MCM-41 (B) during ethanol oxidation. Spectrum of both samples were recorded at (a) 30 °C (under vacuum), (b)-(g) at 30, 100, 150, 200, 250, and 300 °C (under a flow of ethanol and air).

The band assignments of the corresponding vibration modes and cited references are listed in Table 4.6. The spectrum from both samples had several similarities. The band at 1969 and 1875  $\text{cm}^{-1}$  were assigned to overtones of lattice vibrations of RH-MCM-41 structure (Bellat *et al.*, 1999). At the beginning (spectrum b in Figure 4.25A and 4.25B), a broad band in the range of 3015-3640  $\text{cm}^{-1}$  corresponding to the ethanol hydroxyl group (-OH) was clearly observed because the surface was saturated with ethanol. At increased temperature, the band diminished allowing the observation of a sharp band at 3688 and 3711  $\text{cm}^{-1}$  corresponding to silanol groups on the surface of both samples. A strong vibration band of Si-O-Si in the spectrum of both samples was observed at 1266 and 1250  $\text{cm}^{-1}$ , respectively. The peaks of both catalysts before the ethanol reaction contained bands at 2338-2375  $\text{cm}^{-1}$  indicating the presence of  $\text{CO}_2$ , thus, this  $\text{CO}_2$  was not from the reaction. The broad bands at region 3650-3010  $\text{cm}^{-1}$  could be attributed to stretching modes of ethanol hydroxyl group that adsorbed over the support and metal (Akdin *et al.*, 2008). Those bands decreased with the temperature indicating that physisorbed ethanol was removed from the surface or changed to other species.

**Table 4.6** Band assignments and vibration modes during ethanol oxidation on 0.5Pt/RH-MCM-41 and 0.5Pt15Co/RH-MCM-41.

Wavenumber/ $\text{cm}^{-1}$		Assignment	Reference
0.5Pt	0.5Pt15Co		
Species groups on silica surface			
3688	3711	Si-OH outside channel ( $\nu$ OH) (sharp)	(Jentys et al., 1999)
1266	1250	Si-O-Si	(Haga and Watanabe, 1996)
3016-3625	3016-3641	( $\nu$ OH) of physisorbed ethanol	(Akdim <i>et al.</i> , 2008)
Ethoxy species			(Akdim <i>et al.</i> , 2008)
2980	2977	$\nu_{\text{as}}$ CH <sub>3</sub>	
2945	2938	$\nu_{\text{as}}$ CH <sub>2</sub>	
2913	2906	$\nu_{\text{s}}$ CH <sub>3</sub>	
2875	2875	$\nu_{\text{s}}$ CH <sub>2</sub> (shoulder)	
1484	1484	$\delta_{\text{as}}$ CH <sub>2</sub>	
1454	1454	$\delta_{\text{as}}$ CH <sub>3</sub>	
1391	1398	$\delta_{\text{s}}$ CH <sub>3</sub>	
Acetate species			
1735	-	$\nu_{\text{as}}$ CO (monodentate)	(Nagai and Gonzalez, 1985)

**Table 4.6** (Continued).

Wavenumber/ cm <sup>-1</sup>		Assignment	Reference
0.5Pt	0.5Pt15Co		
		Acetate species	
1560	1563	$\nu_{as}$ OCO (bidentate)	(Yee, Morrison, and Idriss, 1999; Song and Ozkan, 2009)
1438	1438	$\nu_s$ OCO (bidentate)	(Yee <i>et al.</i> , 1999; Song and Ozkan, 2009)
-	1344	$\delta$ CH <sub>3</sub> (bidentate)	(Yee <i>et al.</i> , 1999; Song and Ozkan, 2009)
1375	-	$\nu_s$ CO (monodentate)	(Nagai and Gonzalez, 1985)
		Acetaldehyde	
1719	-	$\nu$ CO	(Scott, Goeffroy, Chiu, Blackford, and Idriss, 2008)

**Table 4.6** (Continued).

Wavenumber/ $\text{cm}^{-1}$		Assignment	Reference
0.5Pt	0.5Pt15Co		
		$\text{CO}_2$ physisorption	(Song and Ozkan, 2009)
2363	2375		
2338	2344		
		$\text{H}_2\text{O}_{\text{ad}}$	
1625	1633	( $\delta$ OH)	(Yu and Chuang, 2007)

The *in situ* IR result could lead to identification of intermediate species over the catalysts surface. Figure 4.26-4.31 show IR spectra during ethanol oxidation on both catalysts at 30-300 °C, respectively. These figures could be used to derive mechanism of surface reaction on both catalysts. In the 0.5Pt/RH-MCM-41 case (Figure 4.26), the band of ethoxy species and acetaldehyde were observed at 30 °C after the catalyst was exposed to the stream of ethanol and air. The bands at region 2980-2875  $\text{cm}^{-1}$  were attributed to stretching vibration of  $-\text{CH}_3$  and  $-\text{CH}_2-$  groups of ethoxy species. These bands gradually decreased with the temperature indicating desorption of molecular ethanol as well as transformation to other species. The band at 1719  $\text{cm}^{-1}$  was attributed to stretching vibration of carbonyl of acetaldehyde. This band was the most intense at 100 °C (Figure 4.27), gradually decreased with the temperature, merged with the peak at 1735  $\text{cm}^{-1}$  and was nearly unobservable at 300



°C (Figure 4.31). These results indicated that acetaldehyde was an intermediate of ethanol oxidation produced at low temperatures from the ethoxy species and converted to other species at high temperatures. The band at 1735 and 1375  $\text{cm}^{-1}$  were assigned to carbonyl of monodentate acetate species which could be observed at 150 °C (Figure 4.28) and clearly visible at 200 (Figure 4.29) and 250 °C (Figure 4.30). In addition, weak bands corresponding to bidentate acetate species were observed at 1560 and 1438  $\text{cm}^{-1}$ . From the above result, the mechanism of ethanol oxidation over 0.5Pt/RH-MCM-41 was proposed in Scheme 4.2. First, ethanol adsorbed on the catalysts through its hydroxyl group to form ethoxy species, rearranged on the surface to form parallel adsorbed acetaldehyde (Nagai and Gonzalez, 1985), transformed to monodentate acetate with surface oxygen, and finally dissociated/desorbed as products ( $\text{CO}_2$  and  $\text{H}_2\text{O}$ ).

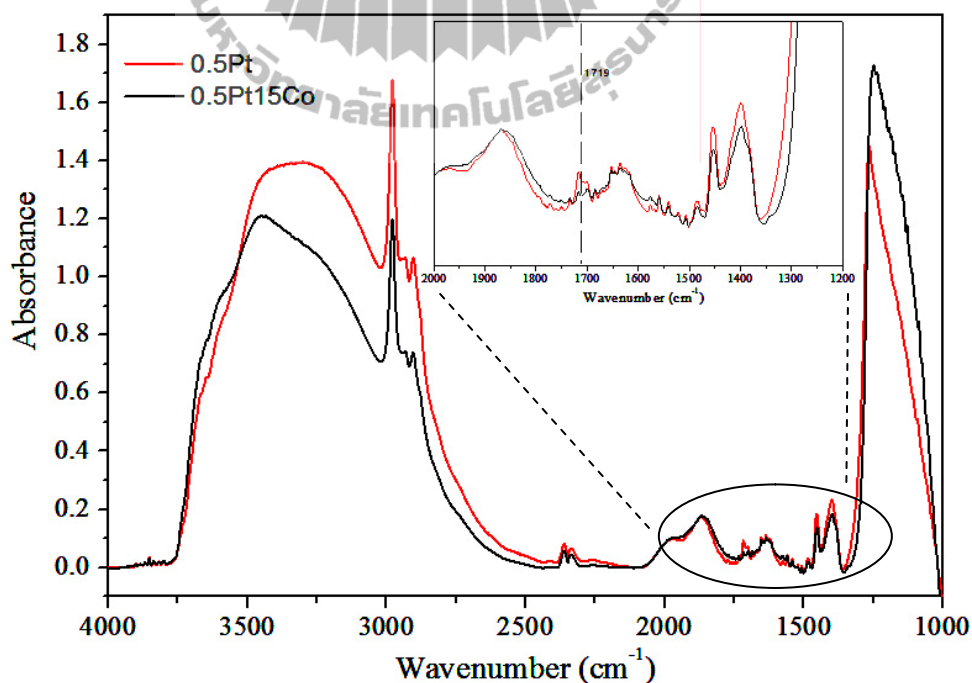


**Figure 4.26** *In situ* IR spectra measured on 0.5Pt/RH-MCM-41 (red line) and 0.5Pt-15Co/RH-MCM-41 (black line) during ethanol oxidation at 30 °C.

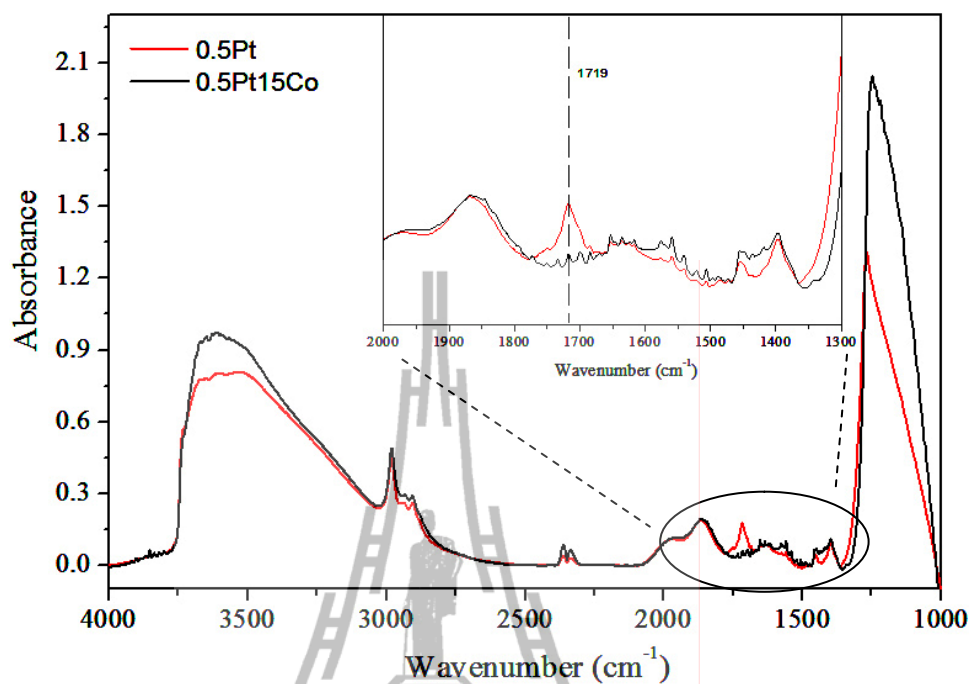


**Figure 4.27** *In situ* IR spectra measured on 0.5Pt/RH-MCM-41 (red line) and 0.5Pt-15Co/RH-MCM-41 (black line) during ethanol oxidation at 100 °C.

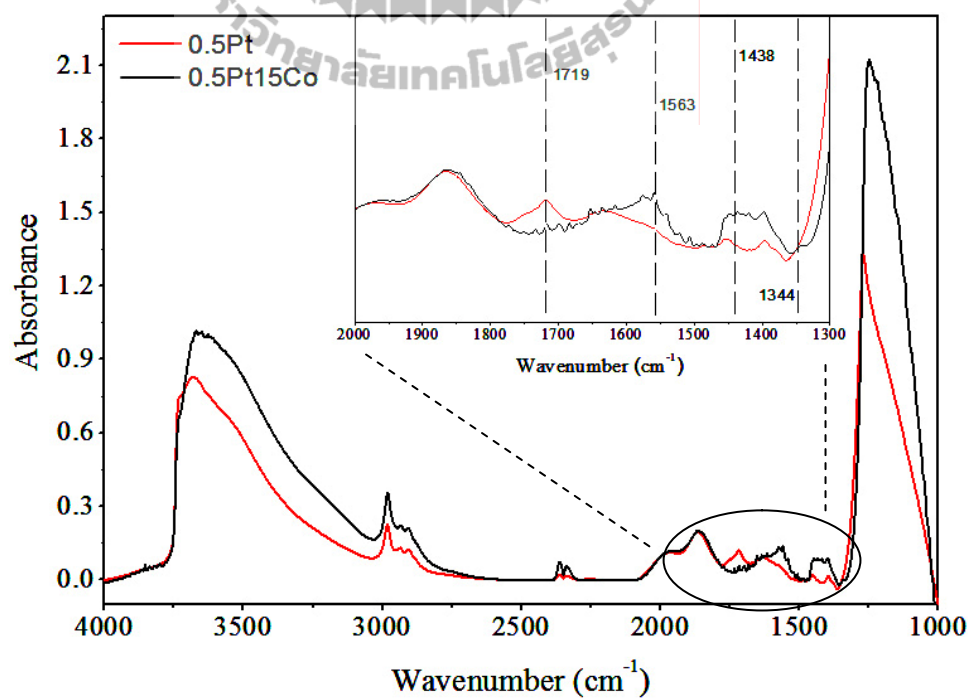


**Figure 4.28** *In situ* IR spectra measured on 0.5Pt/RH-MCM-41 (red line) and 0.5Pt-15Co/RH-MCM-41 (black line) during ethanol oxidation at 150 °C.

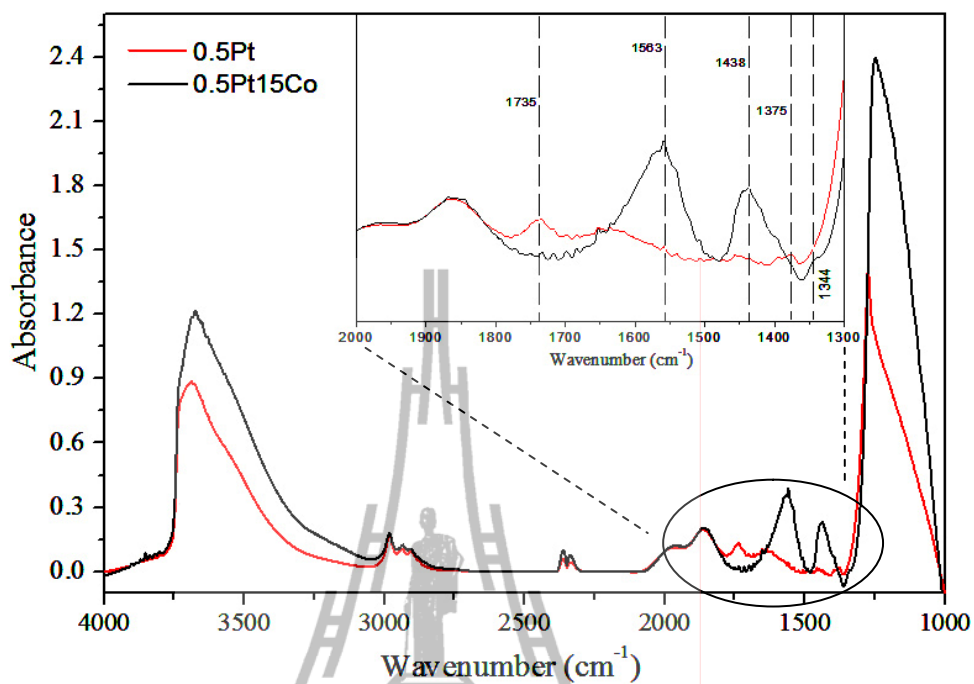


**Figure 4.29** *In situ* IR spectra measured on 0.5Pt/RH-MCM-41 (red line) and 0.5Pt-15Co/RH-MCM-41 (black line) during ethanol oxidation at 200 °C.

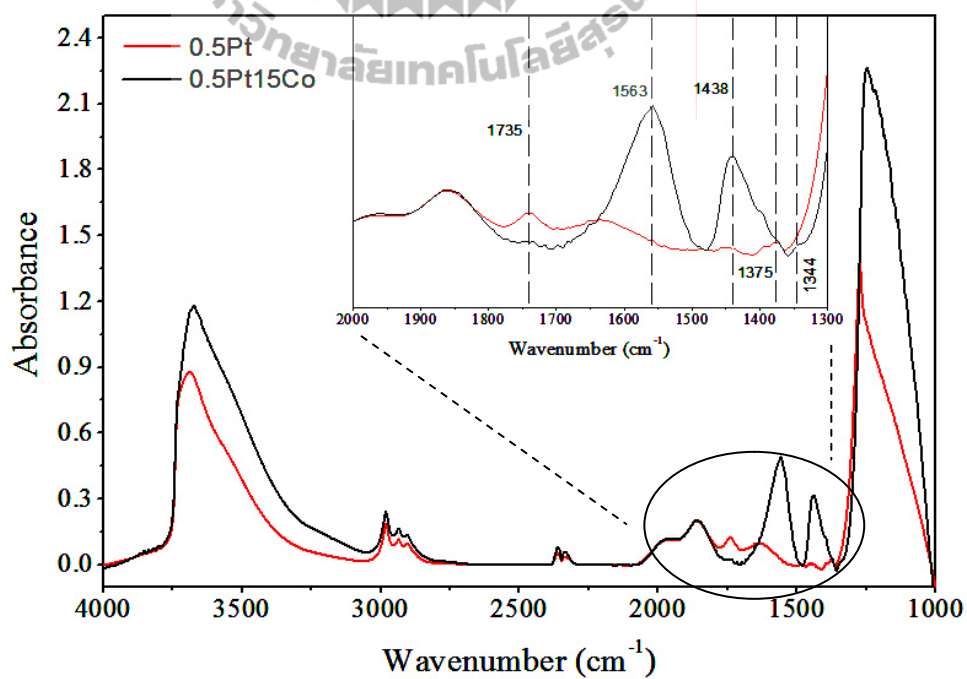


**Figure 4.30** *In situ* IR spectra measured on 0.5Pt/RH-MCM-41 (red line) and 0.5Pt-15Co/RH-MCM-41 (black line) during ethanol oxidation at 250 °C.

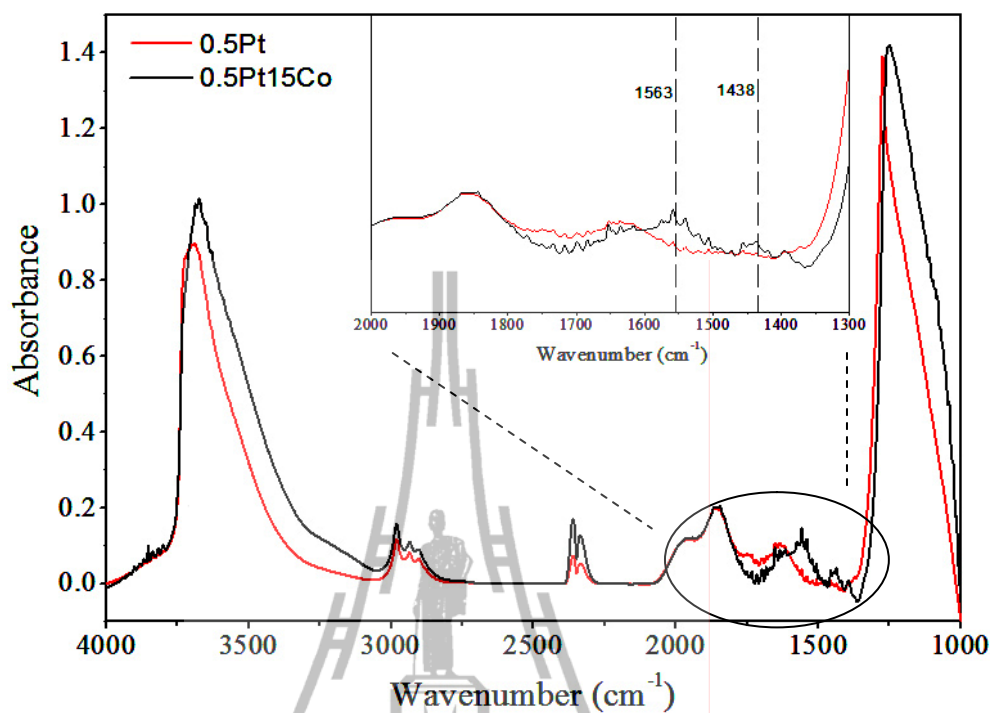
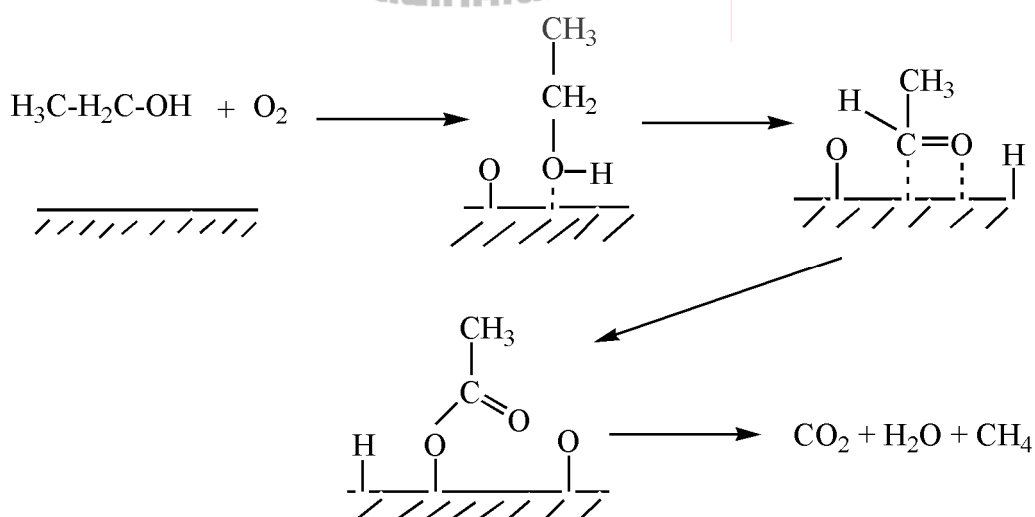
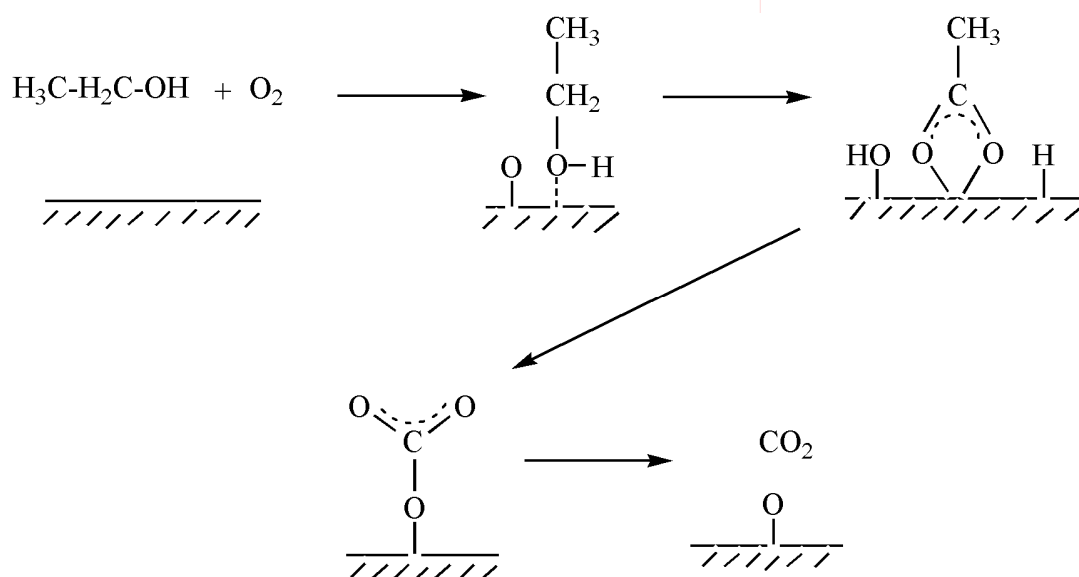


**Figure 4.31** *In situ* IR spectra measured on 0.5Pt/RH-MCM-41 (red line) and 0.5Pt-15Co/RH-MCM-41 (black line) during ethanol oxidation at 300 °C.



**Scheme 4.2** Proposed mechanism of ethanol oxidation on 0.5Pt/RH-MCM-41 from *in situ* IR results.

The *in situ* IR spectrum of 0.5Pt-15Co/RH-MCM-41 showed several similar features to those of the 0.5Pt/RH-MCM-41. However, the characteristic bands of acetaldehyde were not observed. The strong bands at 1563 and 1438  $\text{cm}^{-1}$  were assigned to asymmetric and symmetric stretching modes of bidentate acetate species that were observed start on 100  $^{\circ}\text{C}$  (Figure 4.27). They were clearly observed at 200 (Figure 4.29) and 250  $^{\circ}\text{C}$  (Figure 4.30), much stronger than those in the 0.5Pt/RH-MCM-41. At 300  $^{\circ}\text{C}$  (Figure 4.31), the band of the bidentate acetate decreased significantly and the bands corresponding to  $\text{CO}_2$  increased. The results indicated that the bidentate acetate could generate  $\text{CO}_2$ . The  $\text{CO}_2$  bands from 0.5Pt-15Co/RH-MCM-41 were more intense than that from 0.5Pt/RH-MCM-41 possibly because there was more oxygen supply from oxides of Co for the oxidation. The mechanism of ethanol oxidation on 0.5Pt-15Co/RH-MCM-41 is shown in Scheme 4.3. The surface ethoxy species reacted with surface oxygen to form bidentate acetate which reacted further with the surface oxygen to produce  $\text{CO}_2$ .



**Scheme 4.3** Proposed mechanism of ethanol oxidation on 0.5Pt-15Co/RH-MCM-41 from *in situ* IR results.

#### 4.7 Ethanol oxidation in a flow reactor

Before testing the catalysis for ethanol oxidation, the activity on RH-MCM-41 was first determined. The results are shown in Figure 4.32. There was no conversion in the temperature range of 100-300 °C. The adsorption of ethanol on RH-MCM-41 might be too weak and the desorption occurred spontaneously before converting to any products. The ethanol oxidation that occurred at high temperature could be just a thermal reaction.

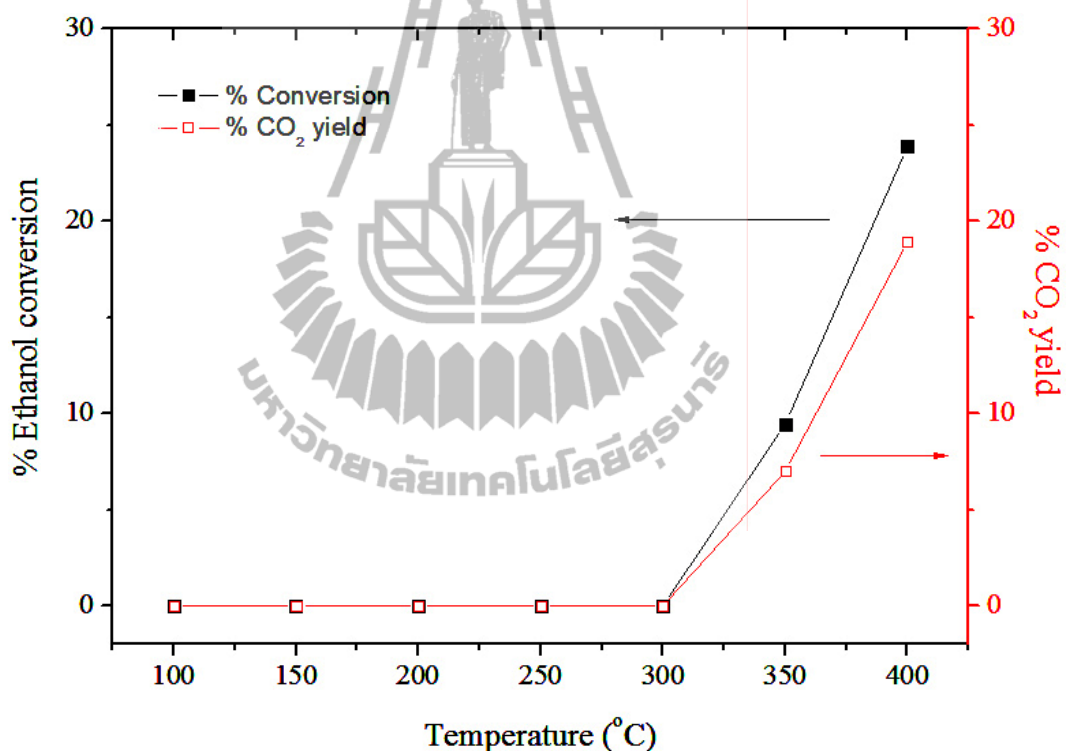


**Figure 4.32** Catalytic performance on RH-MCM-41.

In the rest of the study each catalyst was tested in two cycles. After the first test, the reactor was cooled down to 100 °C under the flow of reactants and the second test was conducted. In the following Figures, the conversions from the first and the second test are represented by filled square and circle symbol, respectively.

The conversions on all catalysts increased with temperature and were complete at high temperature.

The  $T_{50\%}$ , the temperature for 50% ethanol conversion, of 0.5Pt/RH-MCM-41 was the lower than that of the other catalysts suggesting that the Pt catalyst was more active (Figure 4.33). Although acetaldehyde from the fresh 0.5Pt/RH-MCM-41 was observed only at 200 and 250 °C, they were observed at all temperatures in the second run. These results were consistent with the IR spectra that showed acetaldehyde intermediate specie on 0.5Pt/RH-MCM-41. Thus, the monometallic Pt catalyst was susceptible to the reaction condition and likely to be deactivated easily if tested for several times. During the reaction, some intermediates may adsorb strongly on Pt sites preventing further reaction. Therefore, Pt was responsible to the increase of acetaldehyde yield.

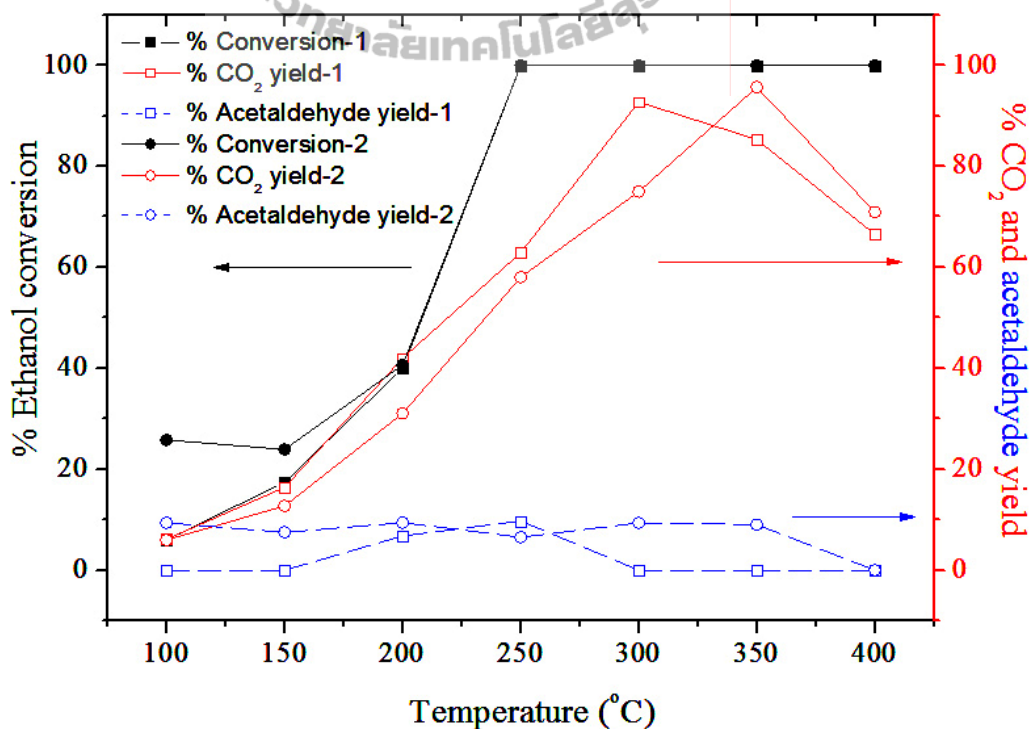


**Figure 4.33** Catalytic performance on 0.5Pt/RH-MCM-41.

The % ethanol conversion and % yield of 5Co/RH-MCM-41 and 15Co/RH-MCM-41 are shown in Figure 4.34 and 4.35, respectively. The ethanol oxidation started at about 200 °C. Thus, the activity of monometallic Co catalyst was lower than the monometallic Pt one. Acetaldehyde yield was not observed on monometallic Co catalysts due to high availability of oxygen on the surface. In addition, the CO<sub>2</sub> yields of 15Co/RH-MCM-41 increased with temperature but decreased after 300 °C. The yields were not 100% suggesting that incomplete oxidation could also take place. However, the analysis of CO, the product from incomplete reaction, by GC in the work was limited due to an overlap of the peak with that of air. There were also other possibilities, for example, CO<sub>2</sub> could be converted to CO by using H<sub>2</sub> from ethanol decomposition (Therdthianwong, A., Sakulkoakiet, and Therdthianwong, S., 2001).

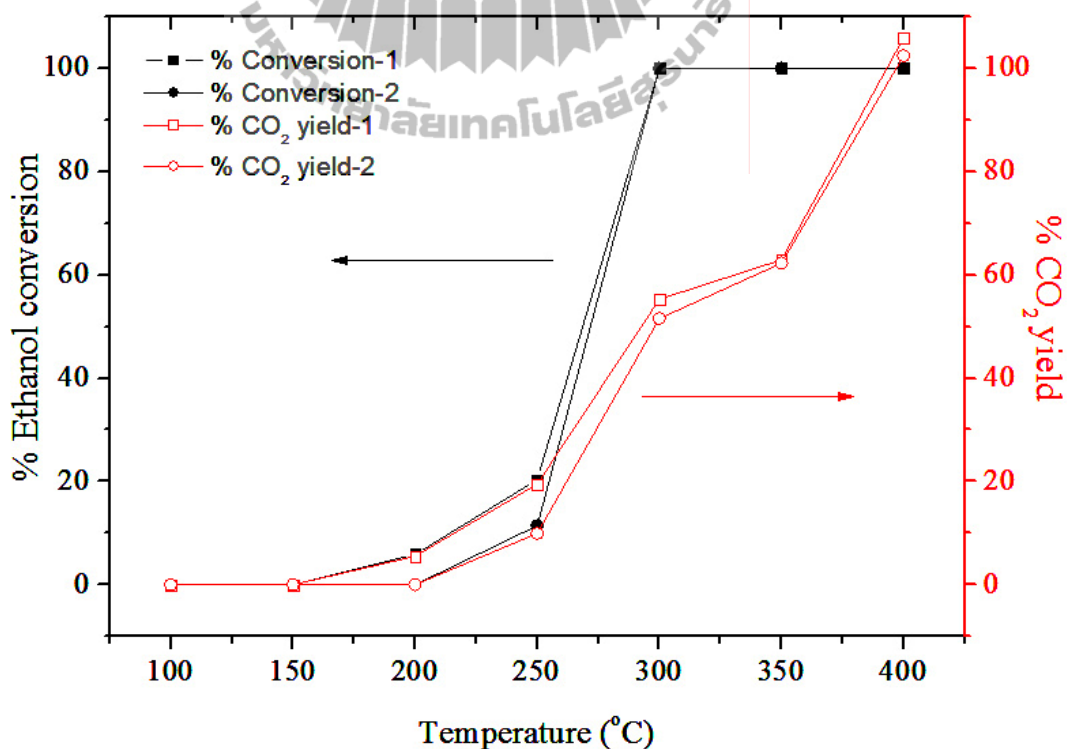


**Figure 4.34** Catalytic performance on 5Co/RH-MCM-41.



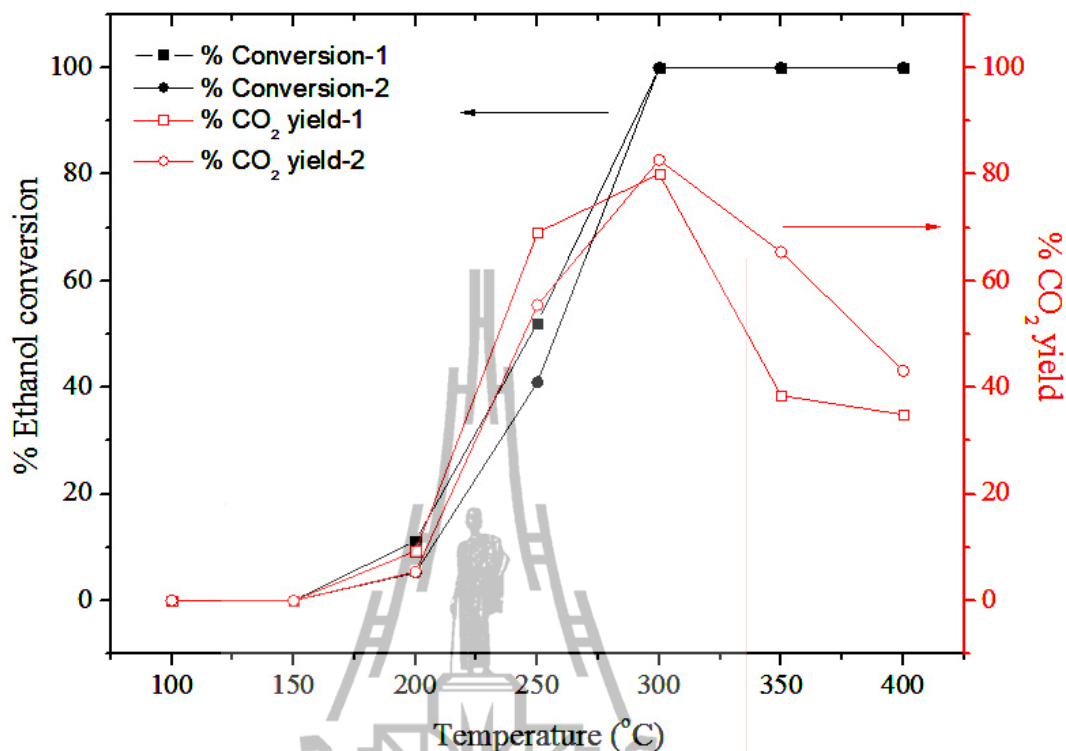


**Figure 4.35** Catalytic performance on 15Co/RH-MCM-41.

The ethanol oxidation of bimetallic Co catalyst was better than monometallic ones because they displayed higher % conversion and % CO<sub>2</sub> yield at low temperature (Figure 4.36). The co-existence of Pt and Co on the same support could improve catalytic activity. In addition, the yields of acetaldehyde on the bimetallic Co catalysts from the first and second runs were similar, but different from 0.5Pt/RH-MCM-41, implying that the co-existence of Pt and Co could maintain the catalyst stability.

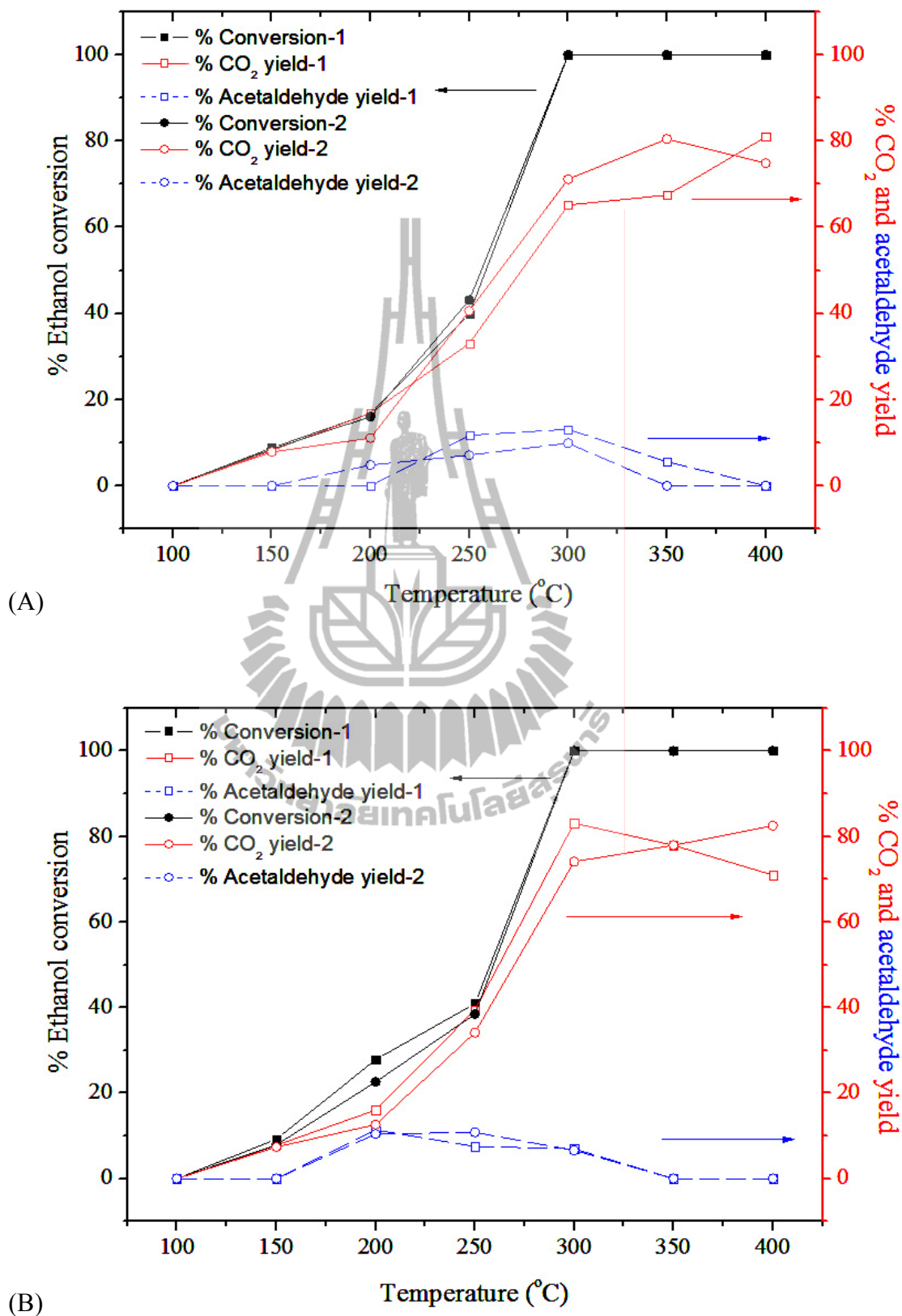


**Figure 4.36** Catalytic performance on 0.5Pt-5Co/RH-MCM-41(A) and 0.5Pt-15Co/RH-MCM-41(B).

Both bimetallic Co catalysts showed similar % ethanol conversion, % CO<sub>2</sub> and acetaldehyde yield. Although, 0.5Pt-15Co/RH-MCM-41 had a higher Co loading but it showed lower dispersion of metal on support. An attempt to observe the difference of dispersion by TEM was not successful (see Appendix). Therefore, optimum catalyst to ethanol oxidation was also depended dispersion of metal, as a 0.5Pt-5Co/RH-MCM-41.

#### 4.8 References

- Akdim, O., Cai, W., Fierro, V., Provendier, H., van Veen, A., Shen, W., and Mirodatos, C. (2008). Oxidative steam reforming of ethanol over Ni–Cu/SiO<sub>2</sub>, Rh/Al<sub>2</sub>O<sub>3</sub>, and Ir/CeO<sub>2</sub> : Effect of Metal and Support on Reaction Mechanism. **Top. Catal.** 51: 22-38.
- Artkla, S., Kim, W., Choi, W., and Wittayakun, J. (2009). Highly enhanced photocatalytic degradation of tetramethylammonium on the hybrid catalyst of titania and MCM-41 obtained from rice husk silica. **Appl. Catal. B: Environ.** 91: 157-164.
- Beck, J. S., Vartuli, J. C., Roth, W. J., Leonowicz, M. E., Kresge, C. T., Schmitt, K. D., Chu, C. T. W., Olson, D. H., and Sheppard, E. W. (1992). A new family of mesoporous molecular sieves prepared with liquid crystal templates. **J. Am. Chem. Soc.** 114: 10834-10843.
- Bellat, J. P., Bertrand, O., Bouvier, F., Broyer, M., François, V., Maure, S., and Weber, G. (1999). Characterization and utilization of MFI zeolites and MCM-41 materials for gaseous pollutant adsorption. **Stud. Surf. Sci. Catal.** 125: 737-744.

- Bhoware, S. S., and Singh, A. P. (2007). Characterization and catalytic activity of cobalt containing MCM-41 prepared by direct hydrothermal, grafting and immobilization methods. **J. Mol. Catal. A: Chem.** 266: 118-130.
- Chumee, J., Grisdanurak, N., Neramittagapong, A., and Wittayakun, J. (2009). Characterization of platinum–iron catalysts supported on MCM-41 synthesized with rice husk silica and their performance for phenol hydroxylation. **Sci. Technol. Adv. Mater.** 10: 1-6.
- de Lima, S. M., Silva, A. M., Graham, U. M., Jacobs, G., Davis, B. H., Mattos, L. V., and Noronha, F. B. (2009). Study of catalyst deactivation and reaction mechanism of steam reforming, partial oxidation, and oxidative steam reforming of ethanol over Co/CeO<sub>2</sub> catalyst. **J. Catal.** 268: 268-281.
- Haga, K., and Watanabe, H. (1996). A structural interpretation of Si-O-Si vibrational absorption of high-photoconductive amorphous a-SiO<sub>x</sub>:H films. **J. Non-Cryst. Solids.** 195: 72-75.
- Jentys, A., Kleestorfer, K., and Vinek, H. (1999). Concentration of surface hydroxyl groups on MCM-41. **Micropor. Mesopor. Mat.** 27: 321-328.
- Khemthong, P., Klysubun, W., Prayoonpokarach, S., Roessner, F., and Wittayakun, J. (2010). Comparison between cobalt and cobalt–platinum supported on zeolite NaY: Cobalt reducibility and their catalytic performance for butane hydrogenolysis. **J. Ind. Eng. Chem.** 16: 531-538.
- Kresge, C. T., Leonowicz, M. E., Roth, W. J., Vartuli, J. C., and Beck, J. S. (1992). Ordered mesoporous molecular sieves synthesized by a liquid-crystal template mechanism. **Nature.** 359: 710-712.

- Lamaita, L., Peluso, M. A., Sambeth, J. E., and Thomas, H. J. (2005). Synthesis and characterization of manganese oxides employed in VOCs abatement. **Appl. Catal. B: Environ.** 61: 114-119.
- Nagai, M., and Gonzalez, R. D. (1985). Oxidation of ethanol and acetaldehyde on silica-supported platinum catalysts: preparative and pretreatment effects on catalyst selectivity. **Ind. Eng. Chem. Prod. Res. Dev.** 24: 525-531.
- Panpranot, J., Kaewkun, S., Praserttham, P., and Goodwin, J. G. (2003). Effect of cobalt precursors on the dispersion of cobalt on MCM-41. **Catal. Lett.** 91: 95-102.
- Paulino, I. S., and Schuchardt, U. (2002). Studies of MCM-41 obtained from different sources of silica. **Stud. Surf. Sci. Catal.** 141: 93-100.
- Pérez, H., Navarro, P., Delgado, J. J., and Montes, M. (2011). Mn-SBA15 catalysts prepared by impregnation: influence of the manganese precursor. **Appl. Catal. A: Gen.** 400: 238-248.
- Rouquerol, F. R. J., and Sing, K. (1999). **Adsorption by powders & porous solids.** Great Britain: MPG Books.
- Scott, M., Goeffroy, M., Chiu, W., Blackford, M., and Idriss, H. (2008). Hydrogen production from ethanol over Rh–Pd/CeO<sub>2</sub> catalysts. **Top. Catal.** 51: 13-21.
- Song, H., and Ozkan, U. S. (2009). Ethanol steam reforming over Co-based catalysts: Role of oxygen mobility. **J. Catal.** 261: 66-74.
- Therdthianwong, A., Sakulkoakiet, T., and Therdthianwong, S. (2001). Hydrogen production by catalytic ethanol steam reforming. **ScienceAsia.** 27: 193-198.

- Trawczyński, J., Bielak, B., and Miśta, W. (2005). Oxidation of ethanol over supported manganese catalysts-effect of the carrier. **Appl. Catal. B: Environ.** 55: 277-285.
- Tsoncheva, T., Ivanova, L., Rosenholm, J., and Linden, M. (2009). Cobalt oxide species supported on SBA-15, KIT-5 and KIT-6 mesoporous silicas for ethyl acetate total oxidation. **Appl. Catal. B: Environ.** 89: 365-374.
- Tsoncheva, T., Rosenholm, J., Linden, M., Ivanova, L., and Minchev, C. (2007). Iron and copper oxide modified SBA-15 materials as catalysts in methanol decomposition: effect of copolymer template removal. **Appl. Catal. A: Gen.** 318: 234-243.
- Wu, Z. Y., Wang, Y. M., and Zhu, J. H. (2005). Direct synthesis of Cu-modified MCM-41 functional materials. **Stud. Surf. Sci. Catal.** 156: 139-146.
- Xu, X., Song, C., Andresen, J. M., Miller, B. G., and Scaroni, A. W. (2002). Novel polyethylenimine-modified mesoporous molecular sieve of MCM-41 Type as high-capacity adsorbent for CO<sub>2</sub> capture. **Energ. Fuel.** 16: 1463-1469.
- Yee, A., Morrison, S. J., and Idriss, H. (1999). A study of reactions of ethanol on CeO<sub>2</sub> and Pd/CeO<sub>2</sub> by steady state reactions, temperature programmed desorption, and *in situ* FT-IR. **J. Catal.** 186: 279-295.
- Yu, Z., and Chuang, S. S. C. (2007). In situ IR study of adsorbed species and photogenerated electrons during photocatalytic oxidation of ethanol on TiO<sub>2</sub>. **J. Catal.** 246: 118-126.
- Zhao, X. S., Lu, G. Q., Whittaker, A. K., Millar, G. J., and Zhu, H. Y. (1997). Comprehensive study of surface chemistry of MCM-41 using <sup>29</sup>Si CP/MAS NMR, FTIR, pyridine-TPD and TGA. **J. Phys. Chem. B.** 101: 6525-6531.

## CHAPTER V

### CONCLUSION

RH-MCM-41 was synthesized by hydrothermal method and used as a support for monometallic Pt, Co, Cu, and Mn as well as bimetallic PtCo, PtCu, and PtMn. After metal loading by impregnation method, surface area and pore volume decreased due to metal deposition but mesoporous ordered structure was still maintained. Metal and metal oxides could be on external surface and inside the pore of RH-MCM-41. The form of Co, Cu, and Mn confirmed by XRD and XANES were  $\text{Co}_3\text{O}_4$ , CuO, and  $\text{MnO}_2$ , respectively.

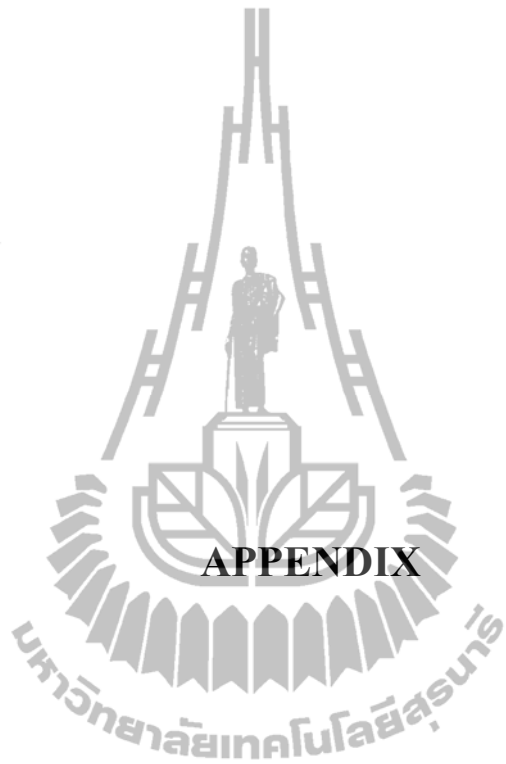
To study ethanol adsorption by thermogravimetric analysis (ethanol-TGA), all catalysts were reduced at 200 °C before exposed to ethanol vapor. Ethanol could adsorb on all catalysts on silanol groups of RH-MCM-41 support as well as on both metallic and metal oxide active sites. In addition, ethanol adsorption was studied by temperature program desorption (ethanol TPD). On the monometallic Pt could adsorb ethanol adsorbed dissociatively, namely, bonds in ethanol were broken and the adsorbed species dissociated further to  $\text{CH}_4$ , CO, and  $\text{H}_2$ . Among oxides of Co, Cu, and Mn, the  $\text{Co}_3\text{O}_4$  displayed the highest potential as an oxygen source for ethanol oxidation.

Only monometallic Pt, Co and bimetallic PtCo catalysts were further studied for ethanol oxidation. Intermediates were analyzed by *in situ* FTIR and the reaction pathway and mechanism were proposed. For monometallic Pt, ethanol adsorbed as

ethoxy species, rearranged on the surface to form parallel adsorbed acetaldehyde, transformed to monodentate acetate with surface oxygen, and finally dissociated/desorbed as products ( $\text{CO}_2$  and  $\text{H}_2\text{O}$ ). On the bimetallic PtCo, surface ethoxy species reacted with surface oxygen to form bidentate acetate which reacted further with the surface oxygen to produce  $\text{CO}_2$ .

Ethanol oxidation testing in a fixed bed flow reactor, the conversion over all catalysts increased with the temperature and  $\text{CO}_2$  was the major product. The activity of monometallic Pt was higher than monometallic Co, but it deactivated easily because monometallic Pt produced increasing acetaldehyde yield if tested for several times. The bimetallic PtCo had the best activity, implying that the co-existence of Pt and Co could maintain the catalyst stability. Besides, the incorporation of  $\text{Co}_3\text{O}_4$  could serve as oxygen source for catalytic ethanol oxidation. Because 0.5Pt15Co/RH-MCM-41 and 0.5Pt5Co/RH-MCM-41 showed similar conversion and product yield, the suitable catalyst to ethanol oxidation depended dispersion of metal.





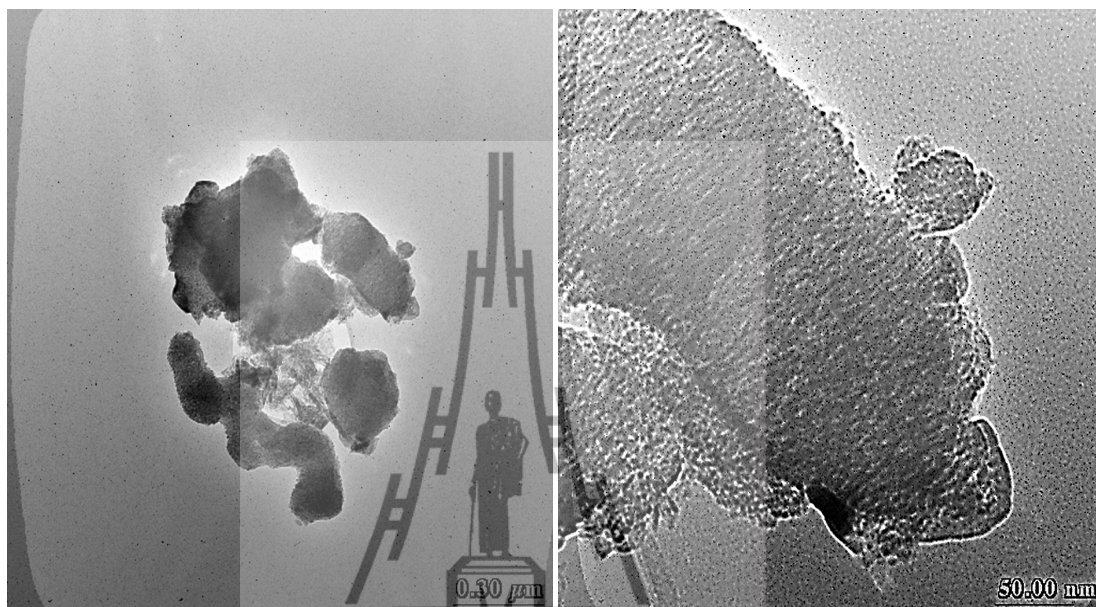
**APPENDIX**

**TEM IMAGES OF 0.5Pt-5Co/RH-MCM-41 and 0.5Pt-10Co/**

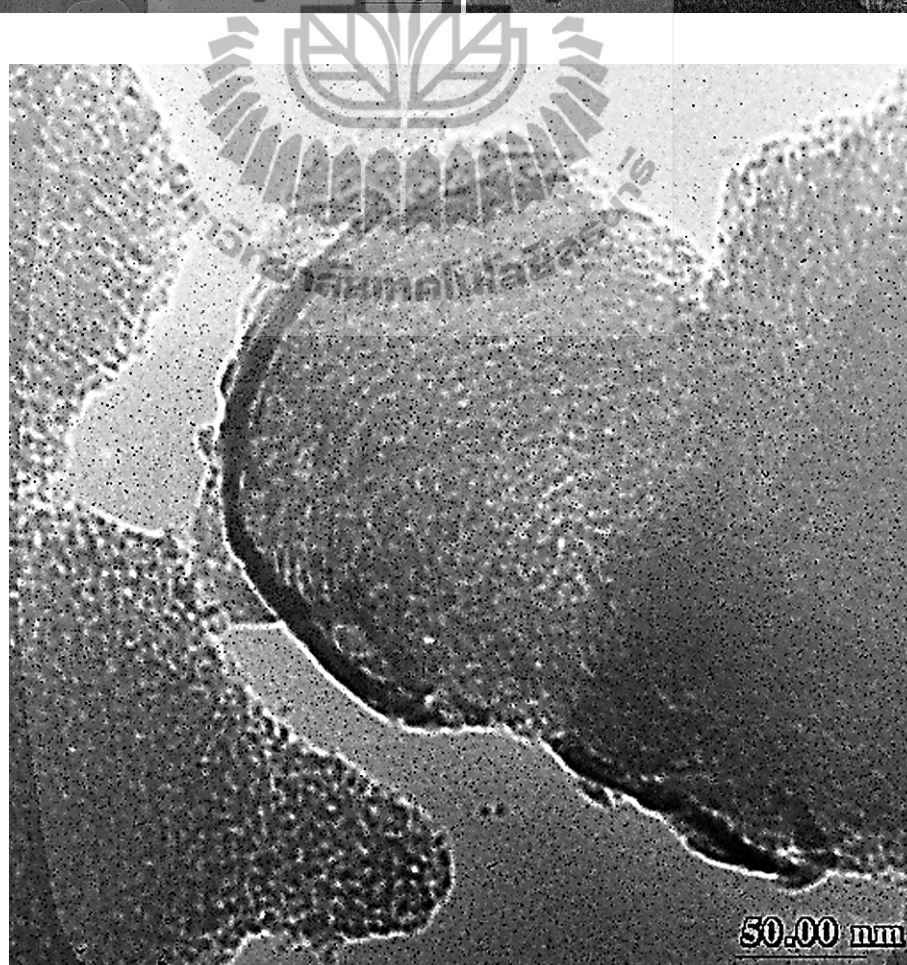
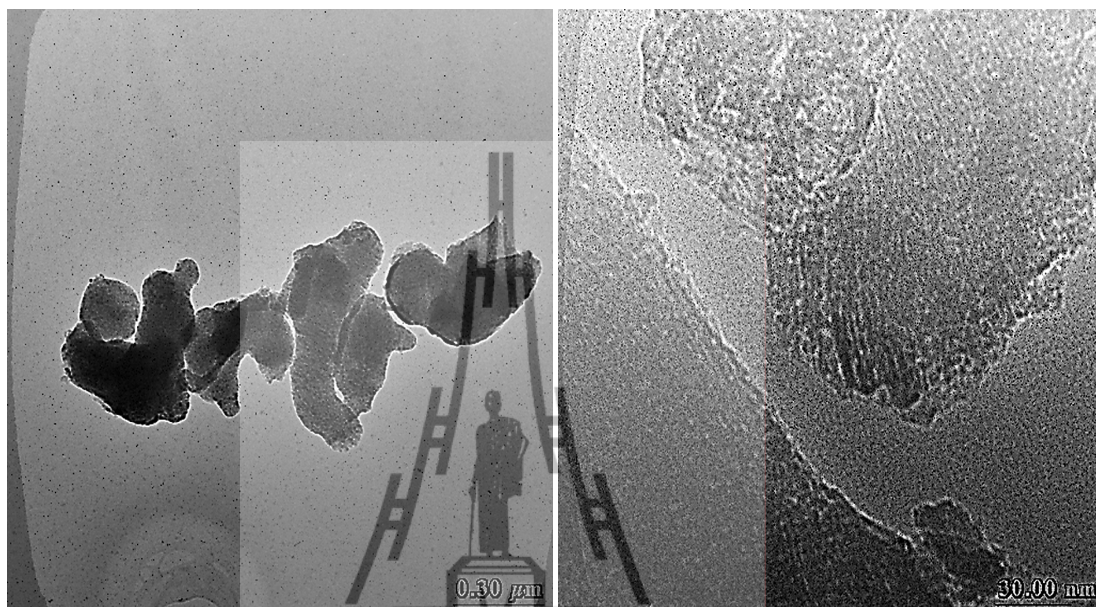
**RH-MCM-41**



## 0.5Pt-5Co/RH-MCM-41



## 0.5Pt-10Co/RH-MCM-41



# CURRICULUM VITAE

- Name** Miss Kamolwan Rinramee
- Education**
- 2002-2006 B.Sc. (Chemistry) Ubon Ratchatane University, Ubon Ratchatani, Thailand
- 2006-2011 Ph.D. (Chemistry) Suranaree University of Technology, Nakhon Ratchasima, Thailand
- Publications**
1. **Rinramee, K.**, Fö
  2. ttinger, K., Rupprechter, G., Wittayakun, J. Ethanol adsorption and oxidation on bimetallic catalysts containing platinum and base metal oxide supported on MCM-41, Applied Catalysis B: Environmental, 115-116 (2012) 225-235.
  3. Saceda, J.-J. F., **Rinramee, K.**, Khabuanchalad, S., Prayoonpokarach, S., de Leon. R. L., Wittayakun, J. Properties of zeolite Y in various forms and utilization as catalysts or supports for cerium oxide in ethanol oxidation, Journal of Industrial and Engineering Chemistry, 18 (2012) 420-424.
  4. Saceda, J.-J. F., de Leon, R. L., **Rinramee, K.**, Prayoonpokarach, S., Wittayakun, J. Properties of Silica from Rice Husk and Rice Husk Ash

and Their Utilization for Zeolite Y Synthesis, *Química Nova*, 34  
(2011) 1394-1397.

